WASM: Minerals, Energy and Chemical Engineering

Advanced borehole seismic imaging techniques for mineral exploration

Sana Zulic

0000-0002-3320-7847

This thesis is presented for the Degree of

Master of Philosophy

of

Curtin University

June 2022

Declaration

To the best of my knowledge and belief this thesis contains no material previously published by any other person except where due acknowledgment has been made.

This thesis contains no material which has been accepted for the award of any other degree or diploma in any university.

Signature: .....

Date: .....27.05.2022.....

Abstract

Several decades ago, seismic methods became a standard tool in oil and gas exploration. However, the mining industry still hesitates to accept seismic as a conventional exploration method in mineral exploration. The most common reasons are complex geological settings, which influence the propagation of seismic waves, and the relatively high cost of seismic operations compared to other geophysical methods. The other geophysical methods (e.g. potential fields, EM methods) are being successfully used at different scales of the exploration; however, they have uncertain depth penetration when regolith is present. Seismic methods can provide high-resolution images and maintain the resolution with depth. Vertical seismic profiling (VSP) is one of a few seismic methods where the receivers (or sources in reverse VSP) are placed at a known depth within the drillhole, allowing a signal to be directly studied and correlated to the identified rock from the core samples. Due to only one way of a signal travelling through the low-velocity layer in a near-surface, the VSP often has a significantly higher resolution than surface seismic methods. However, great illumination is needed to achieve good seismic imaging in a complex geological environment. With conventional VSP equipment and challenging drillhole conditions, three-dimensional VSP surveys are hardly possible. In addition to the low illumination of a single-offset VSP, the geology where mineral exploration occurs is fairly complex and often has steep dips and three-dimensional distribution. Therefore, the wavefield recorded with a poor-illumination survey is difficult to resolve. Furthermore, many processing workflows are based on a horizontally stratified subsurface, and VSP processing is slow and hence expensive.

Throughout my thesis, I examine the current VSP application in mineral exploration in Australia, identify the challenges and study in which domain these challenges could be mitigated. In particular, the advancement in the equipment domain could be seen in applying Distributed Acoustic Sensing (DAS) technology. In the thesis, I compare amplitude registered by DAS to amplitude registered by conventional VSP geophone. This work indicates that strain-rate measurements collected with DAS and geophone have very similar amplitudes. The second advancement can be achieved by utilising the full-waveform

inversion (FWI) techniques for data processing. I test the FWI on synthetic and then on the field dataset. I observe that FWI is a powerful imaging technique that can give detailed physical properties of the subsurface, often needed by geoscientists and is not limited to the horizontally stratified subsurface. The thesis conclusions indicate that applying these advanced VSP techniques could address the abovementioned challenges and introduce an additional high-resolution dataset to assist the subsurface characterisation in mineral exploration.

Acknowledgements

I would like to thank my thesis committee, supervisor Professor Roman Pevzner, co-supervisor Professor Andrej Bona, co-supervisor Dr Konstantin Tertyshnikov and Dr Alexey Yurikov for providing support throughout this research project and for unselfishly sharing their knowledge. I want to thank anonymous thesis reviewers for their feedback and suggestions to increase the quality of the thesis.

In addition to my thesis committee, I would especially like to thank my managers, Dr Greg Turner and Jai Kinkela, and MinEx CRC Education and Training Program Coordinator A/Professor Caroline Tiddy, for providing support while I worked and studied simultaneously. It would be much harder to complete without their help.

I want to thank Red5, Goldfields Ltd and Northern Star Resources Ltd, particularly Mark Williams, Andrew Foley and Carl Young, for allowing me to publish information from the VSP borehole surveys collected by their companies. Big thanks to the acquisition crews who collected the data.

I thank Deco Geophysical, Tesseral, Mira Geoscience, Matlab, and OpendTect for software under their University programs, Sercel and Silixa for providing the equipment used in the research, and the authors of the IFOS FWI package for the codes that allow elastic FWI of VSP data.

I want to thank Dr Sara Jakica, my industry supervisor, for listening to my numerous “dry runs” and giving her valuable comments and feedback. I would also like to thank Dr Don Pridmore and Professor Milovan Urosevic for motivating me to embark on the research journey. And last but not least, thanks to my family for their continuous support.

This research has been supported by Mineral Exploration Cooperative Research Centre, whose activities are funded by the Australian Government's Cooperative Research Centre Program, HiSeis Pty Ltd and the Pawsey Supercomputing Centre with funding from the Australian Government and the Government of Western Australia.

Table of contents

List of figures

List of tables

1 Introduction

1.1. Overview

Early mineral exploration started several dozen thousand years ago, with people collecting minerals from the rocky outcrops and using them to produce the tools for work that improved and advanced the quality of life (Vujić, 2014). However, significant mineral exploration and mining development occurred after one of the greatest human discoveries – turning the rocks into metals by melting them in a fire. The archaeological studies of the early metallurgy imply that this discovery happened eight thousand years ago in Serbia, during the Vinča culture in the Late Neolithic/Early Chalcolithic period (Radivojević and Roberts, 2021). Since this great discovery, the early mining made a long way from melting the rocks found at the surface to digging the pits and developing underground mines. The discovery was a foundation for the technical development of mineral exploration and mining in general (Vujić et al., 2003).

Today, the demand for minerals has never been higher, although almost all rocky outcrops have been explored. A three-monthly report produced in 2020 by the Australian Bureau of Statistics Mineral Exploration data indicates that mineral exploration increased exploration expenditure by 21% compared to the year before. In Western Australia, 62% of national expenditure is reported as mineral exploration (Geoscience Australia, 2020). Major mineral deposits in Australia, located within the areas of outcrops, are well explored, and exploited. However, the overburden covers the vast areas of basement rock. Several nationally coordinated initiatives are formed (e.g., Mineral Exploration Cooperative Research Centre) to unlock Australia's hidden resource potential. The hidden resource potential can be unlocked by utilising different geological and geophysical detection techniques, with seismic methods being one of them. Seismic methods are based on the study of wave propagation through the earth and can provide high-resolution images and maintain the resolution with depth. Vertical Seismic Profiling (VSP) is a type of seismic method in which a seismic source is located on the surface and receivers in a borehole. Such a recording geometry allows VSP to record a full wavefield (direct, converted, reflected

waves), which is one of the major benefits over other seismic methods. The known depths of receivers enable measuring seismic properties of formation (P- and S-wave velocity, attenuation, anisotropy). The measured properties can be directly linked to the rock formations identified on the core.

The major benefits of the VSP survey are that the recorded wavefield consists of a full wavefield (direct, converted, reflected waves), can measure seismic properties of formation (P- and S-wave velocity, attenuation, anisotropy) and can be directly linked to the rock formations identified on the core.

1.2. Research motivation and aim

The main objectives of this research are to investigate the current VSP application in mineral exploration in Australia, identify the challenges and study in which domains these challenges could be mitigated in order to assist the exploration better.

The research examines the advancement in the equipment, processing, and interpretation domain with an overall goal to optimise the VSP to suit mineral exploration specific conditions better. As the VSP imaging in the mining industry is limited due to the equipment and costs involved in the VSP field operation, the application of distributed acoustic sensing (DAS) would allow different VSP geometries to be acquired in significantly reduced acquisition time. It could also reduce the cost of tool loss associated with open hole environments. In the processing domain, the full waveform inversion can be utilised to overcome some conventional processing limitations in imaging complex geology.

The significance of this research study can be seen in:

1. Workflow optimisation of VSP for the mining industry;
2. Application of DAS technology in mineral exploration;
3. Application of powerful imaging technique for mineral exploration and estimation of rock elasticity parameters using VSP data;
4. The cost reduction of VSP acquisition in the mining industry.

1.3. Thesis structure

The thesis is organised into six chapters. The objectives and significance of VSP application in mineral exploration are summarised in Chapter 1. Chapter 2 gives a brief overview of seismic reflection methods, focusing on the VSP development and its specifics. Several VSP field examples from Australian mineral exploration are showcased in Chapter 3. Chapter 4 introduces distributed acoustic sensing and contains the comparison of amplitudes on DAS and geophone. Chapter 5 assesses full-waveform inversion and its application to the VSP data. Finally, the conclusions and further recommendations are given in Chapter 6.

2 Vertical seismic profiling and its application in mineral exploration

2.1. An overview of seismic reflection methods

Several decades ago, seismic reflection methods became a standard tool in oil and gas exploration. However, the mining industry still hesitates to accept seismics as a conventional exploration method in mineral exploration. The most common reasons are complex geological settings, which influence the propagation of seismic waves, and the relatively high cost of seismic operations compared to other geophysical methods. The other geophysical methods (e.g. potential fields, EM methods) are being successfully used at different scales of the exploration; however, they have limitations in spatial resolution, especially with increasing depth of investigation (Malehmir et al., 2012). Seismic methods can provide high-resolution images and maintain the resolution with depth. They are based on the study of wave propagation through the earth.

There are several classifications of seismic methods. Depending on the position of the source that generates the waves and the receivers that record them, the seismic methods can be categorised as surface and borehole methods. In surface seismic methods, the receivers and sources are positioned on a surface (land, water). In borehole seismic methods, the most common configuration is

when the receivers are placed inside a borehole and sources on the surface. The latter is also known as Vertical Seismic Profiling (VSP) (Figure 2-1).

In VSP, there are several benefits due to the nature of its acquisition design. Stable conditions of the sensors inside a borehole, lack of surface waves on the seismograms, and shorter propagation distance from a source to receiver result in data with a better signal-to-noise ratio and higher resolution than surface seismic. Downhole seismics also offer the in-situ measurements of changes in the shape and amplitudes of a propagating acoustic signal. Compared to the land 3D surveys, borehole seismic acquisitions are faster and prone to fewer land access issues. In the case of time-lapse investigations, VSP provides excellent repeatability, as sensors are located in constant conditions in a borehole. These advantages generally allow obtaining high-resolution seismic imaging of complex geological environments in the vicinity of the borehole. To achieve good seismic imaging in a complex geological environment, apart from high resolution, the VSP must have sufficient illumination.

Data collected by seismic methods are recorded in time, measuring how much time a wave needs to travel from a source to a receiver. When receivers are deployed in a borehole, the recorded data comprises two main wavefield components: downgoing part – body waves propagating from a source at the surface to receivers and upgoing part – energy reflecting in the borehole (Figure 2-2a).

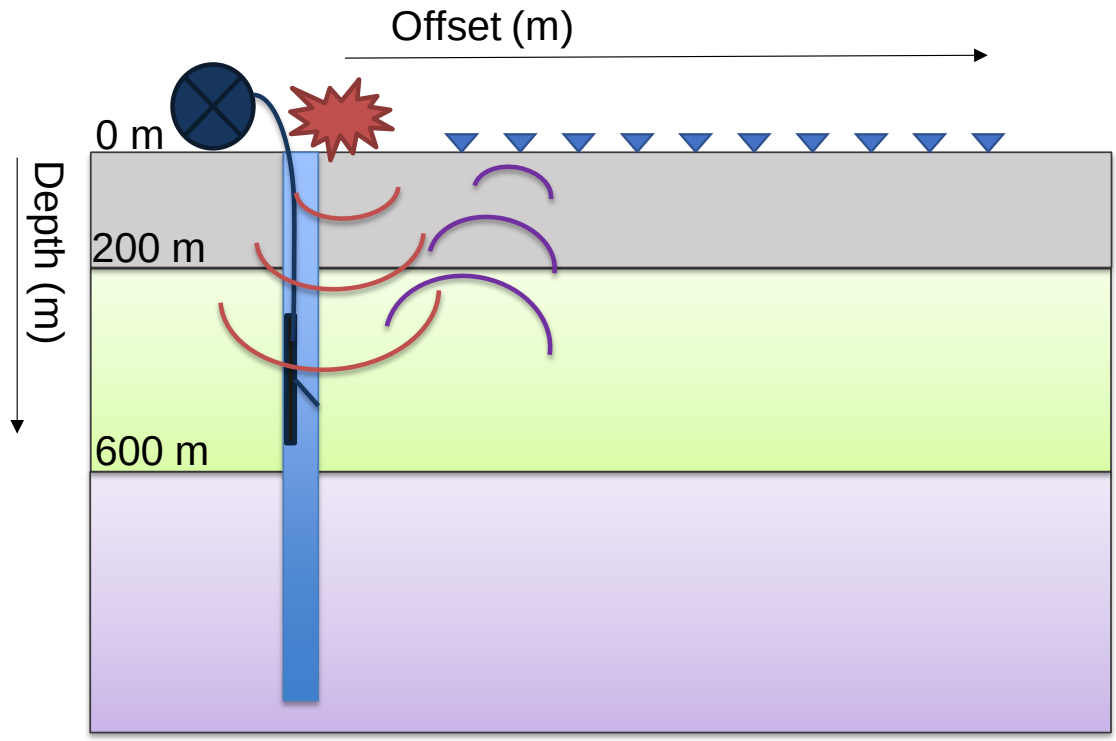

Figure 2-1. A basic principle of the seismic reflection method. Red is the source; blue cones are surface receivers; a dark circle is a winch with a borehole receiver. Red lines are down-going body waves, and purple lines are up-going waves.

In surface reflection seismic, the travel time of a wave, required to travel from a source at the surface to a subsurface reflector and return back to a surface receiver, is utilised to create an image of the subsurface. In this case, determination of the relationship between time and depth of the reflection origin requires information about the wave propagation velocities through a particular medium. In VSP, ambiguity about the time-depth relation is removed as the receiver's depth is accurately recorded with the assistance of gamma-ray logging during acquisition. Furthermore, accurate depth allows identified reflectors to be correlated back to geological interfaces using wireline logs and core data (Juhlin, 1990). As such, the VSP data can be utilised for tying surface seismic reflections to known depths and lithological units. For this purpose, surface seismic often is employed in conjunction with VSP.

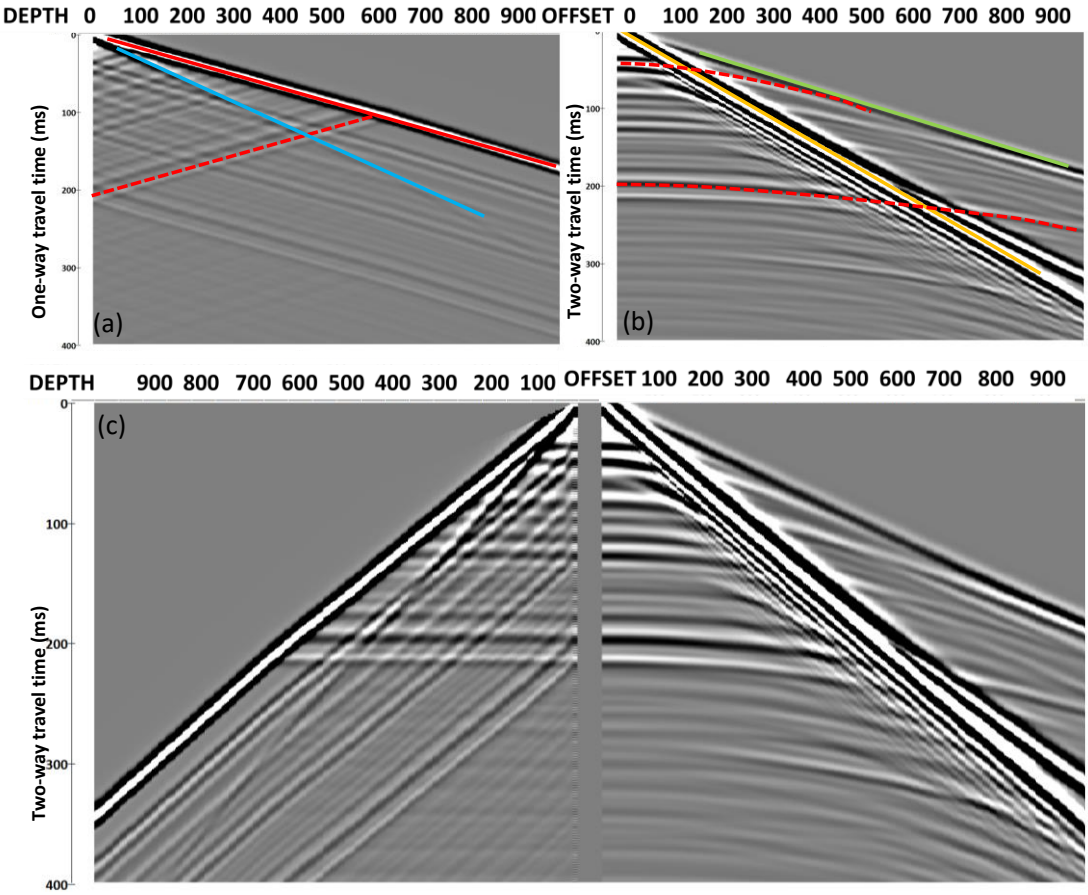

Figure 2-2. Seismogram examples with source at surface and (a) receivers in a borehole (VSP); (b) receivers on a surface; (c) two-way time VSP and surface seismogram. Solid and dashed red line: direct and reflected P-wave, solid blue line: direct S-wave, solid green line: refracted P-wave, solid orange line: direct surface wave.

2.2. Development of VSP and its application in mineral exploration

In his pioneering work on seismic exploration (Fouqué, 1888), Ferdinand Fouqué summarised several important scientific conclusions related to the observation of propagation of seismic waves. Three significant observations from his review are:

- wavefield propagation does not occur in the same way on the surface as when the superficial path is avoided;
- different geological formations have variable velocities;
- there are additional factors, apart from the rock type, on which velocity depends.

The development of the automated seismometer enabled the recording of seismic waveforms and detailed study of their characteristics. Shortly after, other scientists started using boreholes as a location for the deployment of either a seismic source or geophone. Fessenden (1917) was granted a patent for his “Method and apparatus for locating ore bodies”. This patent is one of the first published examples of the application of the borehole seismic method for mineral exploration, in which receivers and sources are placed in a borehole and used to generate and record the energy. These early ideas pushed further forward the development of borehole seismic methods.

Advancements in borehole seismic continued rapidly in the twentieth century. According to Gal’perin (1974), the principal difficulties in seismic exploration are related to the complexity of the actual medium through which seismic waves propagate. In particular, the mineral exploration encounters geological environments, which are usually characterised by a high structural complexity (steeply dipping shear zones, faults, folding, intrusions, etc.) as well as by the presence of high-velocity formations with weakly differentiated acoustic properties. Studies of the full waveforms recorded in boreholes at known depths are quite beneficial to characterise such media. Extensive research in borehole seismic exploration led to the further development of vertical seismic profiling (VSP) by the Institute of Physics of the Earth of the Academy of Sciences of the USSR in 1959 (Gal’perin, 1974).

After decades of continuous improvements in the equipment and computational techniques, VSP was established (Gal’perin, 1985) to complete various exploration tasks:

- determination of in-situ seismic velocities as a function of depth;
- time-depth ties for surface seismic;
- estimation of seismic attenuation;
- analysis of the wavefield propagation;
- imaging of the subsurface.

Since its development, VSP has been implemented in mineral exploration programs around the world to various degrees. In Russia, the government supported the wide use of VSP to characterise different mineral-bearing regions for seismic exploration by deriving appropriate velocity models and enhancing understanding of the reflectivity of different geological sections. As a result of these studies, deep drilling was undertaken for mineral exploration, including drilling of the deepest borehole in the world – the Kola Superdeep borehole (12 km depth). In addition, surface seismic methods were employed in regional surveys and explorations for ferrous, base, precious metals, and diamonds (Karaev and Rabinovich, 2010). Canada, Europe, and Australia followed a similar development path through government initiatives in partnerships with mining companies. Such partnerships allowed extensive knowledge transfer between research institutes and industry. One example of a successful industry-driven application was in South Africa by Anglo-American Corporation, commencing in 1983. This enabled application of 3D VSP in the mining industry through extensive development in optimisation of the field operations, quality control, processing techniques and integration of a variety of datasets (Pretorius, 2003, 2011). Consequently, many deep mineral deposits have been discovered and explored using borehole seismic methods, including massive sulphides (Adam et al., 2000; Eaton et al. 2003; Bellefleur et al., 2004; Cosma et al., 2001, 2003 2011; Mueller et al. 2012), Outokumpu mineral deposits (Kukkonen, 2011), nickel exploration (Greenwood et al., 2013), delineation of kimberlite pipes (Urosevic and Evans, 2000), characterisation of crystalline rocks for nuclear waste storage (Juhlin et al. 1991; Cosma et al., 2003).

Compared to the number of publications on the VSP application in oil and gas exploration, it is fair to say that no matter how many exploration uncertainties it can reduce, the VSP method is still underutilised in mineral exploration. The main challenges for its application in mineral exploration are:

1. High operational costs;
2. Lack of equipment for small-size hole diameter;
3. High risk of losing the equipment in unstable uncased holes;
4. Complex geological targets.

The novel Distributed Acoustic Sensing (DAS) technology has the potential to overcome some listed issues and make borehole seismic affordable and effective. The approach utilises an optical fibre interrogated with a laser pulse to record its interaction with seismic energy. DAS allows the deployment of a fibre optic cable down the entire well and records data with dense spatial sampling (~1 m channel spacing) at once along its full length. In addition, considering the use of inexpensive standard telecommunication fibre optic cables, this approach significantly reduces the operational costs of borehole seismic. It becomes an attractive and cost-effective alternative to geophone. DAS technology has already been applied to various tasks in hydrocarbon exploration and monitoring (Mateeva et al., 2014; Correa et al., 2018a; Yu et al., 2020). Several studies compare DAS performance against conventional receivers, and in some aspects, fibre optic sensors perform better than geophones (Correa et al., 2017b).

Currently, DAS is slowly entering the mineral industry. Bona and Pevzner (2018) showed numerous advantages of DAS over hydrophones (consistent amplitudes, clearer reflections, etc.). Riedel et al. (2018) conducted an underground VSP experiment and agreed that even though DAS gives only single-component data, it reduces the costs and risk compared to conventional geophone VSP surveys. Bellefleur et al. (2020) discussed new logistical factors around DAS, such as cementing the fibre-optic cable and assessed data collected by different fibre-optic cables. Tertyshnikov et al. (2020) used 3D DAS VSP to image a target coal seam in an area around boreholes with installed fibres. They suggested that permanently deployed fibre-optic cable can also be used to monitor mine operations.

Despite the many benefits that DAS offers, there are some specifics related to the novelty of the technology itself. For example, the deployment challenges, variable signal quality between different DAS equipment, measuring different physical properties, effects of interrogator designs on DAS signal, calibration amongst different manufacturers, are some of the factors that need to be studied and addressed.

2.3. Types of VSP and their specifics related to the mineral exploration

VSP can refer to various types of survey designs with various combinations of positioning sources or receivers in and around a borehole. The VSP term is generally used for surveys in which receivers are placed in a borehole and sources on the surface. When a source is positioned in a borehole, the survey is called Reverse Vertical Seismic Profile (RVSP). If source and receivers are placed in adjecent boreholes, than the survey is called crosswell seismic.

Additional classification can be made on survey geometry. The survey geometry is defined by borehole trajectory, receiver coverage and source offsets. It directly affects the results of VSP of how much of the subsurface can be imaged with selected survey parameters.

The common field practice with conventional sensors is to deploy a borehole geophone (or a string of several geophones) to the end of the hole (EOH) and conduct the survey along the bore from EOH to the surface. The borehole geophone is clamped with a special tool arm against the borehole wall to ensure good coupling while the source generates the seismic energy. Once the shot is generated, the geophone is moved to the next depth level. For example, if the borehole is 1000 m deep and the receiver interval is 5 m, then the described procedure is repeated at least 200 times. To reduce the standby of the rig in hydrocarbon exploration, multi-level geophones (string) are developed, which can listen to several depth levels for one shot. Usage of multi-level geophones allows a much more efficient survey (time, costs); however, the increased risk of losing the expensive instrument requires cased boreholes. In hydrocarbon exploration, the casing is a part of the normal well completion. In the mineral industry, boreholes are used for geological exploration, not production, and are usually left uncased after drilling. The casing is present only in case of an unstable top sediment cover (overburden) and usually consists of a 4-5-inch steel drilling rod.

Before presenting several cases from mineral exploration (Chapter 3), I will briefly explain specifics related to various types of VSP approaches and emphasise

what kind of solutions each one can provide. Detailed background information can be found in Gal'perin (1985), Hardage (2000) and Hinds et al. (1996).

2.3.1. Zero-offset VSP

Zero-offset VSP (ZVSP) is a type of VSP in which the source is positioned at the borehole collar (or close to it). The receiver positions are evenly distributed in the borehole at a given spacing. The receiver interval should be chosen to allow efficient survey but, more importantly, to avoid spatial aliasing. It depends on the slowest expected velocity V_{min} and highest frequency f_{max} (Hardage, 2000) :

$$\Delta Z \leq \frac{Vmin}{2f_{max}} \ . \quad (1)$$

In ZVSP, when the borehole is vertical, the wave travels from source to receiver with an incidence angle of ~90 degrees. This means that all reflection points from any interfaces occur in a narrow zone close to the borehole, which is insufficient for imaging. However, ZVSP is extremely valuable for calculating interval velocities and assessing the reflection response of the subsurface by creating the corridor stack. Corridor stack can be correlated to geological log and used to tie surface seismic images to interfaces' depth. This is a unique way to determine what interfaces act as reflectors down the hole and becomes powerful when combined with other available geological datasets.

Mineral exploration often occurs in geological settings with steeply dipping structures and formations. The boreholes are drilled to intersect the lithology normal to its dip, which results in deviated boreholes. Such drilling has implications for the ZVSP illumination area as it becomes possible to image some parts of the media close to the borehole trajectory.

Although ZVSP imaging becomes possible in a deviated borehole, it is not possible due to 2D nature of the survey and the small illumination area to uniquely determine the origin of the reflection points (Greenwood, 2013).

This type of VSP can assist significantly with interpreting the surface seismic collected over complex terrains and can be acquired with minimal equipment (single-level geophone, seismic recorder, cable winch and source).

2.3.2. Offset VSP (2D VSP)

Offset VSP survey geometry incorporates a source placed at an offset from a borehole to form a subsurface 2D image using receivers in the borehole. The image is built along a plane passing through the borehole trajectory and the source location. An increase in offset allows a larger subsurface volume to be imaged, expanding the imaging away from the borehole. Therefore, increased offset allows the identification of major structures and formations away from the borehole.

Single offset VSP has limited illumination, especially in complex terrains. The product is a 2D image of the subsurface that can be constructed by VSP-CDP transformation or migration.

Expansion of imaging areas around a borehole can be achieved by increasing the number of sources/shot locations (multi-offset VSP) at various azimuths. To expand the lateral extend of a 2D image transect and increase its fold, one can introduce sources along a line walking them away from the bore (walkaway VSP). However, these survey options increase the source effort and preferably require more active receivers in the borehole at different depths simultaneously. Therefore, multi-offset and walkaway surveys are time- and equipment-wise consuming and have higher associated costs.

2.3.3. 3D VSP

A three-dimensional VSP survey employs a grid of source locations around a borehole at different azimuths and offsets to regularly illuminate the adjacent subsurface. Such design delivers high-resolution 3D image volumes of media around the borehole, which can be utilised for numerous exploration purposes (targeting, development, high-resolution infill to 3D surface seismic data). The resulting images display geological dips and reflectors and generally have higher resolution than surface seismic data. However, to utilise 3D VSP, it is necessary to use a multi-level borehole tool, which poses an additional logistical risk and cost in an open-hole environment.

This type of survey is expected to benefit most from DAS technology.

2.4. VSP Sensors

Geophones, accelerometers, and hydrophones are conventional sensors used as borehole receivers. In addition to these options, distributed acoustic sensing has been gaining more and more attention in the last decade as a versatile sensor, enabling coverage of the full length of a borehole with receivers at once. However, DAS works fundamentally on a different principle compared to conventional sensors.

The geophones are electro-mechanical sensors that sense the Earth's motion in the form of particle velocity. In contrast, DAS observes a change in elongation of an optical fibre that acts as a sensor.

Therefore, it is reasonable to question whether these systems can obtain the same information about the same physical properties. I address this question in chapter 4, in which I compare the same physical property (strain-rate) collected with DAS and geophone data.

2.5. VSP Imaging

VSP data are recorded in a time-depth domain. VSP-CDP transformation is a procedure to transform a time-depth gather into an offset-depth (CDP domain) image (Wyatt and Wyatt, 1981). These transformed traces start at the receiver depth and extend laterally to the furthest illuminated imaging point. The transformation utilises the velocity model estimated from the P-wave direct arrivals and determines the depth and offset of the reflections arriving after the first arrivals from this velocity and survey geometry. This method is a single-channel process, so events on one trace are mapped independently to events on nearby traces. It is a robust and quick method; however, the main disadvantage is that it assumes horizontal layering and does not handle well complex structures.

For imaging more complex structures, it is more appropriate to use migration. Migration is a process in which the subsurface image is created at the coincident time of direct and reflected wavefield (Claerbout, 1971). There are different migration algorithms depending on what theory (ray or wave theory) they are based on or in which domain (time or depth) they are implemented. For the VSP

application, the migration is typically done in the time domain. The most commonly used algorithm is based on the Kirchhoff integral (Schneider, 1978), which can handle most of the VSP geometries and dip angles (Dillon, 1988). However, its implementation often does not take into account the lateral velocity changes.

Another type of imaging that gains much attention with the development of high computational power is the full-waveform inversion. Full-waveform inversion (FWI) attracts much interest as it produces quite an accurate velocity model often needed for seismic imaging in complex geological environments. This accuracy is achieved by minimising the difference between modelled and field data using least square methods (Tarantola, 1984). It is mainly used for inverting the surface reflection seismic data, where it relies on low frequencies and very large offsets that produce diving waves. However, Charara et al. (1996) showed that due to the rich wavefield information (presence of transmitted, converted, and reflected waves) in VSP datasets, such data are also suitable for the inversion. Furthermore, the FWI can be applied to VSP data collected using geophones as well as distributed acoustic sensors (DAS) (Egorov et al., 2018).

2.6. Conclusions

Borehole seismic method provides valuable in-situ measurements of the propagating seismic energy. Its various configurations can address a multitude of exploration tasks: study the changes in a transmitted wavelet, estimate the attenuation of the seismic signal, determine anisotropy in the area, and obtain a 2D or 3D image of the geological structures around a borehole. Currently, the employment of borehole seismic in mineral exploration is quite limited despite all offered benefits for reasons attributed in this chapter. However, modern developments of new types of sensors, particularly the introduction of distributed fibre optic sensing, dramatically changed the view of VSP in mining and made it an attractive and cost-effective tool for exploring new mineral targets and monitoring operations and infrastructure. Nevertheless, novel technologies such as DAS require more fundamental research before overtaking conventional sensors. In parallel to equipment development, the development of high

computational power allows utilising full-waveform inversion as a powerful imaging tool.

3 Case studies from mineral exploration

In this chapter, I present three case studies related to the VSP application in mineral exploration in which I was actively involved (data acquisition, processing, and interpretation). For each of them, I give a brief geological overview, followed by the goals, results and learnings from the VSP survey. The cases reflect typical commercial ZVSP surveys in mineral exploration in Australia, with an additional DAS field trial added to one of the surveys.

3.1. ZVSP at Darlot Gold mine

3.1.1. Geological setting

The Darlot-Centenary gold deposit is located in the Yandal Greenstone Belt in the Eastern Goldfields Province of the Archean aged Yilgarn craton, region of Western Australia, 900 km north-east of Perth (Foley at el., 2018). This part of the belt comprises lower banded iron formations, extensive basalt and dolerite sills, ultramafic rocks, intermediate to felsic volcanic rocks and variable clastic sedimentary rocks. Gold mineralisation is associated with quartz veins and

alteration halos controlled by major structures and is found in a structurally complex series of faults and folds.

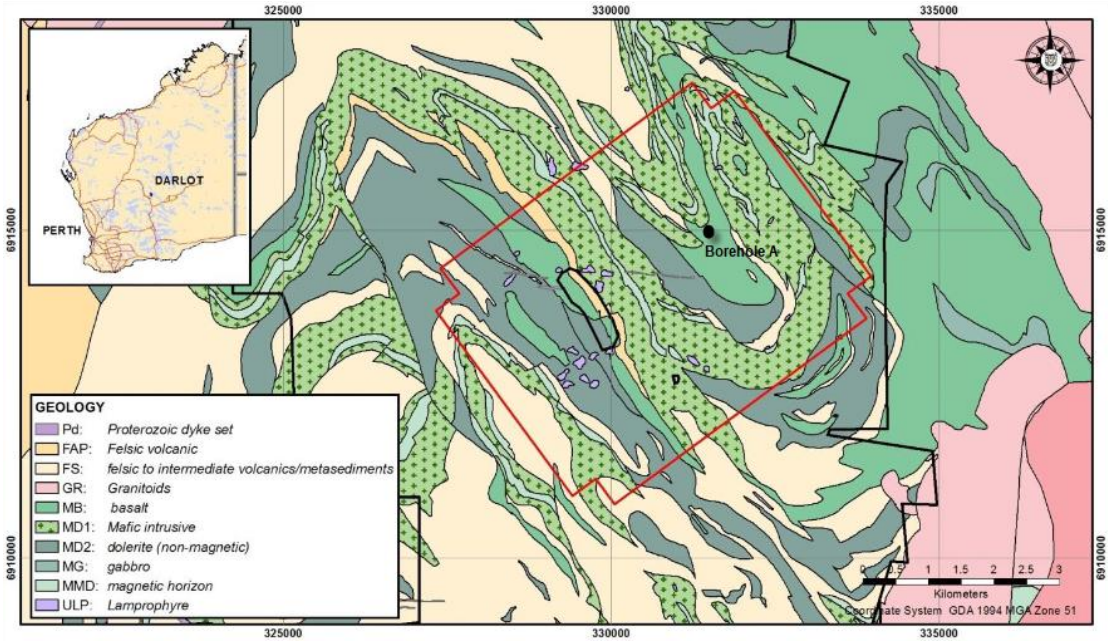

Figure 3-1. Location/geology map for the Darlot Gold mine. The outline of the 3D seismic survey is shown in red. Borehole A is shown as a black circle. (modified after Foley et al., 2018).

3.1.2. Survey details

A detailed surface 3D seismic programme was conducted in late 2016 to map out all potential geological structures that could have been primary controls in locating economic mineralisation (GoldFields, 2016). A borehole seismic program was carried out in early 2017 to measure in-situ velocities and identify which geological interfaces act as reflectors in a surface seismic survey. In this section, I will discuss details related to the borehole seismic program at Borehole A.

Borehole A is located in the north-central section of the survey (Figure 3-1). A plan view of the drillhole is given in **Error! Reference source not found.**. The b orehole is 630 meters deep and deviated, with a maximum inclination of 30 degrees from vertical. The hole was cased through the unconsolidated regolith, from the surface to 107 meters.

The VSP data were acquired with a single component (1C) downhole geophone. The seismic signal was generated by 60,000 lbs AHV vibroseis truck. Acquisition parameters are given in Table 3-1 .

Table 3-1. Acquisition Parameters

VSP Survey Information	
Recording System	ARAM Aries II
Software acquisition	Aries II
Logging cable	4C 1500 m electric winch
Geophone Information	
Downhole tool	1C downhole geophone
Receiver step	5 m
Sweep and listen time	12s + 2s
Sample rate	1 ms
Sweep per receiver	1
Source information	
Source type	60,000 lbs AHV IV
Source sweep	8 – 120 Hz linear sweep
Sweep duration	12 seconds
Tapers	0.3 s
Force	70 %
Source control	Pelton VibPro
Source position	30 m east from borehole collar

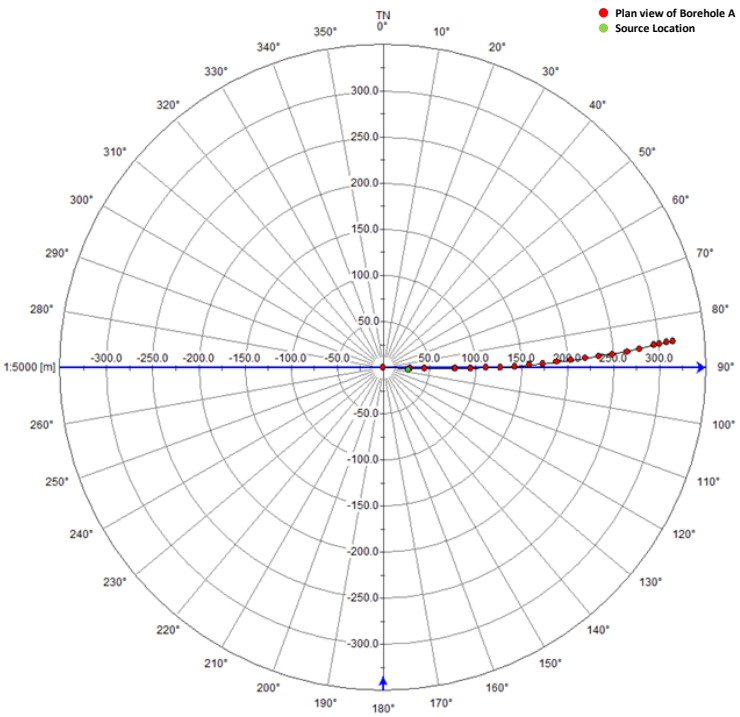

Figure 3-2. Plan view of Borehole A (red dots) with source location (green dot). Distance is in meters.

3.1.3. Data Processing and Interpretation

The processing flow applied to the field VSP dataset involves the following steps: loading data to seismic processing software, correlating with the pilot sweep, assigning the field geometry, editing bad traces, stacking, deconvolution, wavefield separation, building the velocity model and creating the corridor stack. In this case, the reflections appear to have a dip, and after moving to two-way time to create a corridor stack, the reflections did not stack well.

Due to hole deviation, the illumination increases compared to standard ZVSP, with a maximum horizontal offset of 300 meters between source and receiver. Therefore, the migration is performed in addition to the standard ZVSP processing flow.

The full and upgoing wavefields are shown in Figure 3-3, respectively on left and right. The most evident waves on left image are direct (dotted) - and reflected (dashed) P-waves marked in red. The red arrows indicate presence of strong multiples of the direct P-wave, most likely caused by the strong impedance contrast at the geological boundary of overburden and fresh rock. The dotted blue

line refers to direct S-wave. The yellow arrows refer to the primary (dotted) and reflected (dashed) tube waves. After removal of the direct/downgoing wavefield, the upgoing wavefield reveals strong reflections which intersect the borehole (first-break times marked with red dots).The interpretation is carried out by integrating VSP results to other available geophysical and geological logs: P- and S-wave velocities (Vp and Vs, respectively) from the full waveform sonic survey (FWS), specific gravity (SG) measured on core samples, calculated acoustic impedance, lithological log, corridor stack and upgoing wavefield from the VSP (Figure 3-4).

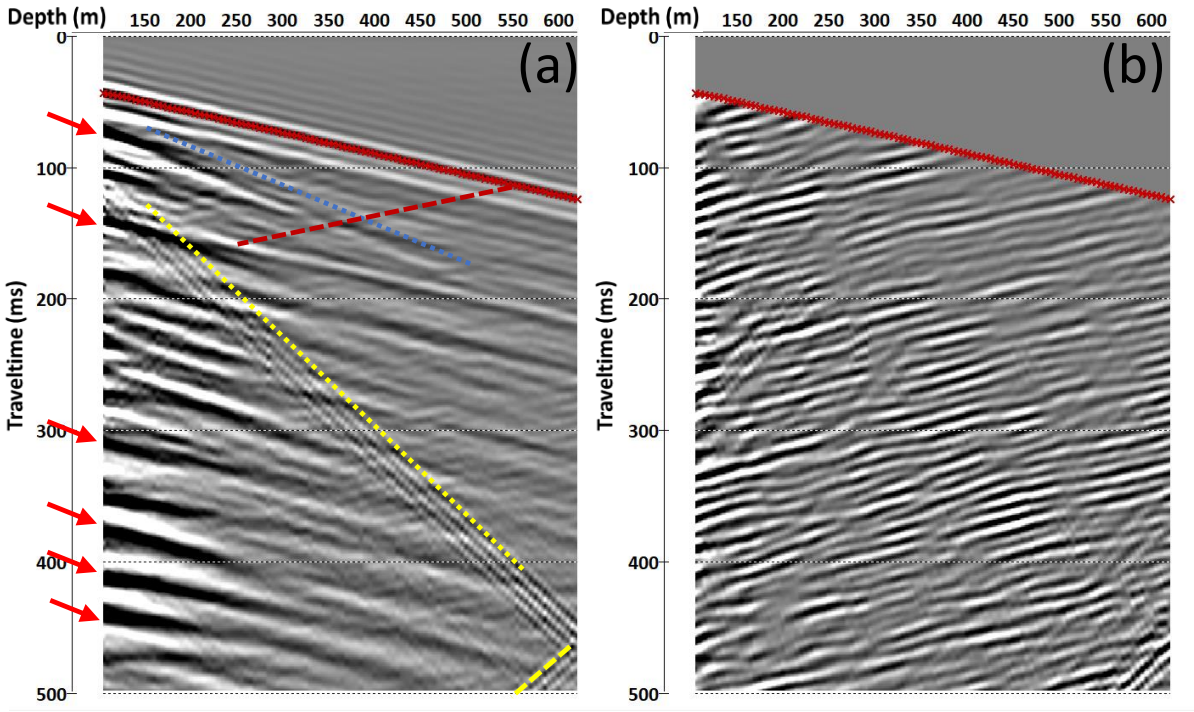

Figure 3-3. Borehole A: (a) Full wavefield and (b) upgoing/reflective wavefield. The red dotted line (picks) is the first-break times of the direct P-wave, while the blue and yellow dotted lines represent direct S- and tube waves. The red dashed line is an example of a reflected P-wave and the dashed yellow of a reflected tube wave. Red arrows indicate multiples of direct P-wave.

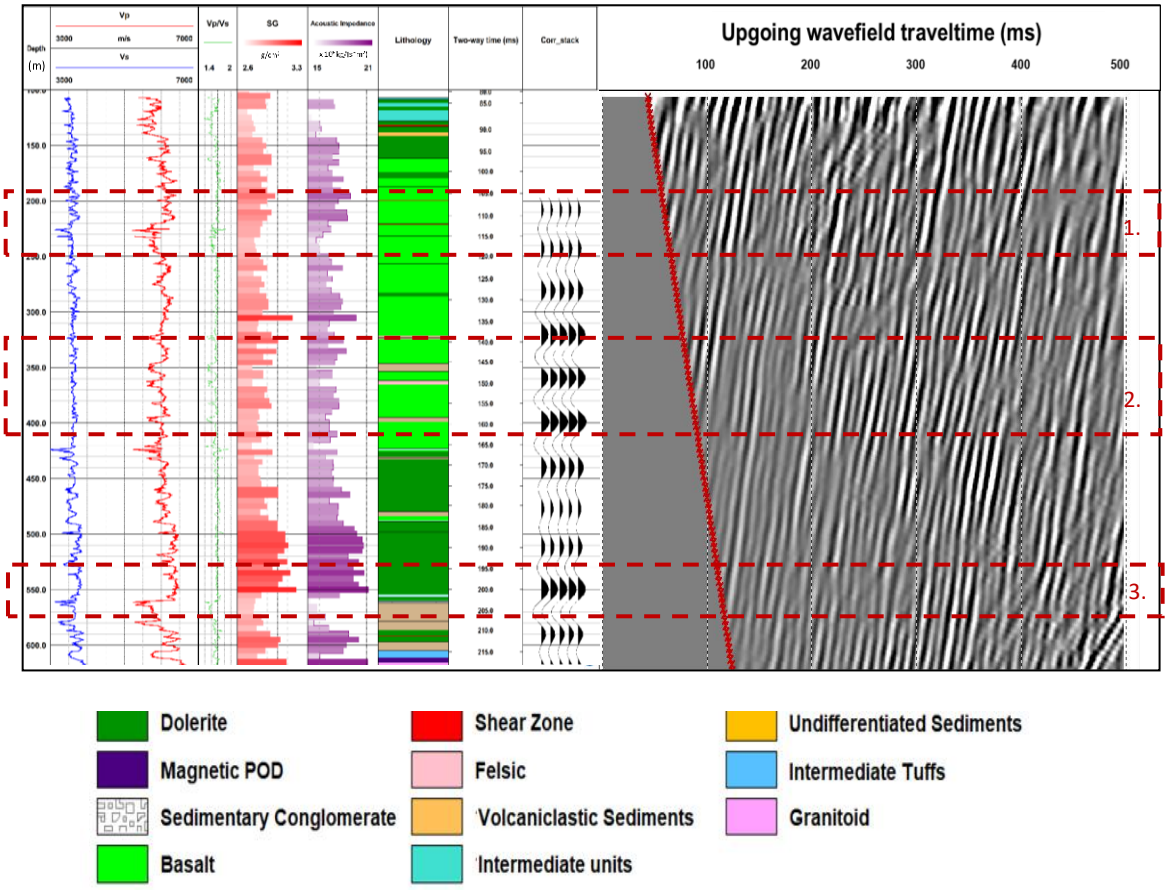

Figure 3-4. Borehole A - Composite plot with a legend below. Major depth intervals (zones) with a good correlation between the logs, lithology and upgoing reflectors are marked with red boxes and numbered 1-3.

The lithological log comprises mainly mafic (green units), such as dolerite and basalt. These units have relatively high velocities (~ 6100 m/s) and, therefore, higher acoustic impedance since the trend of measured specific gravity coincides with velocity trends. Sharp velocity lows within basalt in zone 1 indicate several fractures and faults within mafic units (e.g., at 200 m), which are confirmed by logging and appear reflective in the VSP. The next example of good correlation is zone 2, where metasediments and felsic units occur. These units have relatively lower velocities, and strong reflector correlates to interbedded siltstone and felsic within basalt (e.g. at 350 m). Zone 3 is identified around the most distinctive VSP reflector at a depth of 550 m. This reflective event correlates to the major geological boundary (dolerite/siltstone contact) and, according to logs, it has the greatest acoustic impedance contrast. Migrated VSP data is overlaid against the pre-stack time migrated 3D cube (Figure 3-5). Strong VSP reflections related to the base of dolerite match well with the reflector observed on surface

seismic. The VSP observations, confirmed by geology and surface seismic, can be used to extrapolate reflectors away from the borehole and assist with interpreting other reflectors observed in datasets.

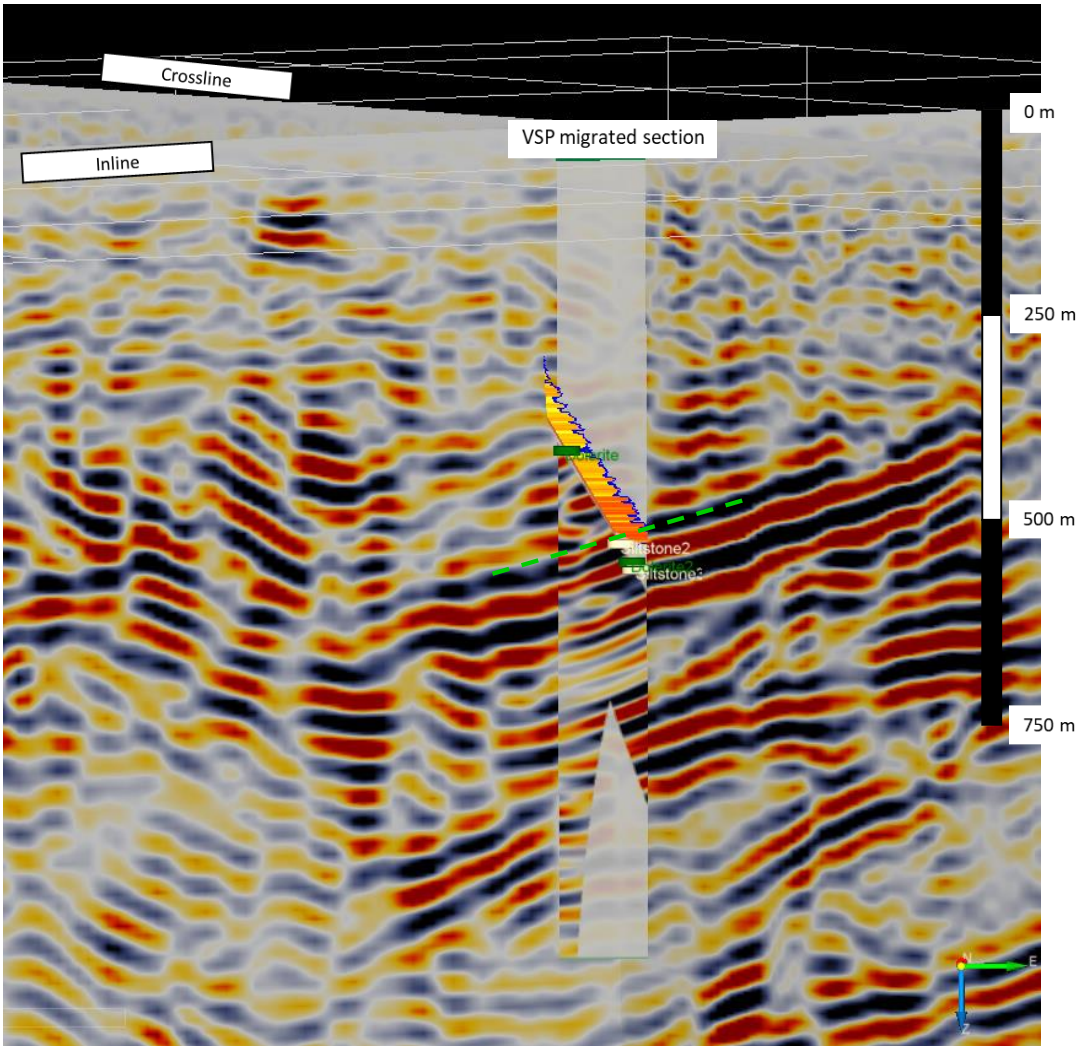

Figure 3-5. Pre-stack time migrated 3D seismic data with the migrated VSP image around borehole A and the P-wave velocity log displayed down the hole trajectory and major lithological markers. The green dashed line shows reflection from the lithological contact of dolerite and siltstone.

3.2. ZVSP at Karari / Carosue Dam Operations

3.2.1. Geological setting

Carosue Dam Operations include the Carosue Dam Project, the Porphyry Project and the Deep South Project. The main deposits (Karari, Dervish) are located along the regional NNW-trending Keith-Kilkenny fault zone within the eastern

edge of the Norseman-Wiluna Greenstone belt. These deposits are controlled both lithologically and structurally. The lithology consists of primarily intermediate felsic volcaniclastic sandstones, intermediate tuffs and intermediate porphyry units intruded by granites of varying composition. Large lamprophyre units are intruded post-mineralisation. The stratigraphy is generally dipping to the east (approx. 60 degrees). Pyrite mineralisation is hosted in broad hematite altered sandstone units (Northern Star Resources, 2021).

3.2.2. Survey details

A borehole seismic programme was conducted in late 2019, with goals to assist surface seismic 2D and 3D programs in mapping the most important mine sequences and overall subsurface architecture. In particular, the objective of the borehole seismic program was to give geological meaning to the observed reflectors and build confidence about the reprocessed pre-stack depth migrated 3D cube. In this section, I will discuss details related to the borehole seismic program at Borehole B.

The borehole B is located in the central section of the survey (Figure 3-6), at the edge of the Whirling Dervish deposit. It is 1620 meters deep and deviated borehole, with a maximum inclination of 40 degrees from vertical. The hole was cased through the unconsolidated regolith, from surface to 105 meters.

The VSP data were acquired with a single component (1C) downhole geophone. The seismic signal was generated by a 60,000 lbs AHV vibroseis truck. Acquisition parameters are given in Table 3-2.

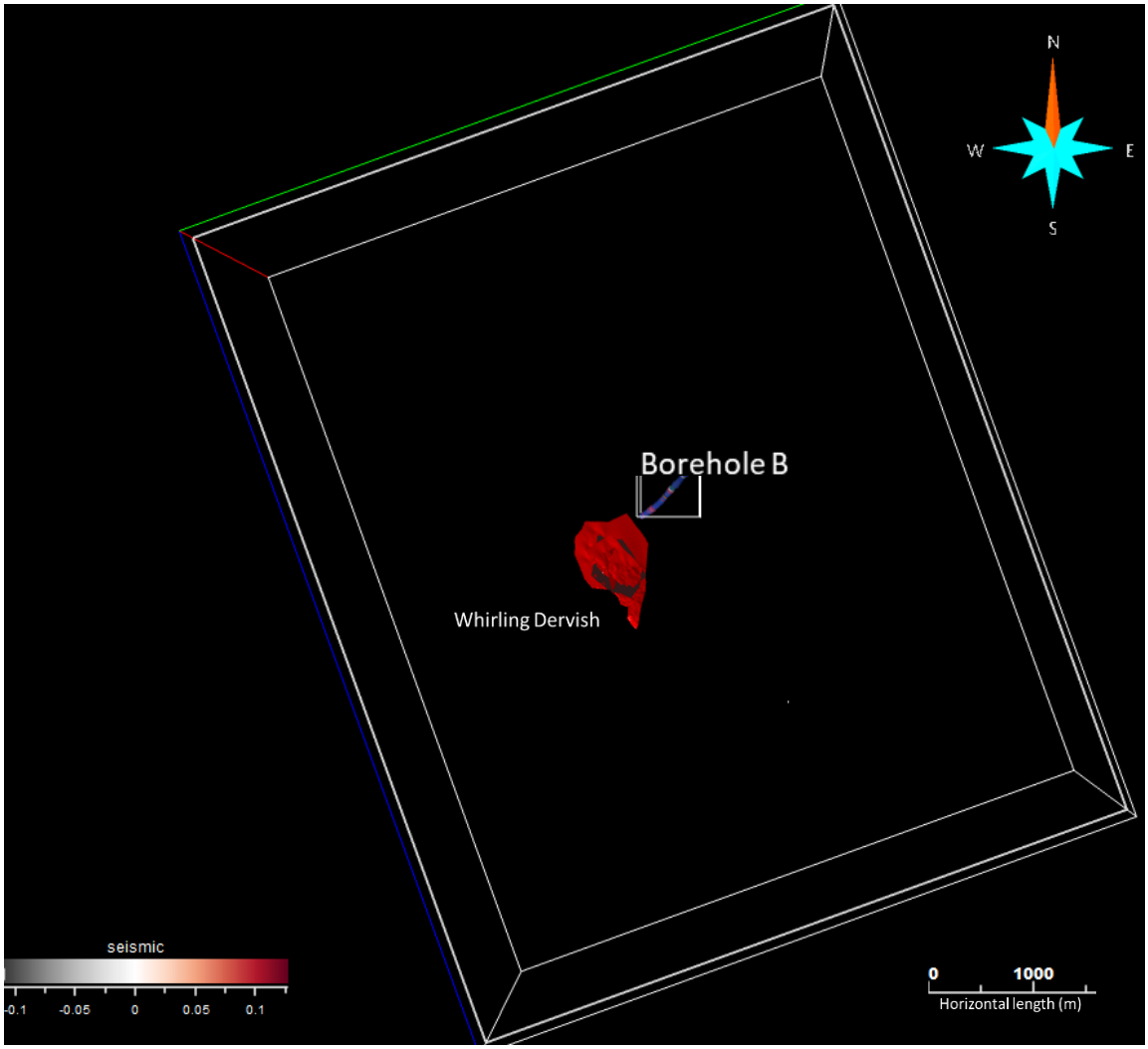

Figure 3-6. Position and plan view of Borehole B in relation to 3D seismic cube boundaries and one of the known mineralisation zones marked in red.

Table 3-2. Acquisition parameters

VSP Survey Information	
Recording System	DAQ IV
Software acquisition	DAQ
Logging cable	4C 2000 m electric winch
Geophone Information	
Downhole tool	1C downhole geophone
Receiver step	5 m
Sweep and listen time	12s + 2s
Sample rate	1 ms
Sweep per receiver	1
Source information	
Source type	60,000 lbs AHV IV
Source sweep	8 - 120 Hz linear sweep
Sweep duration	12 seconds
Tapers	0.3 s
Force	70 %
Source control	Pelton VibPro
Source position	23 m north-east from borehole collar

3.2.3. Data Processing and Interpretation

The processing flow applied to the field VSP dataset involved the following steps: loading data to seismic processing software, correlating with the pilot sweep, assigning the field geometry, editing bad traces, stacking, deconvolution, wavefield separation, building the velocity model and creating the corridor stack. Due to hole deviation, the illumination increases compared to standard ZVSP, with a maximum horizontal offset of 750 meters between source and last receiver. Therefore, the migration was performed in addition to the standard ZVSP processing flow. The full and upgoing wavefields are shown in Figure 3-7.

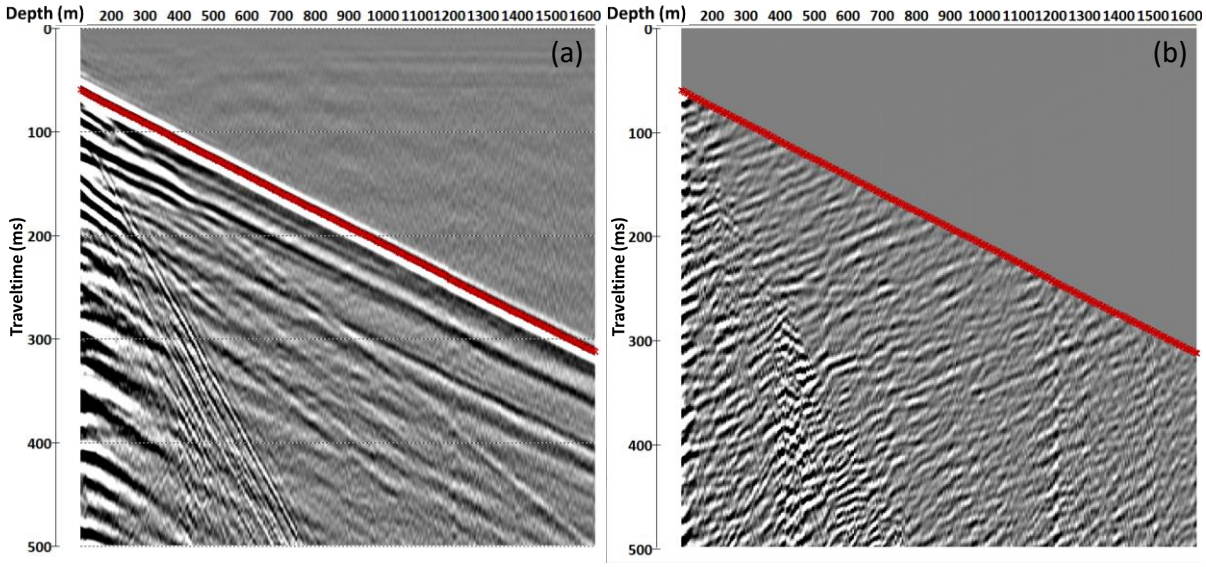

Figure 3-7. Borehole B: (a) Full wavefield and (b) upgoing/reflective wavefield. The red picks are the first-break times.

The upgoing wavefield reveals strong reflections which intersect the borehole (first-break times). The interpretation is carried out by integrating VSP results to other available geophysical and geological logs: P- and S-wave velocities (Vp and Vs, respectively) from the full waveform sonic survey (FWS), specific gravity measured on core samples (SG), calculated acoustic impedance (AI), synthetic seismograms, corridor stack and upgoing wavefield from the VSP, lithological, alteration, and structural logs (Figure 3-8).

The change in velocity and acoustic impedance shows subtle changes within volcaniclastics rocks. The main increase marked as zone 1 is observed around the intruded mafic units at 870 m measured depth. In addition to lithology, it appears that reflectivity is influenced by the textural and structural features/rock deformations observed on the core, such as schistosity, fracturing/faulting, and shearing. The bottom part of the borehole pierces the mineralisation zone (marked as zone 2) and both 3D seismic and VSP show strong reflections and structural complexity originating from that zone.

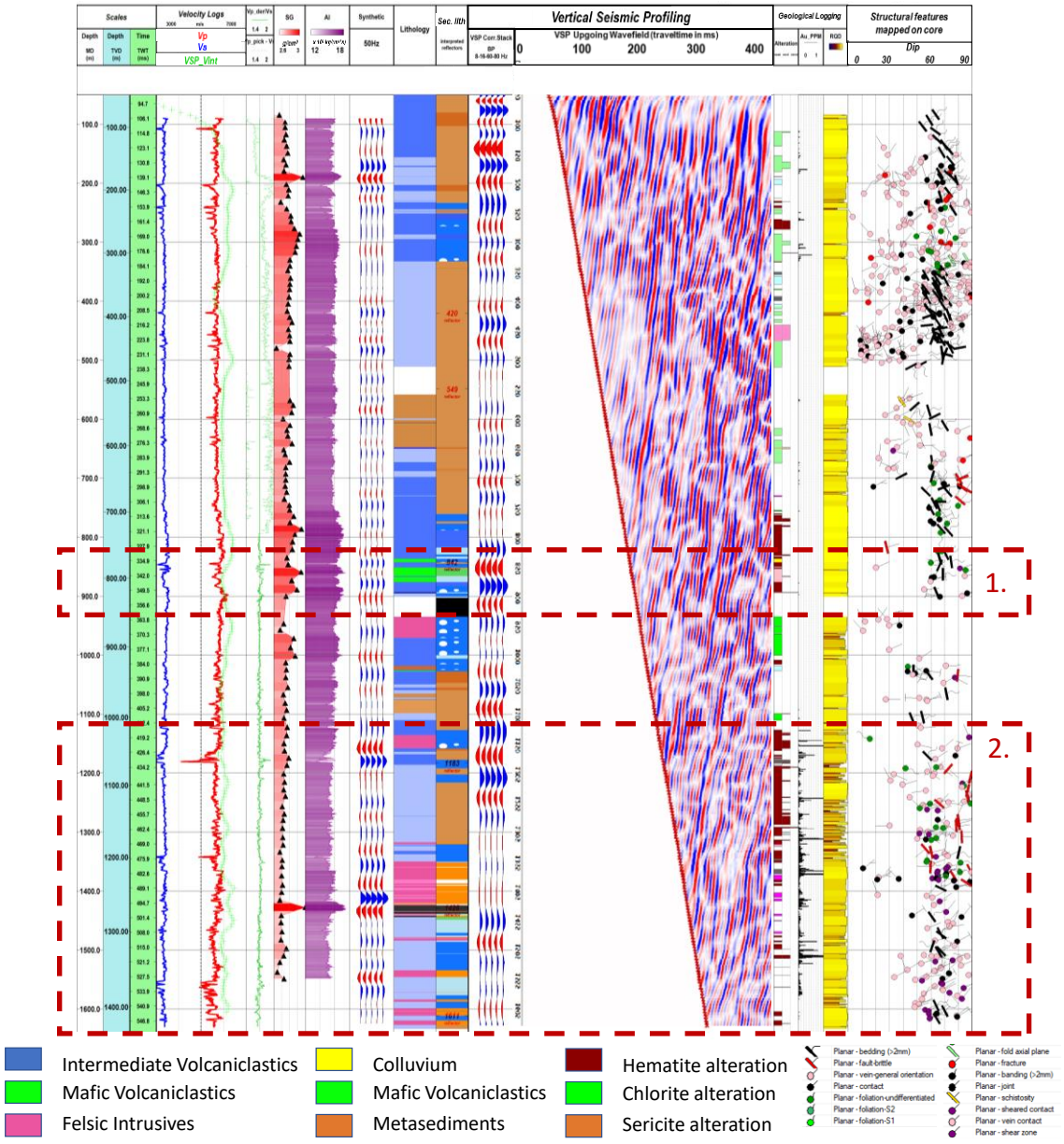

Figure 3-8. Borehole B - composite plot with a legend below.

Migrated VSP image (Figure 3-9) shows rich reflectivity in the zone above the hole trajectory in the second half of the borehole. However, dips of these reflections should be taken as apparent due to the low illumination, particularly with moving away from the borehole trajectory. Compared to 3D surface seismic, the resolution of VSP is much higher and allows better identification of seismic events. This figure indicates that in the case of a proper VSP illumination, as in

the case of a 3D VSP, the mineralised area around the borehole could be imaged at a much higher resolution and tied accurately to the geology.

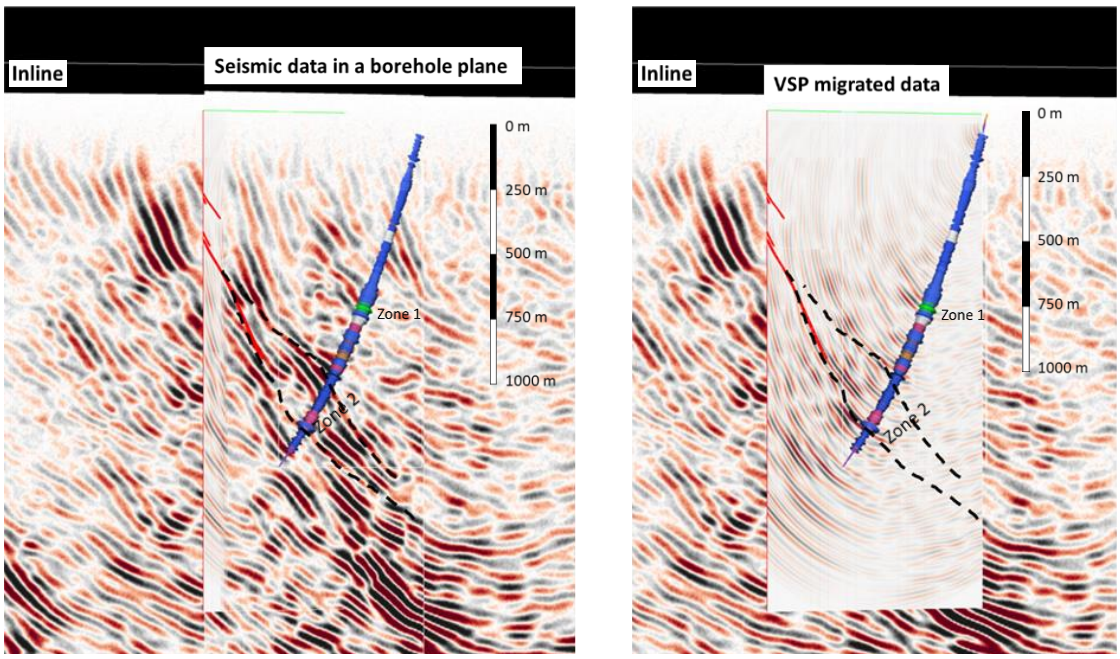

Figure 3-9. Pre-stack depth migrated 3D data with a slice through the Borehole B plane (left) and overlaid migrated VSP data (right). The trajectory is coloured by lithology. Red lines show parts of the mineralised zone, and black dashed lines are interpreted as the dilatation zone.

3.3. ZVSP and DAS deployment experiment at St Ives mine

3.3.1. Geological setting

St Ives mine consists of several underground mine areas and open pits, near Kambalda, in the Eastern Goldfields (WA). It is part of the Norseman-Wiluna Greenstone Belt in Yilgarn Craton, which is bounded by Boulder-Lefroy Fault and Zuleika Shear. The belt comprises abundant tholeiitic and komatiitic volcanic rocks, albitic and sulphidic sedimentary rocks, chert and a chain of discrete felsic volcanic centres. (GoldFields, 2012). The generalised stratigraphic sequence consists of three mafic-ultramafic units, two felsic volcanic units, and an uppermost epiclastic sequence (Steffen et al., 2004). Lithologically, the gold mineralisation is hosted most commonly in dolerites (Defiance, Condenser and Junction dolerite) and structurally is related to fault and shear zones.

3.3.2. Survey details

A borehole seismic program was carried out in early 2018 to measure in-situ velocities and identify which geological interfaces act as reflectors in a surface seismic survey. In this section, I will discuss details related to the borehole seismic program at Borehole C. This hole was part of the research experiment to trial Distributed Acoustic Sensing (DAS) technology, which utilises a fibre optic cable as a downhole seismic receiver, controlled by a surface laser box - interrogator.

The borehole C is located in the eastern part of the survey (Figure 3-10). This is 990 meters deep and deviated borehole, with a maximum inclination of 23 degrees from vertical. However, due to the hole blockage, the bottom 200 meters has not accessible for logging. The hole had a steel casing through the unconsolidated regolith, from surface to 73 meters. The hole diameter changes at 468 m, from HQ (96 mm) to NQ (75.7 mm).

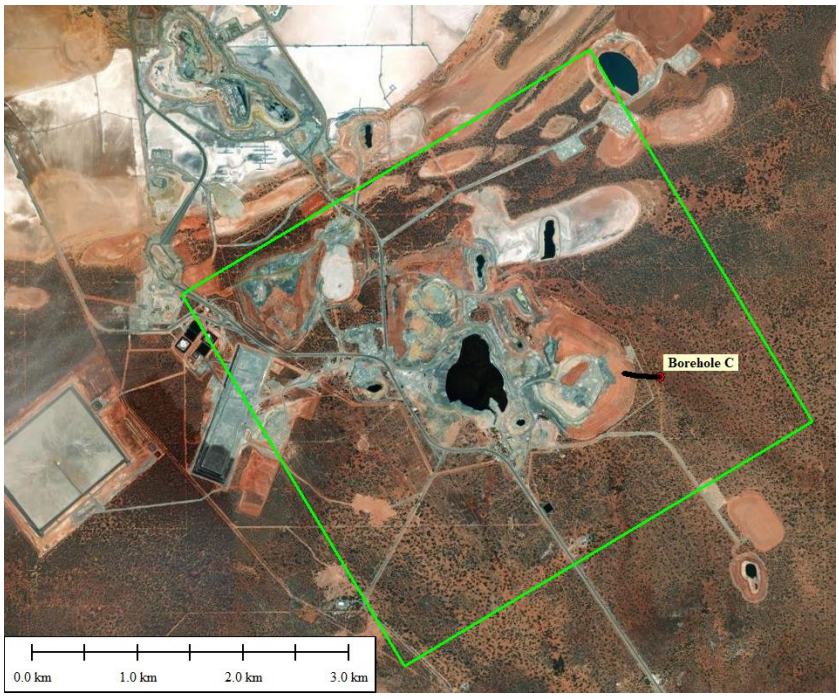

Figure 3-10. Position and plan view of Borehole C in relation to 3D seismic cube boundaries.

The VSP data were acquired with a single component (1C) downhole geophone. The seismic signal was generated by a 60,000 lbs AHV vibroseis truck. Acquisition parameters are given in Table 3-3.

In addition to the conventional VSP survey, DAS data were collected to test deployment with different types of fibre-optic cables. Data were collected by deploying the loose fibre optic cable as a downhole receiver and using the same source (vibroseis) in the same position as for the conventional zero-offset VSP. More details about the experiment are given in section 3.3.4. DAS Experiment.

Table 3-3. Acquisition Parameters

VSP Survey Information	
Recording System	ARAM Aries II
Software acquisition	Aries II
Logging cable	4C 1500 m electric winch
Geophone Information	
Downhole tool	1C downhole geophone
Receiver step	5 m
Sweep and listen time	12s + 2s
Sample rate	1 ms
Sweep per receiver	1
Source information	
Source type	60,000 lbs AHV IV
Source sweep	8 - 120 Hz linear sweep
Sweep duration	12 seconds
Tapers	0.3 s
Force	70 %
Source control	Pelton VibPro
Source position	30 m east from borehole collar

3.3.3. Data Processing and Interpretation

The processing flow applied to the field geophone VSP dataset involved the following steps: loading data to seismic processing software, correlating with the pilot sweep, assigning the field geometry, editing bad traces, stacking, deconvolution, wavefield separation, building the velocity model and creating the corridor stack. Due to hole deviation, the illumination is increased compared to standard ZVSP, with a maximum horizontal offset of 250 meters between source and last receiver. Therefore, the migration was performed in addition to the standard ZVSP processing flow. The full and upgoing wavefields are shown in Figure 3-11.

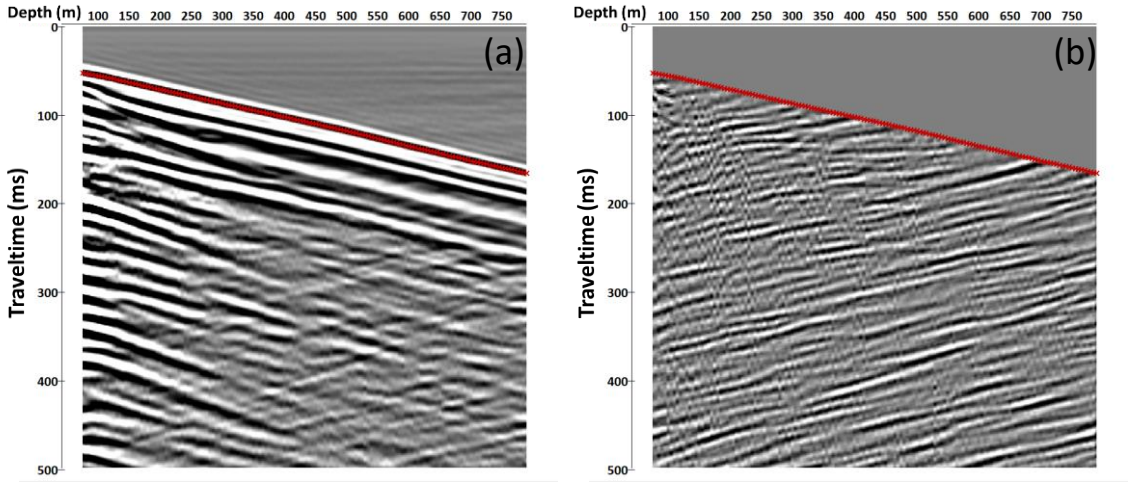

Figure 3-11. Borehole C: (a) Full wavefield and (b) upgoing/reflective wavefield. The red picks are the first-break times.

The upgoing wavefield reveals strong reflections which intersect the borehole (first-break times). The interpretation is carried out by integrating VSP results to other available geophysical and geological logs: P- and S-wave velocities (Vp and Vs, respectively) from the full waveform sonic survey (FWS), specific gravity measured on core samples (SG), calculated acoustic impedance (AI), synthetic seismograms, corridor stack and upgoing wavefield from the VSP, lithological, alteration, and structural logs (Figure 3-12).

The measured physical properties, both velocity and specific gravity, clearly distinguish between the mafic units on one side (green lithological units on the composite plot) and the felsic intrusive, volcanoclastic and metasediments on the other side. The velocities measured by the FWS are in excellent agreement with

the velocities measured by the VSP. However, when in-situ measured velocities (both FWS and VSP) were compared to those measured on core samples drilled several years ago, a discrepancy was observed in every dataset, particularly within the deeper mafic units. There are several potential reasons for the discrepancy, such as the dispersion of seismic velocity due to different frequencies used by VSP, FWS and core (lab) measurements. Secondary porosity increased due to atmospheric conditions can also influence discrepancy. In the hardrock environment, the core can often be strongly foliated, as in this case, or altered (as seen in Malehmir at el., 2013), and often is both. Therefore, the interpretation of rock properties from core measurement should be done with caution for seismic purposes. If numerous in-situ measurements are difficult to get, an example of good practice would be to get at least FWS data from one drillhole within the representative geology and validate against core velocities before the interpretation. Understanding physical properties is of great value for successful seismic interpretation.

The mafic units have the highest acoustic impedance values; therefore, this interface should act as a reflector when the other lithological units are in contact. In some cases, these contacts can be used as marker horizons to interpret 3D seismic data. The second reflector type correlates to the structural features as faults and shear zones. The intense foliation and alteration often characterise these zones (e.g., at 400 m depth in Figure 3-12), which can lower the velocity, hence the acoustic impedance. The structures, by their nature, often coincide with lithologic/stratigraphic boundaries, which affects the overall reflectivity.

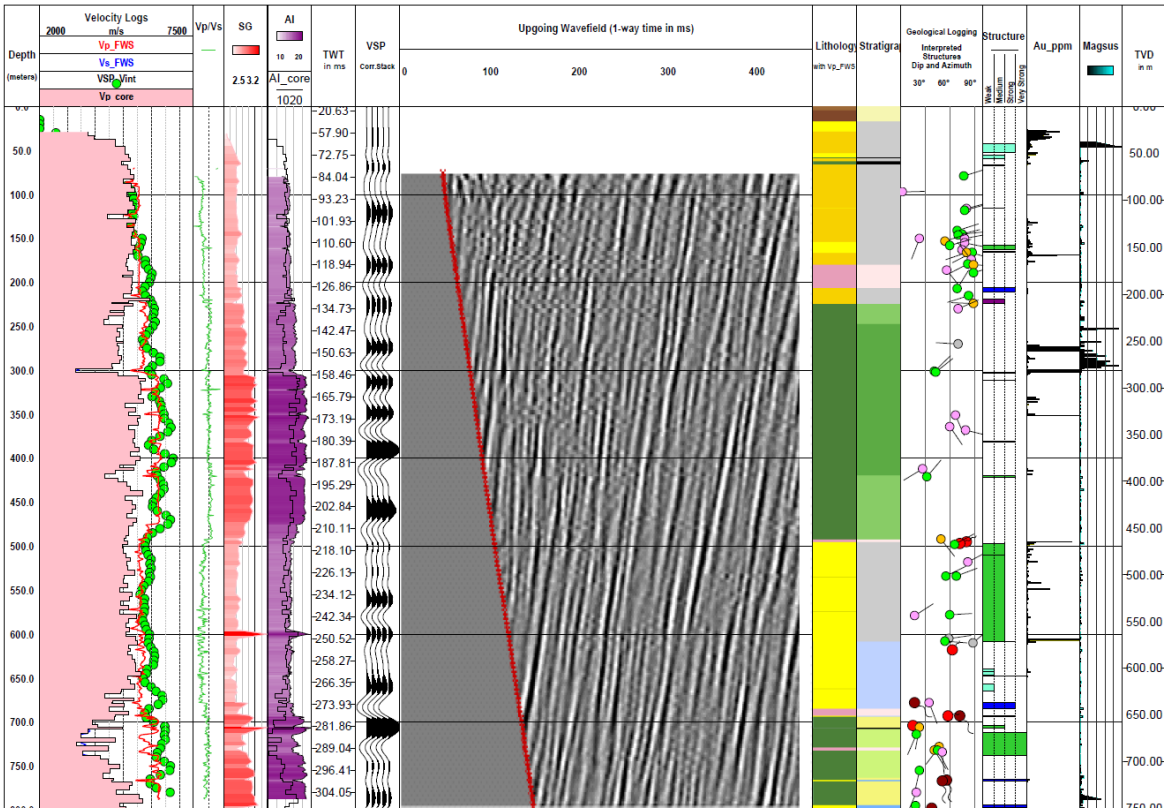

Lithology

- Meta sediments
- Mafics
- Felsics

Stratigraphy

- Black Flag Beds
- Condenser Dolerite 2
- Condenser Dolerite 3
- Paringa Basalt
- Defiance Dolerite
- Blag Flag Beds Felsic conglomerate

Structure

- TL - Foliation Unclassified
- SH - Shear
- TR - Fracture
- FOC - Fold Unclassified
- BC - Breccia Crackle
- TF - Fault
- JO - Joint
- CL - Cleavage
- MY - Mylonite
- FY - Fold Asymmetrical
- BU - Breccia Unclassified

- TL - Foliation Unclassified
- SF - Foliation with shear fabric
- LI - Lineation
- IC - Intrusive Contact
- SC - Sheared Contact
- CL - Cleavage
- IV - Irregular Vein
- JO - Joint
- VN - vein
- SH - Shear
- TF - Fault
- BD - Bedding
- RC - Sharp Contact
- LC - Chilled Contact
- DC - Diffuse Contact
- WC - Wavy/Irregular Contact

Figure 3-12. Composite plot for Borehole C

3.3.4. DAS Experiment

One of the DAS experiment objectives was to test the affordable deployment of several widely available fibre-optic (FO) cables. The time available for the experiment was limited by a short time window between two commercial borehole logging works.

There are several methods for deploying a FO cable down the hole. The FO cables can be cemented behind the casing or inserted inside the casing and are conventional deployment types in hydrocarbon exploration (Hartog, 2017). However, the cementation of any downhole cable in mineral exploration is not common. Therefore, it seemed obvious to trial a free-floating cable suspended in the well based on successful trials of this deployment type (Correa et al., 2017b; Bona and Pevzner, 2018). Furthermore, compared to cementation, free-floating cable deployment is relatively simple and inexpensive.

Three different fibre-optic cables were trialled: a special-order single-mode helically wound loose tube cable with 30 degrees pitch, a single-mode 72 fibre (72F) stranded loose tube cable, and a single-mode tight buffer cable. The helical cable was deployed only to 235 m depth since it did not sink further due to its buoyant coating. The other two cable types were deployed to 800 meters. Due to their light weights, the deployment of tight buffer fibre-optic cables required additional weight at the cable bottom (Figure 3-13). Nevertheless, the deployment was relatively simple, and the acquisition was significantly faster (10 times) to geophone ZVSP.

The Helios Theta interrogator, made by Fotech Solutions, was used to record the data. The gauge and pulse lengths were 7.5 m and 2.5 m, respectively, with a channel spacing of ~ 0.7 m.

Figure 3-13. Details from the field experiment – tight buffer FO cable deployment.

One of the challenges related to DAS acquisition is depth uncertainty (Verliac et al., 2015; Correa, 2017b; Mateeva et al., 2021). The uncertainty arose from the fact that, in general, most DAS systems require fibre optic cable to be mapped. The mapping is achieved by defining the depth of the two beginning and ending points, and all the channels are then linearly interpolated as per defined recording parameters. This calculation depends on factors like the physical parameters of the mud (temperature, pressure), the refractive index of the cable and its axial strain, etc. (Verliac et al., 2015). Such depth determination differs from the depth determination in standard wireline operations, where depth is usually determined by the wireline encoder and the gamma-ray log. Therefore, considering that different types of cables were deployed during this experiment and challenges

related to the depth calibration, I choose to show the DAS data in the channel domain, followed by an estimated depth taken from the geophone data. Additionally, all three cables were longer than the length of the drillhole, so during the acquisition, the extra cable was left coiled to the stationary cable reel, close to the drillhole and recording truck. Therefore, the first 100+ channels in the following figures are DAS channels which are still coiled on the cable reel, and therefore every trace is alike.

A single-shot and stack of eight shots DAS correlated seismogram collected with a tight buffer FO cable are shown in Figure 3-14. The channels from the reel are marked in the orange box. The strongest recorded events are induced tube waves, marked in dotted and dashed yellow, for downgoing and upgoing waves, respectively. A hint of the P-wave is present only below channel 2500, which corresponds to 470 m depth, where a change of diameter is reported. The dashed red line shows the expected arrival of a direct P-wave; however, the strong P-wave amplitudes are absent. The absence of the P-wave could be due to having too much tension on a cable.

To better understand drillhole conditions and DAS data, I looked at raw FWS waveforms from different outputs/modes. An example of the raw FWS data from the same drillhole is given in Figure 3-15 for the depth interval from 319 m to 330 m. FWS data are collected with the ALT QL40-FWS tool, which has a broadband ceramic-piezoelectric transducer. The transducer excites the formation in a way that waves of different frequencies are developed and propagated. The different frequencies are useful to create different outputs, which can enhance the identification of various wave propagation modes (P-, S-, tube waves) and perform analysis such as fracture or cement bond analysis, permeability index, etc. From the raw FWS data, I selected “WideBand” and “Chevron” outputs/modes, as these are preferred outputs for velocity analysis and fracture analysis, respectively (ALT, 2014). The origins of observed tube waves, channels 1980 (depth ~ 140 m) and 2250 (depth ~ 325 m), correlate strongly to the fractures observed in both “WideBand” and “Chevron” modes of raw FWS data (Figure 3-15); which confirms the source of induced tube waves. “WideBand” dataset was used to determine P- and S-wave sonic velocities. An indication of

the P-wave is slightly increased with an increased source effort, but only below channel 2250, which correlates to a reduction of hole diameter. It remained unclear why P-wave was not recorded with DAS. Potential reasons may be related to the cable tension, fractures presence in the vicinity of the cable and a change in diameter.

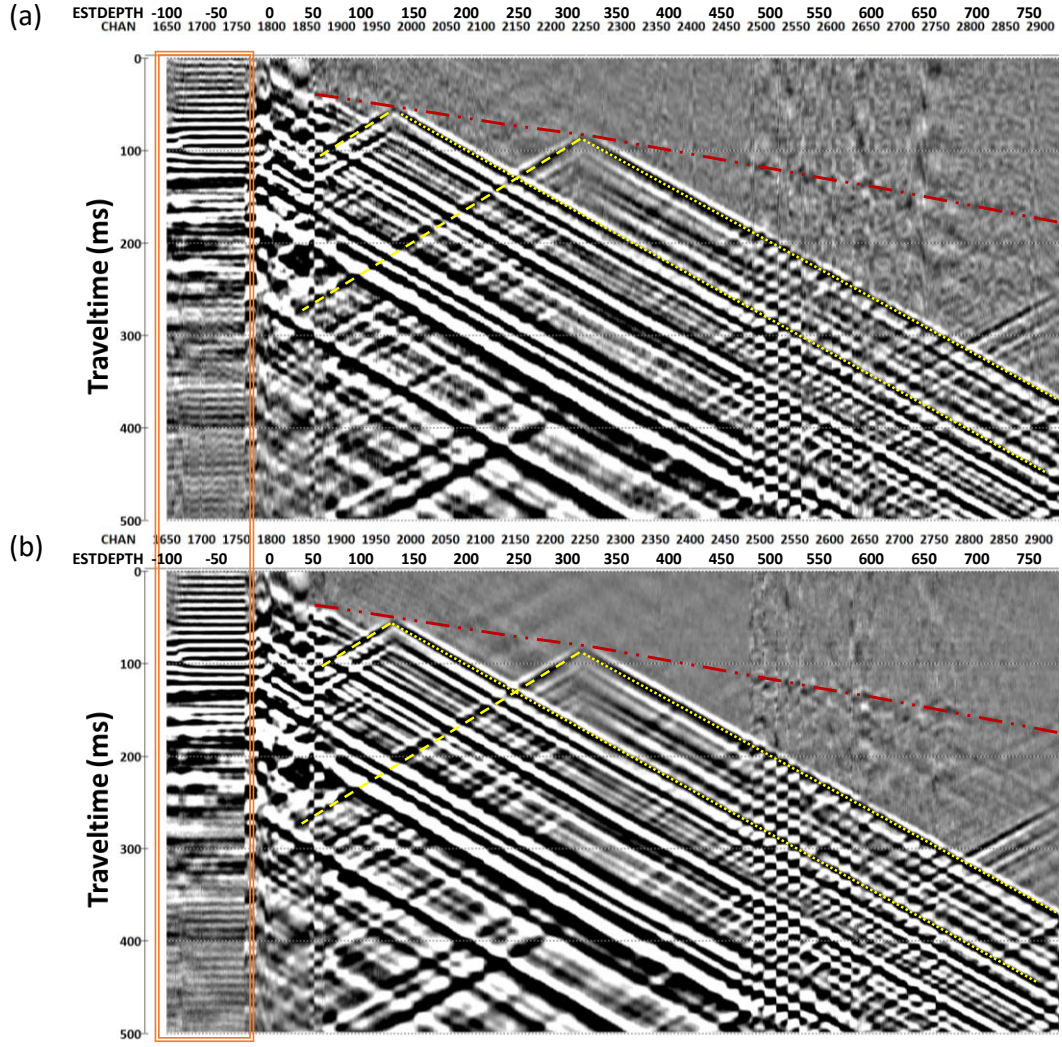

Figure 3-14. a) Single-shot -, b) stack of 8 shots correlated DAS seismograms recorded with a tight-buffer fibre-optic cable. The orange box shows DAS channels coiled on the reel. Induced tube waves are shown in yellow, and the expected arrival of the P-wave is shown in red (estimated from the geophone dataset). A different character of traces below 470 correlates to a reduction of hole diameter.

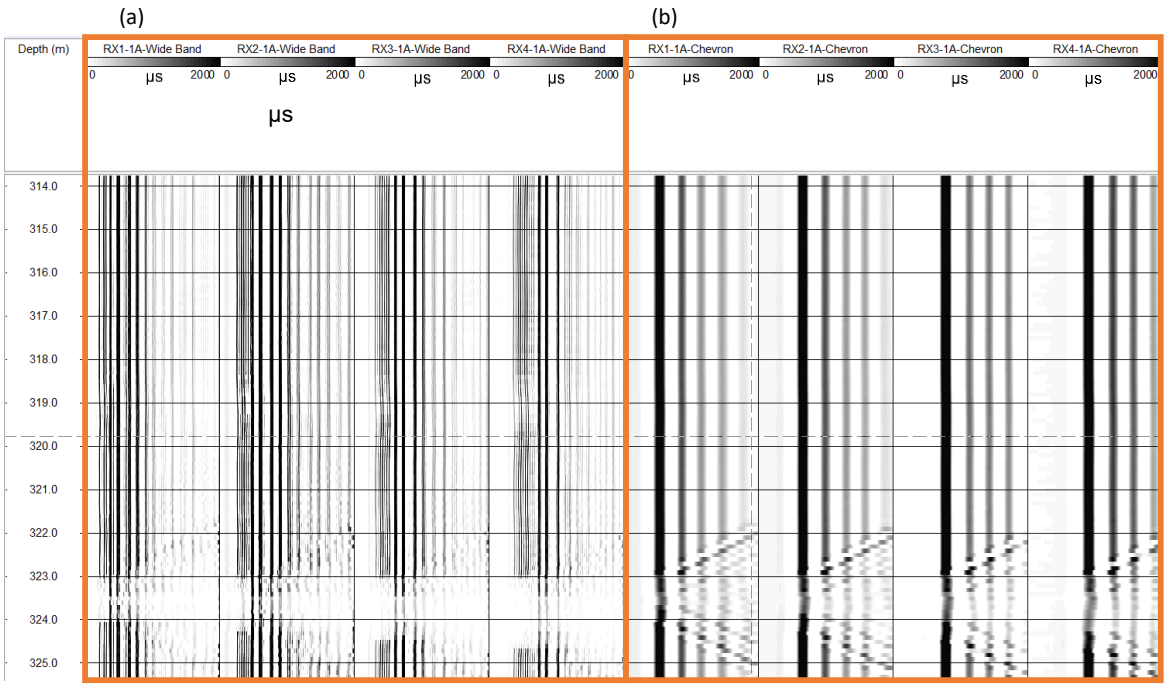

Figure 3-15. Example of full-waveform sonic data collected by four receivers, shown in two modes: (a) WideBand and (b) Chevron, for depth interval 320 – 330 m. The vertical scale is depth in meters, and the horizontal is time in microseconds.

The same acquisition parameters were used to collect data with a 72F cable. A single-shot and stack of two shots DAS correlated seismograms are shown in Figure 3-16. The first break times (red line) from geophone measurements are laid over the DAS measurements to confirm the depth calibration. The strong tube waves are also present, similar to those observed in Figure 3-14. The P-wave is slightly better captured with this cable; however, its absence is observed from 290 m – 460 m. This depth interval corresponds to the high-velocity dolerite zone. The P-wave can be observed below the high-velocity dolerite zone, where a reduction of hole diameter is reported.

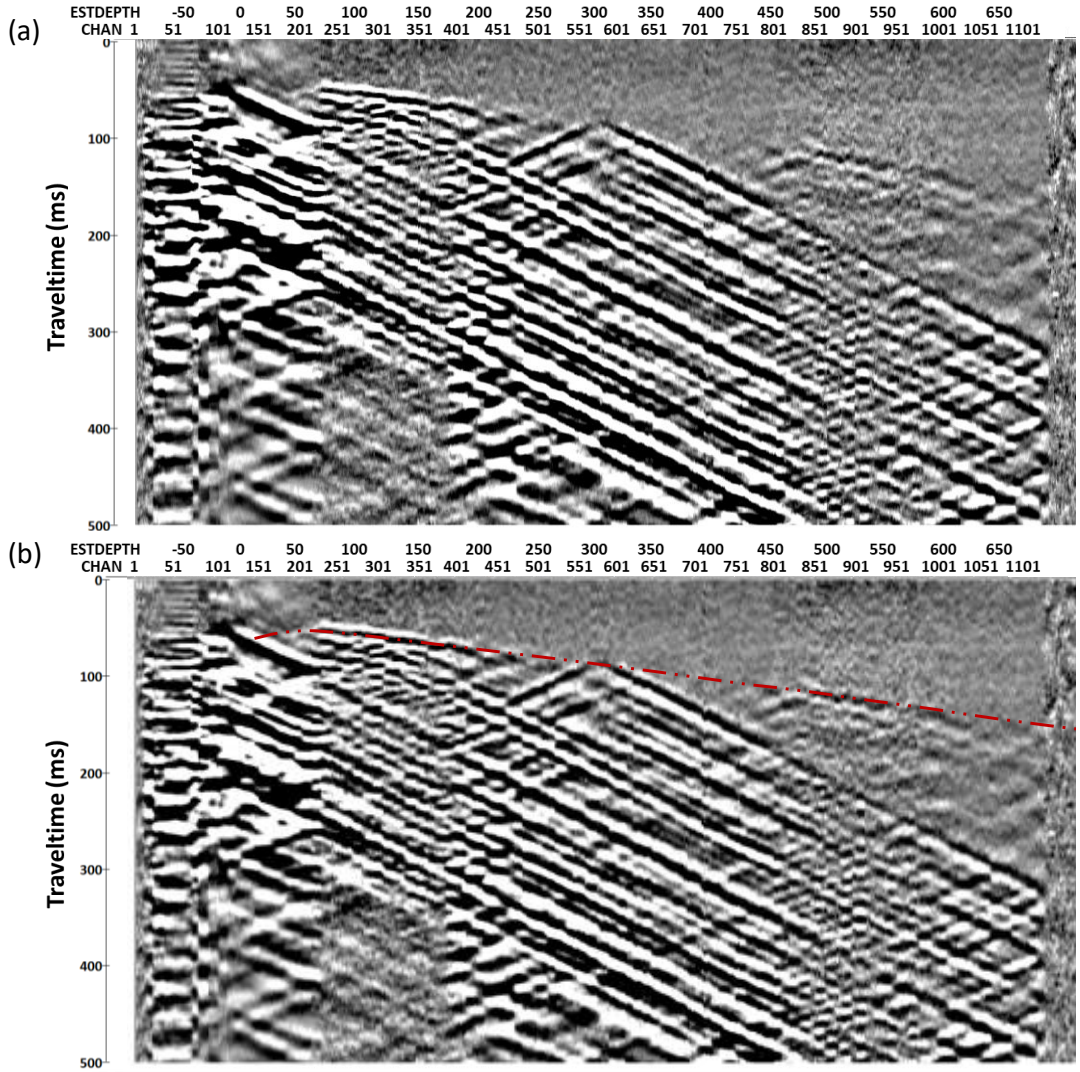

Figure 3-16. a) Single-shot -, b) stack of two shots correlated DAS seismograms recorded with a single-mode 72F cable. The red crosses are the first-break times from the geophone measurements.

In addition to these two straight cables, a helical cable was also trialled. Deployment of the helical cable was more challenging than the other two cables due to a larger diameter. Moreover, the coating of the cable had buoyant properties, which increased the deployment challenge since the groundwater was naturally present in the drillhole. The cable was deployed only to 235 m depth since it did not sink further due to its coating. Data collected with a helical cable are shown in Figure 3-17. Similar to the previous cases, the strongest events on seismic gathers are caused by tube waves (marked in yellow), with a glimpse of the P-wave present in stacked sections.

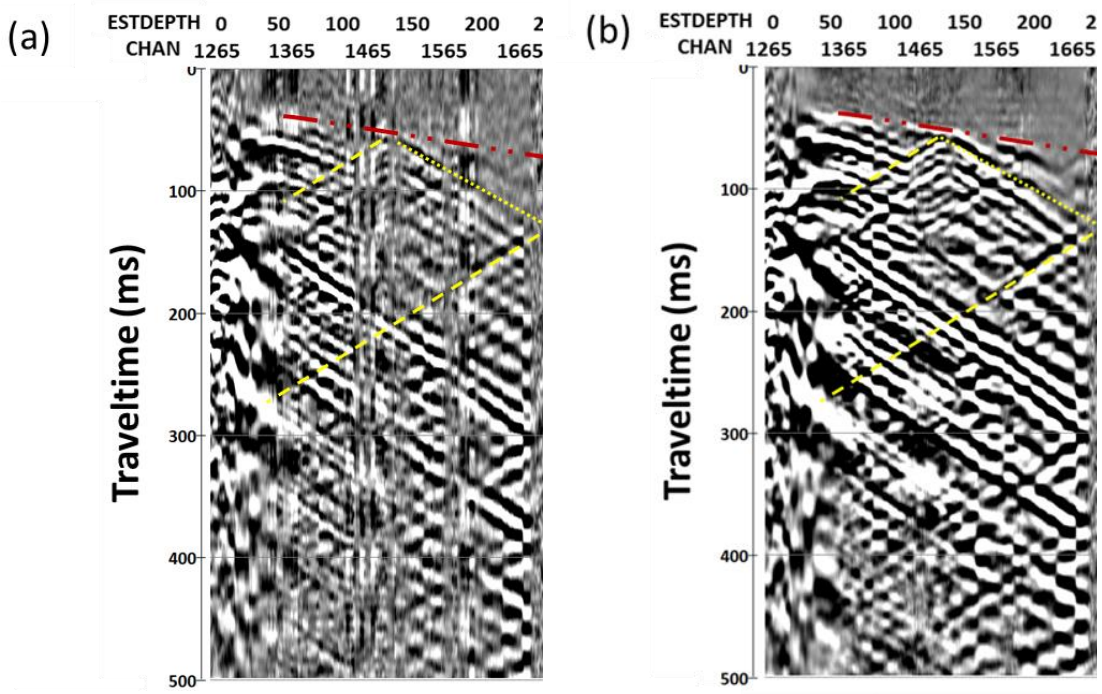

Figure 3-17. a) Single-shot -, b) stack of eight shots correlated DAS seismograms recorded with a single-mode helically wound loose tube cable with 30 degrees pitch. Induced tube waves are shown in yellow, and the expected arrival of the P-wave is shown in red (estimated from the geophone dataset).

In this DAS experiment, none of the cables successfully captured the P-wave energy. Major differences to previously reported successful cases with a free-floating cable suspended in the hole were:

- an open-hole environment (non-cased drillhole) with changing diameter;

- the hole was deviated and filled with groundwater.

Strong tube waves dominated the recorded data. Therefore, a cable coupling in the abovementioned environment could be unsuitable for capturing the P-wave. Furthermore, a different character of tube waves can be observed below the diameter reduction. In future experiments, the tube waves could be potentially suppressed by adding the viscosifiers to the mud, which Greenwood (2013) suggested for similar hydrophone VSP acquisition problems. Besides the coupling and tube waves, the acquisition system and recording parameters were also different than in successful cases. More field DAS experiments are needed to understand how these factors affect the data.

3.4. Conclusions

All presented VSP cases from the three hard rock settings show rich reflectivity, which is often questioned due to the low reflection coefficient in this type of environment. These cases support that the seismic reflectivity is controlled by the contrast of the acoustic impedance, which is strongly affected by numerous structural and textural features. The structural-textural features like shears, faults, foliation, bedding, fracturing, etc., often indicate a zone of significant change or interest within mineral deposits, and their imaging is important for exploration.

Comparison of velocity measurements collected in-situ (borehole) and on rock samples (core) at atmospheric conditions shows a great discrepancy, particularly within strongly foliated dolerite units. The dispersion of seismic velocity can explain this discrepancy due to the different frequency content of VSP, FWS and ultrasonic (core) measurements and the increased secondary porosity of rock samples. The latter is very common, with the core exposed to surface/atmospheric conditions for extended periods. Therefore, interpretation of rock properties from core measurement should be done with caution for seismic purposes and only if wireline measurements are not available. Validation of core velocities against in-situ velocity is recommended.

The VSP survey must be acquired in a 3D recording geometry to accurately image the complex subsurface features. Novel technologies, such as DAS allow for 3D VSP geometry to be collected significantly shorter and at a much lower risk than 3D VSP acquisition with conventional equipment. The DAS trial at St Ives shows that deploying the cable and collecting the data can be done in a matter of hours, but it also shows there are DAS-specific challenges that need to be addressed. For example, a variable presence of a P-wave indicates that the cable tension has an important role in such a deployment. Also, the absence of a P-wave in a high-velocity layer (6500 m/s) indicates that physical properties may greatly be important when selecting the acquisition parameters.

A good understanding of a novel technology is best achieved in a controlled environment at designated test sites that can allow for the repetition of the experiment using different parameters and sensors in stable conditions. Once the technology is well understood in such conditions, DAS VSP surveys should

become a routine during a seismic program in mineral exploration. Furthermore, unique VSP characteristics allow the reflections to be correlated to known geological features with great confidence and depth accuracy and be used to control the time-depth conversion of surface seismic. Therefore, their contribution to understanding and imaging the mineral systems is of great value.

4 Understanding DAS at designated field laboratory GeoLab / Comparison of Amplitude Measurements on Borehole Geophone and DAS Data

This chapter is based on material submitted in a form of a manuscript for Journal of Applied Geophysics. The manuscript title is “Comparison of Amplitude Measurements on Borehole Geophone and DAS Data”, and at the time of thesis publication is in phase “Under Review”. The manuscript is written in collaboration with Evgenii Sidenko, Alexey Yurikov, Konstantin Tertyshnikov, Andrej Bona, and Roman Pevzner.

The chapter also uses material from the following publications:

> Zulic, S., Tertyshnikov, K., Yurikov, A., Sidenko, E., Isaenkov, R., Pevzner, R. (2020). *Curtin Geolab Research Facility: Walkaway VSP with DAS and Geophones* [Paper presentation] EAGE Workshop on Fiber Optic Sensing for Energy Applications in Asia Pacific ;
>
> Zulic, S., Sidenko, E., Yurikov, A., Tertyshnikov, K., Bona, A., Pevzner, R. (2021). *Comparison of Amplitude Measurements on Borehole Geophone and DAS Data* [Paper presentation] AGU Fall Meeting 2021 .

As most of the chapter’s content is based on a collaborative work, I use the first-person plural narrative to acknowledge my collaborators. Particularly, my involvement was in data processing, analysis and writing.

4.1. Introduction

The rapid uptake of distributed acoustic sensing (DAS) for borehole seismic acquisition prompts fundamental research to identify how its performance compares to the performance of conventional borehole geophone sensors.

These two types of sensors, DAS and geophones, are fundamentally different. The geophones are electro-mechanical sensors that sense the motion of the earth in the form of particle velocity. In contrast, DAS observes a change in elongation of the optical fibre that acts as a sensor. The geophone consists of a permanent magnet mounted on a spring with a conductor (copper wire or coil) around it. When the earth moves, the magnet and coil also move. This movement generates a voltage across the coil's winding, which is proportional to the rate at which the coil cuts the magnetic flux, that is, to the velocity of the earth's motion (Evenden and Stone, 1971). In the case of a borehole geophone, the geophone is mounted inside a downhole probe's housing, suspended in the borehole by an armoured cable and clamped to the formation at each desired depth. DAS utilises a fibre-optic (FO) cable, along which the interrogator unit (IU) emits a light pulse and registers how the phase of the backscattered light changes over time in sampling points (Parker et al., 2014). The change in phase of backscattered light is proportional to the fibre deformation caused by the earth's motion. Although there is no standard for a DAS system in terms of its generic architecture, in summary, DAS measurements are said to be proportional to the average strain or strain rate between two sampling points separated by a gauge length.

For borehole seismic measurements, a fibre-optic sensing cable is deployed in the well. Borehole geophones and DAS have different factors that affect the measured signal. For example, the geophone measurements are affected by the geophone type and its performance, probe's housing, the quality of the probe's coupling to the formation or the casing, etc. (Gal'perin, 1985; Hardage 1985). The DAS measurements are affected by the cable design, the cable's coupling to the formation, optical parameters, the interrogator design, etc. (Mateeva et al., 2014; Parker et al., 2014; Schilke et al., 2016; Correa et al., 2017; Dean et al., 2017; Pevzner at al., 2018a; Sidenko et al., 2021). Therefore, it is reasonable to question whether these systems can obtain the same information about the same physical properties.

Initial DAS tests for borehole seismic application used preinstalled cables behind the casing or on tubing inside the casing and demonstrated that seismic energy could be detected on FO cable at a depth over 4 km (Mestayer et al., 2011;

Barberan et al., 2012; Mateeva et al., 2012). Daley et al. (2013) showed a variety of DAS deployment and acquisition possibilities, in which data quality varied significantly depending on these. Mateeva et al. (2014) qualitatively compared geophone to DAS and concluded that DAS polarity is independent of the wave propagation direction and that while transmitted waves have the same polarity as on geophone dataset, the reflected DAS waves have opposite polarity to reflections on geophone dataset. Dean et al. (2015) attempt to clarify the nature of DAS measurements, and on examples from synthetic and real data, they show their DAS system measure instantaneous strain and that the time derivative of strain (the strain rate) is proportional to the average velocity measured at all points along the gauge length. In addition to this, they showed that DAS has highly complex directionality that is dependable on wavenumber and angle of incidence. Correa et al. (2017a) compared seismic data obtained by DAS and conventional borehole seismic sensors to understand DAS data more and showed that DAS could provide similar or better data quality. As DAS measures strain or strain rate, and geophone measures particle velocity, several methods could be used to convert one property to the other. Most of the published literature is related to the conversion of DAS data to particle velocity, where is either necessary to rescale the time-integrated DAS data (Daley et al., 2016) or apply a conversion filter (Bona et al., 2017) which accounts for pulse and gauge length. The former requires the knowledge of local propagation velocity, while the latter needs to be regularised by adding the noise to DAS data to avoid division by zero that may occur for certain wavenumbers. However, Isaenkov et al. (2020) had difficulties applying the filter for larger wavenumber and suggested that internal interrogator processing may contribute to DAS response deviating from a strain rate.

Moreover, various DAS interrogators can have very different designs. The differences in the design of DAS recording units and selection of acquisition parameters significantly affect the data quality (Parker et al., 2014; Dean et al., 2017; Pevzner et al., 2018a; Sidenko et al., 2020). Therefore, further research on DAS is required to better identify the strengths and limitations of DAS technology and assess how DAS measurements correspond to standard borehole geophone recordings.

These tasks are best accomplished in a controlled environment at designated test sites that should allow for the repetition of the experiment using different sensors in stable conditions. In addition, such test sites should enable the comparison of different seismic receivers for both borehole and surface arrays using different types of seismic sources. There are several test facilities for carbon capture and storage (CCS) around the globe, where DAS technology is used, including CaMI (Lawton et al., 2017), Otway International Test Centre (Correa et al., 2018a), CSIRO In-Situ Laboratory (Tertyshnikov et al., 2019), and RITE (Sun et al., 2020). However, access to the data from these project-based sites is often restricted and not publicly available. Furthermore, this type of testing is not limited to these CCS sites; standard telecommunication fibre-optic (FO) cables as seismic DAS sensors were compared to conventional seismometers by Lindsey et al. (2017, 2019) and Ajo-Franklin et al. (2019). Lastly, the fundamental research on DAS is conducted at specifically developed test sites for trialling DAS technology: Aramco Houston Research centre built for testing borehole arrays (Aldawood et al., 2020); NOR-FROST (Wuestefeld et al., 2021) used to study the performance of surface DAS arrays and their coupling in different mediums; and the GeoLab Research facility at Curtin University (Tertyshnikov et al., 2021), where DAS response can be studied from both surface and borehole DAS array, and compared to the reference geophone datasets.

4.2. Test Site: Curtin GeoLab Research Facility

The Curtin GeoLab Research Facility was established at Curtin University, Western Australia, with aims to conduct applied geophysical research, equipment testing and training of students and industry personnel. The key components of the GeoLab are a 900 m vertical well drilled on Curtin campus and state-of-the-art seismic equipment, which includes surface and borehole three-component geophones, impulse and vibroseis seismic sources, and a variety of fibre optic cables (including a cable permanently deployed in the borehole). The Geolab Well (NGLd) is previously referenced as the NGL training well (e.g., Correa et al., 2018a).

From the geological perspective, the GeoLab well is situated at the eastern onshore margin of Perth Basin (Figure 4-1). The basin is covered with unconsolidated quaternary sediments, while the Archean rocks are outcropping on the east side of the Darling Fault. The cross-section over the three nearby wells reveals that the basin comprises Quaternary (Q), Tertiary (T), Cretaceous (K) and Jurassic-aged sediments (J) (Figure 4-2). Almost half of the GeoLab well depth is drilled through the Kings Park Formation. This formation occupies a deeply eroded valley incised through the Cretaceous sediments. Two sandstone sequences, the Mullaloo Sandstone Member and Como Sandstone Member, lie within the formation. These may occupy secondary channels eroded into the shaly sequence at the top and near the base of the formation (Department of Water, Government of Western Australia, 2008).

The well is cased with fibreglass slotted between 650 and 890 m depth. A fibre optic cable is cemented behind the casing with the loop at the bottom. The cable contains two single-mode fibres for distributed acoustic sensing and two multimode fibres for distributed temperature sensing. Since the entire length of the well is covered with fibre cores four times, this facility allows multiple FO interrogators to be used simultaneously (Pevzner et al., 2018a). It is also possible to deploy FO cables directly into the well to test the performance of different types of cables and the effect of the coupling on the measurements.

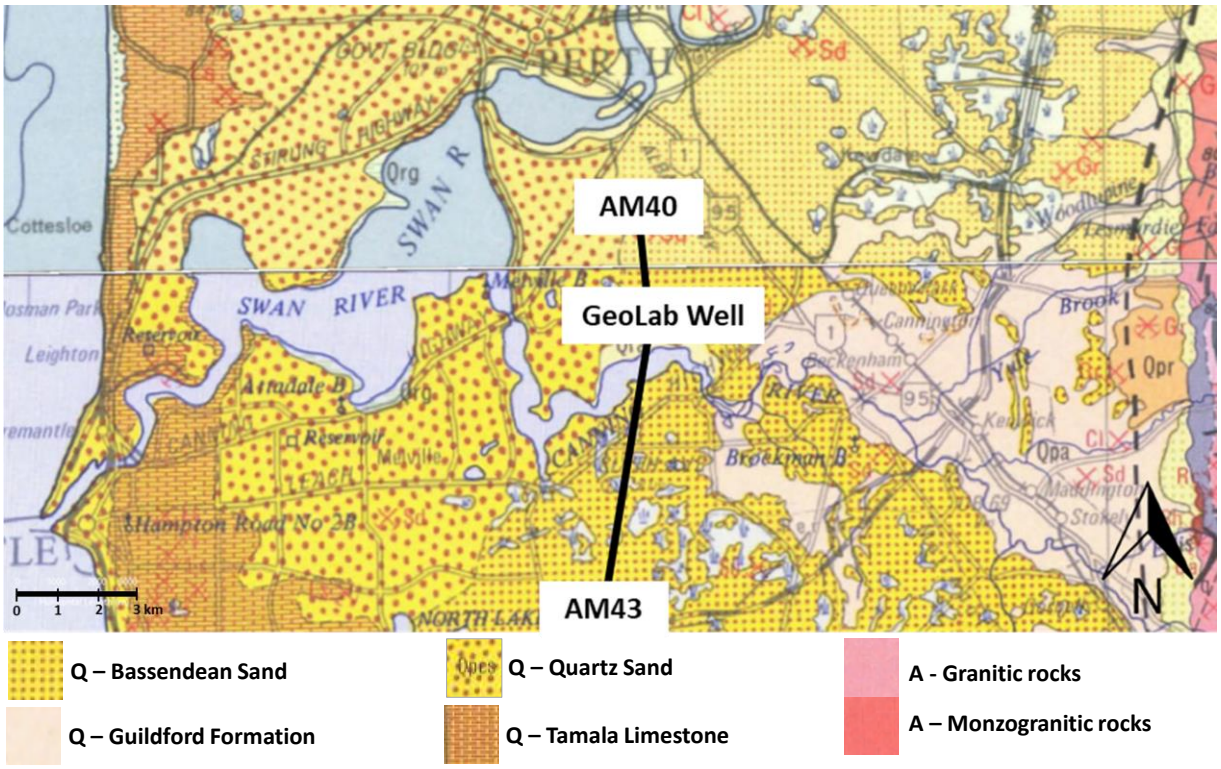

Figure 4-1. Geological map of the area around GeoLab Well-01 (© State of Western Australia (Department of Mines, Industry Regulation and Safety, 2020).

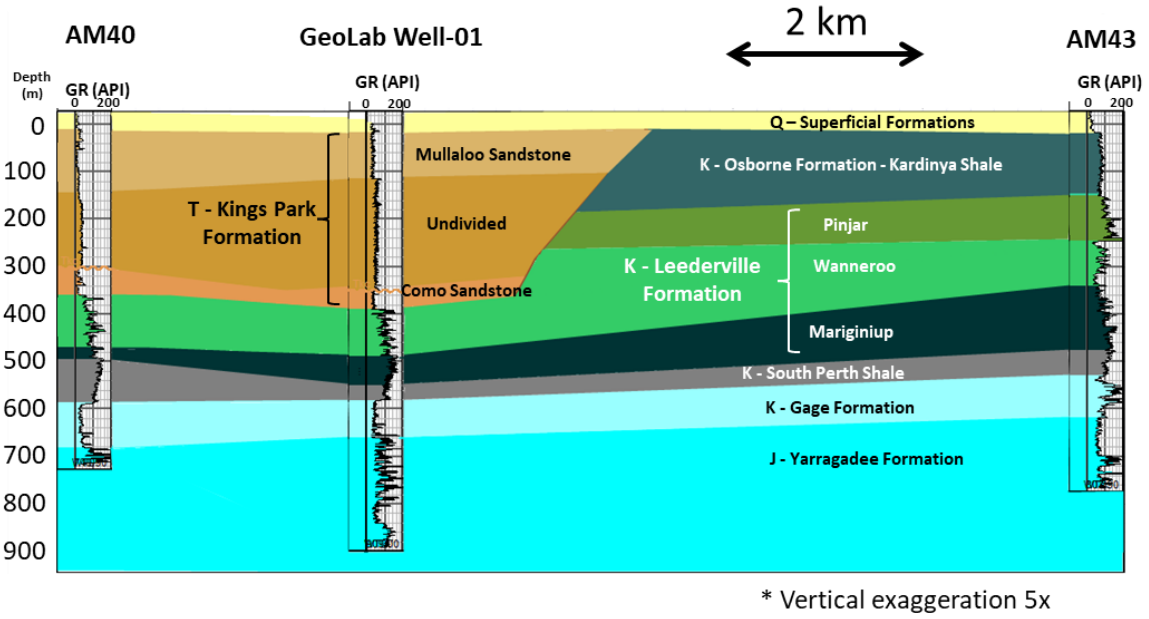

Figure 4-2. Geological cross-section along with three selected wells: AM40, GeoLab Well-01 and AM43.

The GeoLab facility was previously used for a wide range of geophysical experiments. Correa et al. (2017a, 2017b, 2018a) and Van Zaanen et al. (2017) compared different borehole seismic receivers. Pevzner et al. (2018a), Dean et al. (2019) and Sidenko et al. (2020) utilised different interrogator units and studied their internal characteristics. The GeoLab was used to test three-component VSP with DAS (Tertyshnikov and Pevzner, 2020) and the performance of different seismic sources (Tertyshnikov and Pevzner, 2019). Pevzner et al. (2018b) and Shulakova et al. (2020) examined the use of the GeoLab well for passive registration of earthquakes and technogenic activities using DAS. Additionally, experiments on locating the dark fibre cables on the Curtin campus were done at the GeoLab (Tertyshnikov et al., 2021).

This study uses data acquired during a walk-away VSP experiment carried out at the GeoLab in June 2020 (Zulic et al., 2020). The survey area with all source locations is shown in Figure 4-3. The data were acquired with a conventional three-component borehole geophone and a single-mode straight FO cable cemented behind the casing of the GeoLab Well-01. The seismic signal was generated by a 26,000 lbs Univib vibroseis truck. Acquisition parameters are given in Table 4-1.

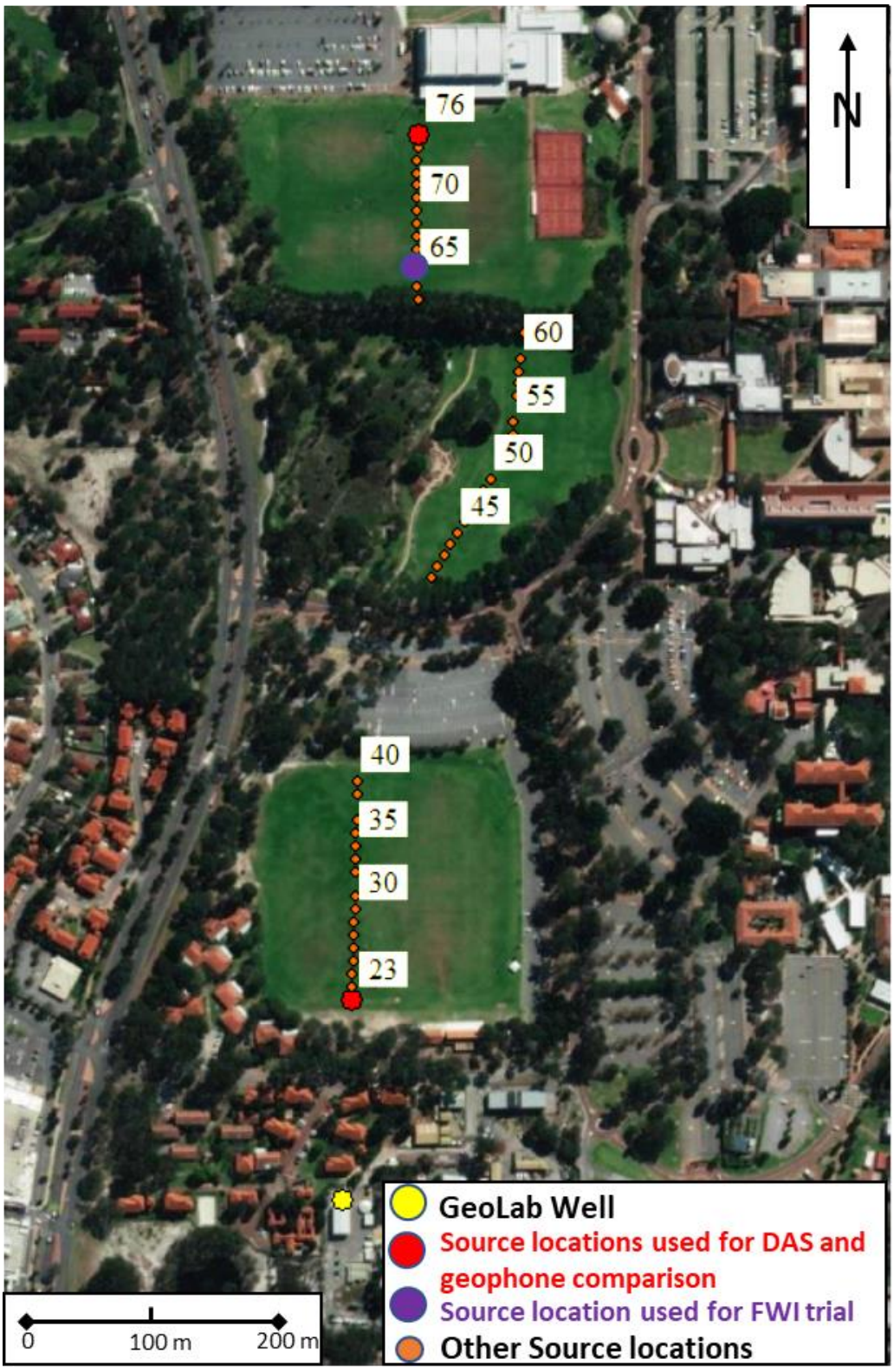

Figure 4-3. Aerial map shows the well's surface location (blue) and source positions (red); every fifth source station is labelled.

Table 4-1. Seismic acquisition parameters

VSP Survey Information	
Geophone Recording System	WaveLab II
Software acquisition	WaveControl
Logging cable	2500 m 4 conductor cable + electric winch
Geophone Information	
Downhole tool	Sercel 3C SlimWave with ten downhole shuttles Sensor: Omni 2400 15Hz
Receiver step	10 m
Sweep + listen time	24s + 4s
Sample rate	1 ms
Sweep per receiver	1
DAS Information	
Interrogator unit	Silixa iDAS v2
Fibre optic cable	Single-mode straight loose tube cable
Sampling interval raw / binned	1 m / 5 m
Pulse length	5 m
Gauge length	10 m
Sweep per receiver	9
Source information	
Source type	26,000 lbs UniVib
Source sweep	8 - 150 Hz linear sweep
Sweep duration	24 seconds
Tapers	0.5 s
Force	70 %
Source control	Pelton VibPro
Number of source locations	48

4.3. Method

Direct comparison of geophone and DAS performance requires converting the data to the same physical property. In practice, DAS response is often converted to the particle velocity for comparison with geophone data (Daley et al., 2016; Correa et al., 2017). However, Bakku (2015) indicated that when we assume that DAS measures the strain rate, then it is given by the difference in the particle velocities measured by two vertical component geophones separated by a gauge length L:

$$\dot{\varepsilon}_{zz}^{DAS} = \frac{v_z(z+\frac{L}{2}) - v_z(z-\frac{L}{2})}{L}, \quad (2)$$

where, $\dot{\varepsilon}_{zz}^{DAS}$ is the strain rate along the vertical direction measured by a DAS system, v_z is the vertical component of particle velocity, and z is the depth. We use this approach to convert the vertical component of particle velocity to the vertical component of strain rate.

We apply the following processing flow to get an absolute strain rate from the geophone dataset (summarised in Table 4-2). After loading raw geophone data, we apply descaling and geophone factors to calibrate the native system units (mV) to particle velocity (m/s). Then we differentiate data over the 10-meter interval (the same interval as the gauge length used during the acquisition of the DAS data) and assign the field geometry. The output dataset represents the strain rate (nanostrain/s), and we refer to it as converted geophone data. In addition to this, DAS data containing native measurements of phase variation over time are calibrated to the absolute strain rate (nanostrain/s) by applying the descaling factor. Then the geometry is assigned. The geophone and DAS equipment manufacturers provided geophone's and descaling factors.

We firstly visually compare gathers from geophone, DAS and converted geophone datasets. Then we compare the amplitude spectrum of the entire absolute strain-rate wavefield (uncorrelated) and the first-break amplitudes (correlated) for DAS and converted geophone.

The gauge length is one of the most important DAS parameters as it affects both the resolution and signal-to-noise ratio of the acoustic signal (Dean et al., 2017).

The IU used in this survey has a fixed gauge length, and therefore it was not possible to study the effect of the gauge length change. The proposed conversion allows adjustment of the gauge length. We can simulate different gauge lengths by differentiating the geophone data over various depth intervals. This simulation can assist with understanding this parameter and potentially use it for the sensitivity optimisation for a target wavelength. In addition to amplitude spectrum analysis and differentiation over a 10-meter interval, we simulate the DAS response with two additional gauge lengths of 50 m and 90 m.

Table 4-2. Processing workflow for getting the absolute strain rate from geophone and DAS measurements

Step	Converted Geophone	iDAS
1	Read raw SEG-Y	Read relative strain-rate iDAS data
2	Apply descaling factor to get the voltage in millivolts	Apply descaling factor to get absolute strain rate
3	Apply geophone factor to get particle displacement rate in m/s	Assigning geometry
4	Assigning geometry	
5	Differentiate over the GL interval	

4.4. Data Analysis

To compare the performance of the DAS system and geophones, we use data from two source locations at the near offset (source location 23, 160 m) and the far offset (source location 76, 845 m).

Figure 4-4 and Figure 4-5 show the comparison of the correlated vertical component geophone, DAS and converted geophone datasets for near and far offset, respectively. The geophone data have noisy channels because of the malfunctioning of two geophones in the receiver string, which is more prominent in the far offset data as the amplitude of the signal decays. This type of noise is

consequently carried through to the converted geophone dataset. Apart from that, DAS and converted geophone records look similar, as shown in the selected trace view displayed at the bottom of the figures. The red arrows indicate the difference in phase of P- and S direct waves between recorded DAS and converted geophone data.

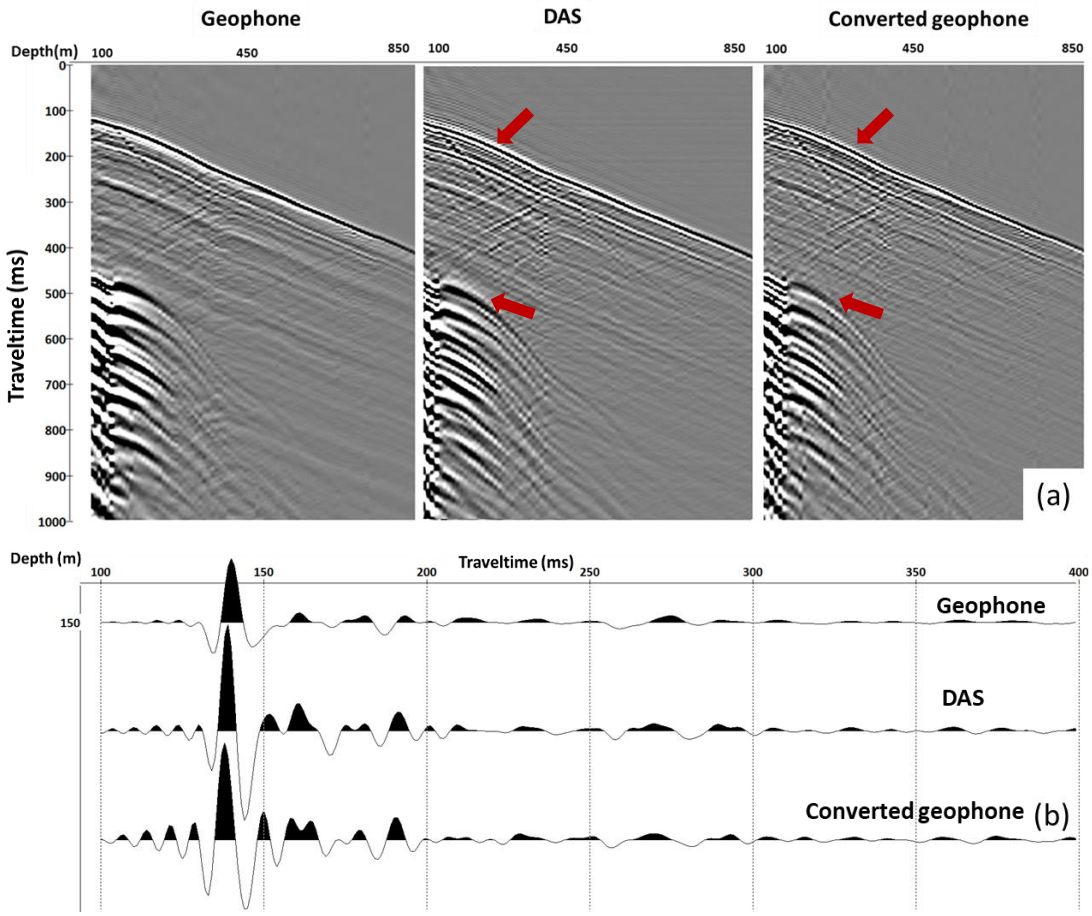

Figure 4-4. Near offset example: (a) from left to right gathers of Geophone, DAS and converted geophone response; (b) from top to bottom: trace at a depth of 150 m of Geophone, DAS and converted geophone response. We exclude every second trace from DAS data to match the same receiver interval for Geophone/Converted Geophone and DAS. The red arrows indicate the difference in phase of P- and S direct waves between recorded DAS and converted geophone data.

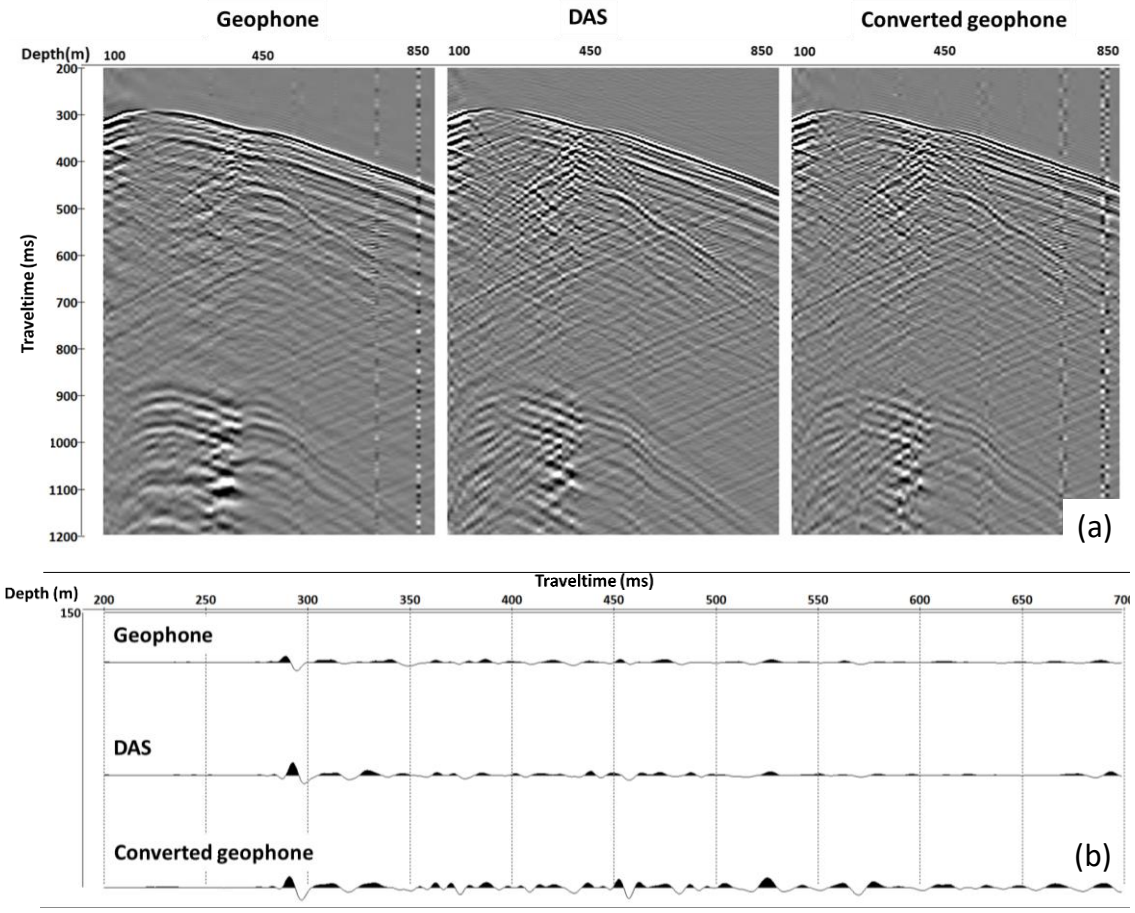

Figure 4-5. Far offset example: (a) gathers of Geophone, DAS and converted geophone response; (b) trace at a depth of 150 m of Geophone, DAS and converted geophone response. We exclude every second trace from DAS data to match the same receiver interval for Geophone/Converted Geophone and DAS.

Then, we analyse the entire wavefield to compare the absolute values of the strain rate obtained using both types of sensors. We apply Ormsby bandpass filter 5-8-150-200 Hz to denoise the data. We also adjust the length of uncorrelated datasets to 27 s and compute the amplitude spectrum of the recorded signal for all the traces.

Figure 4-6 shows the amplitude spectrum for near (a) and far (b) offsets for both types of receivers. The frequency spectrum of DAS and converted geophone data are similar for the near offset shot. However, we observe more discrepancy in the spectrum with increased offset. The low-frequency signal at the DAS data has a

lower amplitude compared to the converted geophone data, and towards the high frequency, the entire spectrum is biased (Figure 4-6b).

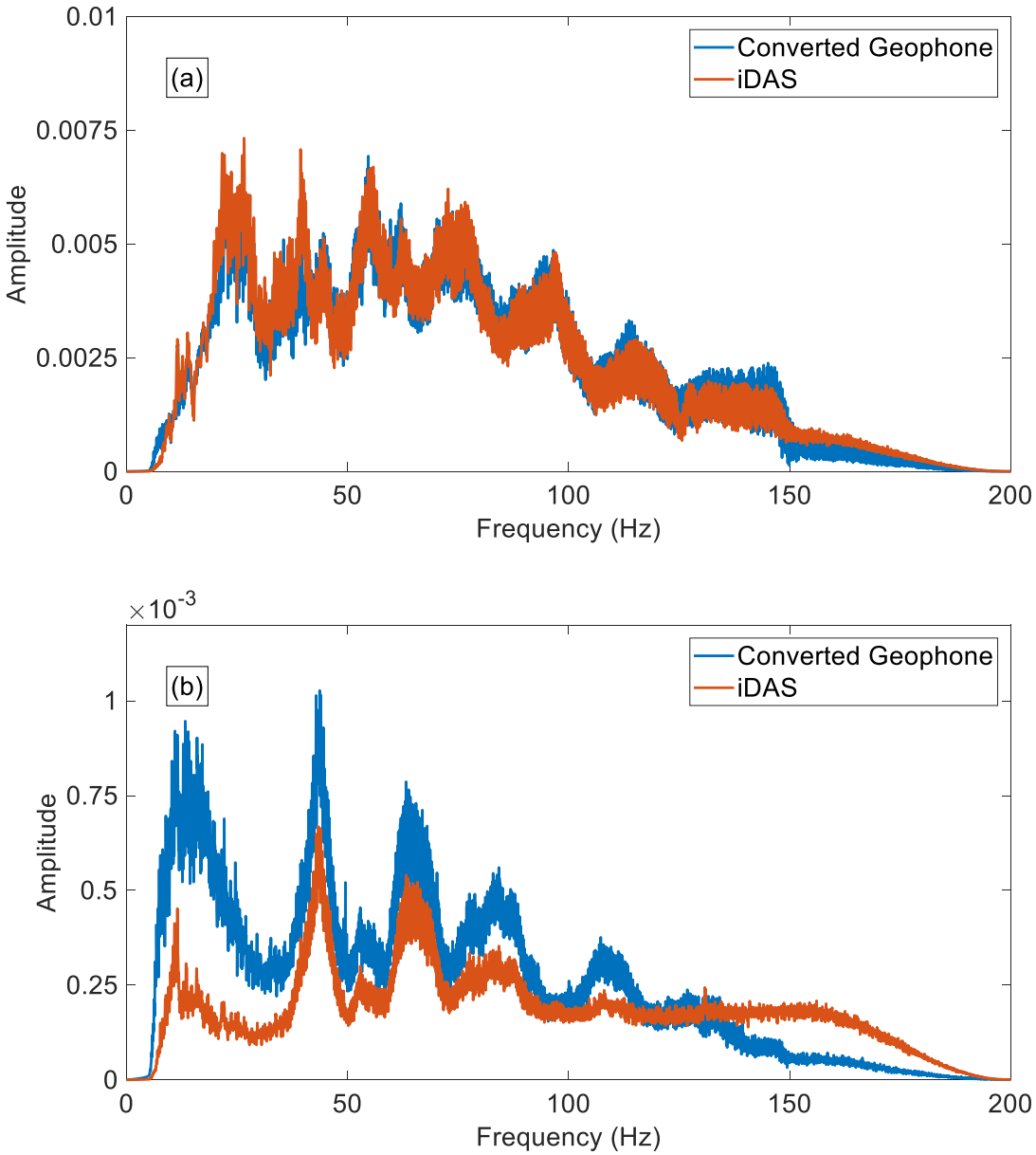

Figure 4-6. Amplitude spectrum comparisons for (a) near and (b) far offsets. The blue line is the strain rate from Converted Geophone, and the red is the strain rate from DAS.

Then we correlate the data with the pilot sweep and compare the first-break amplitudes for near and far offsets (Figure 4-7a and Figure 4-7b, respectively).

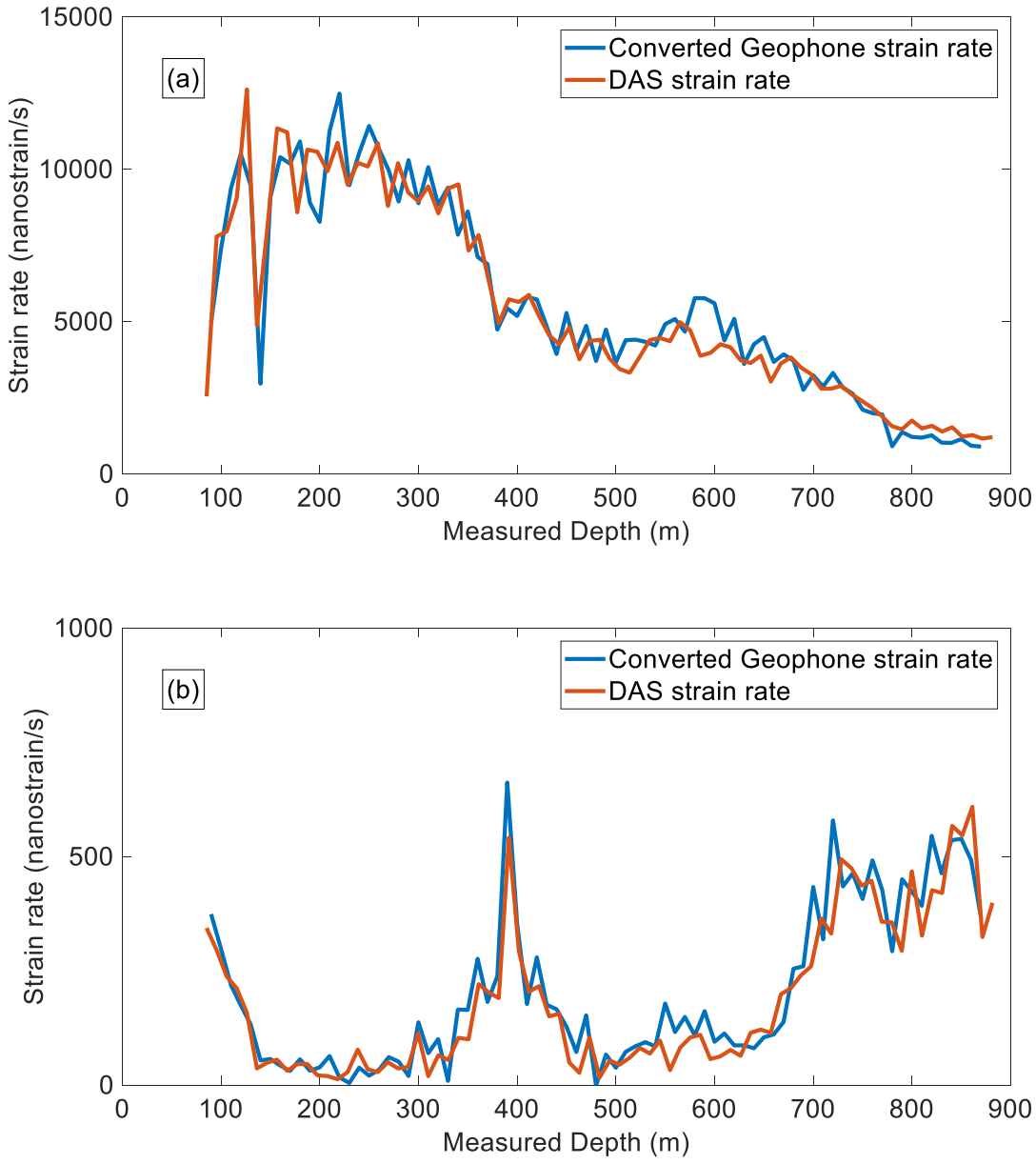

Figure 4-7. First-break amplitude comparison for (a) near and (b) far offset. The blue line is the strain rate from Converted Geophone, and the red is the strain rate from DAS.

In addition to amplitude spectrum analysis, we simulate the DAS response with two additional gauge lengths by differentiation of geophone data over different depth intervals. The examples of converted geophone datasets obtained by differentiation over three simulated gauge lengths are shown in Figure 4-8, where the simulated gauge lengths are 10 m, 50 m and 90 m, from left to right.

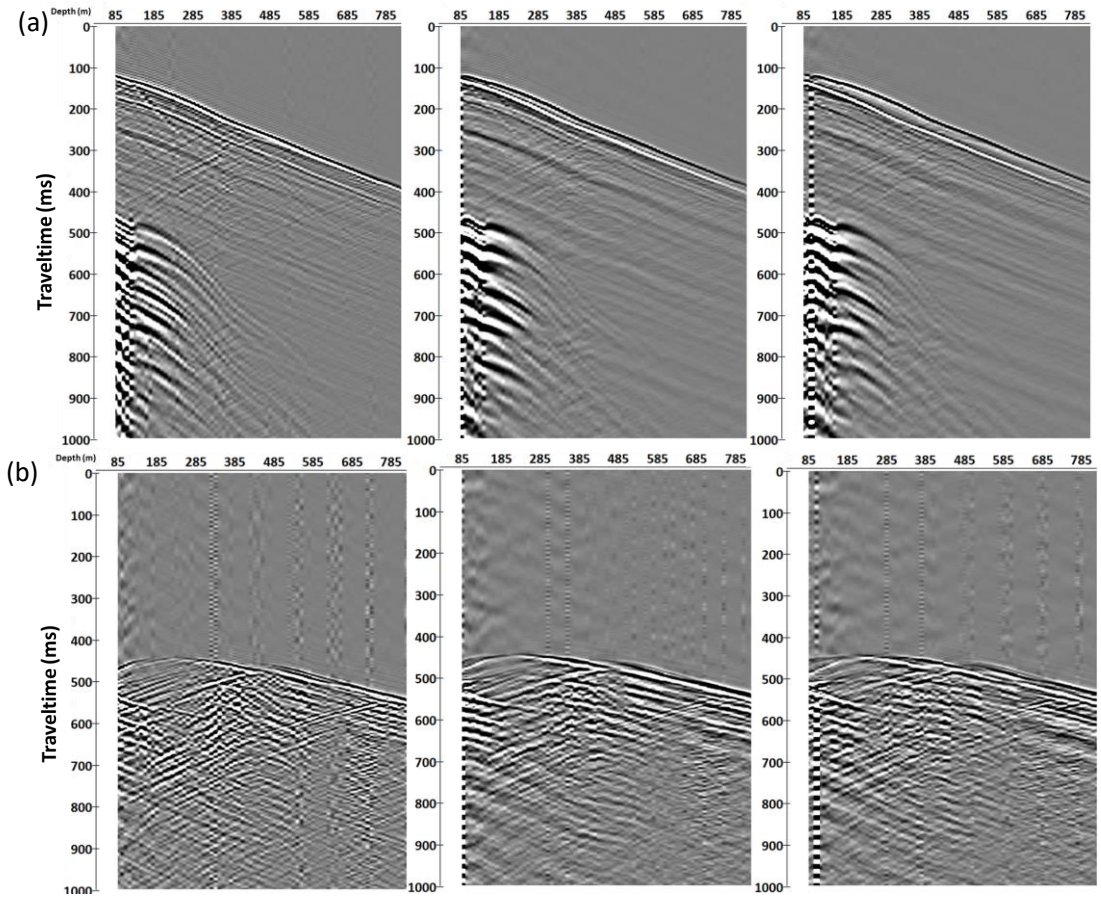

Figure 4-8. Gauge length simulation of 10 m (left), 50 m (middle) and 90 m (right), for (a) near and (b) far offset converted geophone.

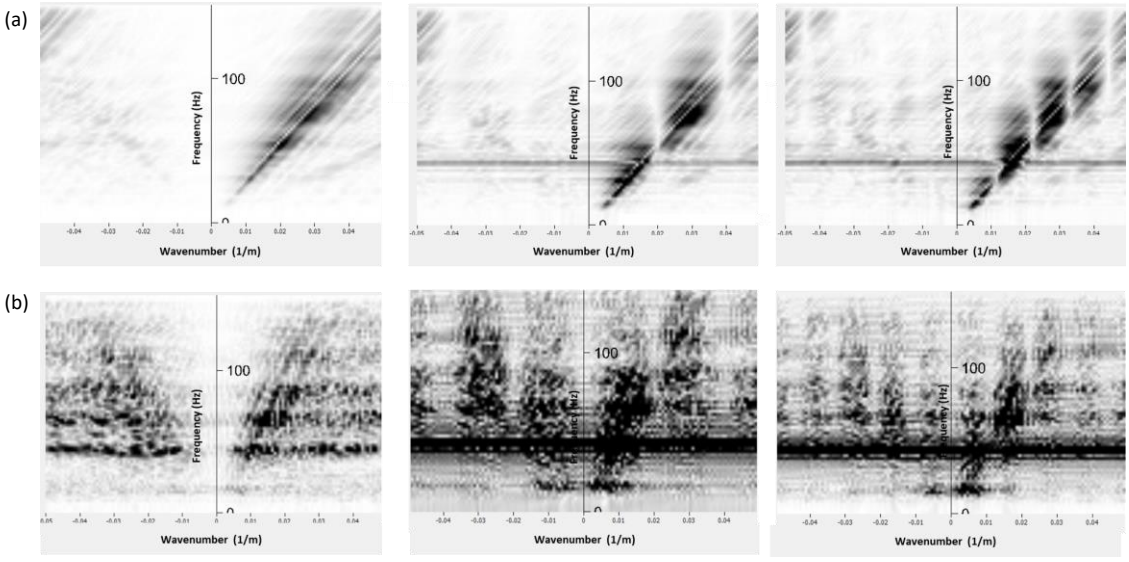

Figure 4-9. F-K spectrum for the converted geophone data with a simulated gauge length of 10 m (left), 50 m (middle) and 90 m (right) for (a) near and (b) far offset.

4.5. Discussion

Our analysis shows that the conversion of geophone data (vertical particle velocity) to vertical strain rate brings the phase of the direct wave closer to the phase of DAS data (Figure 4-4 and Figure 4-5). The polarity of the reflected waves in the converted geophone dataset also matches the DAS data. The amplitude response of the studied borehole geophones and DAS is similar after converting both datasets to strain rates (Figure 4-6 and Figure 4-7). This is a surprising result considering that different factors affect geophones and DAS measurements. For example, the geophone amplitudes are affected by the type of a geophone and its performance, probe's housing, and the quality of the probe's coupling to the formation or the casing. The DAS amplitudes are affected by the designs of a cable and an interrogator, the cable's coupling with the formation, and selected optical parameters. Nonetheless, the amplitude spectrums of the two datasets show similar absolute values (Figure 4-6), and the variations of the first-break amplitudes with depth are similar as well (Figure 4-7).

Apart from the higher noise level on geophone data observed for far offset, DAS and converted geophone records look similar. However, near offset data with higher frequencies present in the record show a significant discrepancy in the phase of the direct arrivals (arrows in Figure 4-4). The discrepancy is better observed at shear waves, which could be caused by how fibre reacts to S-waves. While we can assume that the effect linked to the gauge length dominates for relatively low frequencies, high frequencies may require the pulse length effect also being taken into account.

For the same source effort (single shot), DAS and converted geophone amplitudes are similar for near offset. However, for far offset, the high-frequency part of DAS spectrum (>100 Hz) looks constant even beyond the frequency of the sweep (150 Hz), which might indicate that this part of the spectrum is mostly noise (Figure 4-6). This agrees with earlier findings that geophone has higher sensitivity with increased offset than DAS.

Similar strain rate response between DAS and converted geophone datasets suggests using dense geophone data to simulate DAS measurements. Simulation of DAS response allows analysis of strain rate wavefields and further

understanding of DAS data (e.g., adaptation of existing particle velocity processing workflows to DAS workflows). For example, the gauge length is one of the most important parameters for the DAS survey (Dean et al., 2017), as it affects not only signal to noise ratio but also the wavefield distortion. Changing the gauge length can introduce a ghost wave if the gauge length is not optimal for the recorded wavelength (Figure 4-8). In addition to this, we can observe the notches in k-spectrum, which are caused by the gauge length effect (Figure 4-9). In the absence of standardisation of DAS systems (i.e., different DAS systems may have fixed or variable gauge length parametrisation), one can study the gauge length effect from the converted geophone wavefield and potentially use it for the sensitivity optimisation for a target wavelength.

For purposes of comparing the same physical property collected with a different type of sensors, the conversion approach by differentiation of particle velocity over the gauge length could be better than the integration of strain proposed by Bona et al. (2017) because the division with zero (for certain values of k) is avoided.

The first-break strain rate amplitudes are calculated from the vibroseis data correlated with a pilot sweep. This process affects the phase of a signal. The vibrator output is defined in terms of its baseplate motion (e.g., displacement, velocity, or acceleration). When correlation with a pilot sweep is performed on motion data, the resulting correlogram is assumed to be zero-phase (Sallas, 1984). Therefore, correlating strain data with a pilot sweep (represent of motion) may impact a phase of correlated DAS data. In addition to this, the effects of DAS parameters (pulse and gauge length) are shown to have a considerable effect on phase (Bona et al., 2017). Therefore, correlation with a pilot sweep needs to be studied further and considered when interpreting the DAS data.

4.6. Conclusions

We brought geophone and DAS measurements to the same property and calibrated them to the absolute strain rate. We compared the amplitude spectrum of the entire absolute strain-rate wavefield (uncorrelated) and the first-break amplitudes (correlated) for DAS and converted geophone. In addition to

amplitude spectrum analysis, we simulated the DAS response with two additional gauge lengths.

We observed that DAS and geophone have similar absolute values of strain rate amplitudes, despite different factors affecting the performance. The losses of seismic energy due to the geophone coupling and housing are similar to the losses in fibre-optic cable construction and installation. Although similarity in absolute response is surprisingly good, we do not expect this finding to be universal. Different cable designs, coupling, etc. can produce situations where geophone and DAS responses can be different.

A denser geophone dataset can be used to simulate DAS response.

GeoLab provided an excellent opportunity for such kind of research. Different equipment can be tested and assessed versus the reference dataset. Data is publicly available.

5 Full-waveform inversion

This chapter is adapted after the following publication:

> Zulic, S., Bona, A., Tertyshnikov, K., Yurikov, A., Pevzner, R. (2021). *Subsurface characterisation using full waveform inversion of vertical seismic profile data: Example from the Curtin GeoLab well* [Paper presentation] 3rd Australasian Exploration Geoscience Conference 2021.

As most of the chapter's content is based on collaborative work, I use the first-person plural narrative to acknowledge my collaborators. Particularly, my involvement was in data preparation, processing, applying the FWI workflow, troubleshooting, geological interpretation and writing the paper.

5.1. Introduction

Full-waveform inversion (FWI) attracts much interest due to its potential to give an accurate velocity model often needed for seismic imaging in complex geological environments. This accuracy is achieved by minimising the difference between modelled and field data using the least-squares methods (Tarantola, 1984).

It is mainly used for inverting the surface reflection seismic data, where it relies on low frequencies and very large offsets. Large offsets allow detection of diving waves, a special type of refracted waves, which are of great importance for reconstructing the velocity models as they carry information about the velocity gradient and enable converging to the solution in less iteration.

Typical VSP (zero and single offset) surveys are considered to have low illumination. However, Charara et al. (1996) showed that due to the rich wavefield information (presence of transmitted, converted, and reflected waves) in vertical seismic profile (VSP) datasets, the VSP data is also suitable for the inversion. Furthermore, the FWI of VSP data can be applied to data collected using geophone and distributed acoustic sensors (DAS) (Egorov et al., 2018).

To test the FWI of the VSP dataset, we utilised data acquired during the walkaway VSP experiment was conducted in June 2020 (Zulic et al., 2020) at GeoLab Research Facility. The aerial map of the experiment is shown in Figure 4-3, with a geological map Figure 4-1 and a cross-section in Figure 4-2. At this stage, we chose to do a single-shot inversion to see what can be obtained from such inversion. We selected the source station 715 meters north of the well, referred to as S63 (purple dot in Figure 4-3). Initial velocity analysis of near-offset gather from this experiment indicated very low shear wave velocity within the near-surface layer. Since the lowest expected velocity affects FWI workflow (more details in 5.2.1. FWI workflow), we limit the analysis of the recorded dataset to invert the data recorded with a 3C geophone from 130 m to 870 m depth. The complete acquisition parameters are given in Table 4-1.

5.2. Methods

5.2.1. FWI workflow

We applied 2D elastic FWI workflow (Egorov et al., 2017) to synthetic and field datasets. The workflow is implemented in an open-source software package IFOS2D (Köhn, 2011, Bohlen et al., 2016). The main steps are shown in Table 5-1 and briefly explained below. For the forward problem of FWI, finite-difference modelling (Virieux, 1986; Bohlen and Saenger, 2006) is used, while for the

inverse problem, we use the L-BFGS optimisation method for the minimisation of the misfit function (Nocedal and Wright, 2006), both embedded in IFOS2D.

Table 5-1. Main steps of FWI workflow.

2D Elastic FWI Workflow		
1.	**Parameter model building**	P-wave velocity S-wave velocity Density
2.	**Parametrisation for forward and inverse modelling**	FD grid order Domain decomposition Discretisation Time stepping Source function Modelling type Boundary conditions Receiver definition Inversion parameters Gradient method Step length estimation Misfit definition
3.	**Pre-processing of field data**	Correlation Field geometry assignment Orientation of horizontal component towards the source Stacking Conversion to minimum-phase Correction to 2D amplitudes
4.	**An iterative process of inversion**	Minimising the misfit through the gradient optimisation method

Parameter model building

The parameter model building step defines a starting model in parameter space. These parameters are P- and S-wave velocity and density for the elastic inversion. They can be created from the well data or other sources. We use MATLAB, RadexPro and OpendTect software packages for data preparation, processing and interpretation, as explained in the following sections.

The parameterisation for forward and inverse modelling

Forward modelling is done by solving the elastic wave equation with a time-domain eight-order finite difference (FD) staggered grid scheme (Virieux, 1986).

The geometry of the grid and other parameters such as domain decomposition, order of FD operator, discretisation, time-stepping, source function, type of modelling, boundary conditions, receiver definition, inversion parameters, gradient method, step length estimation, misfit definition are all defined in a parameter file. However, special care must be taken to avoid numerical artefacts (dispersion) and instability. The stability is achieved by fulfilling the wavefield's spatial and temporal sampling conditions. The conditions are related to grid size (how many grid points per minimum wavelength) and time-step (it must be smaller than the time for the wave to travel between two neighbouring grid points) for the given order of FD operator. The conditions for an FD operator can be found in the IFOS2D manual.

We also set the boundary conditions for the forward modelling in this step. We apply a free surface at the top of the global grid (Levander, 1988), and on each side and bottom of the grid, we apply a convolutional perfectly matched layer (Komatitsch and Martin, 2007). Finally, receivers are placed within the grid and mimic the scenario from the field experiment. We use a wavelet extracted from the field data for the source function.

For the inverse problem, minimisation of misfit function between modelled and field data is done using local iterative gradient-based techniques, where the gradient is obtained by the adjoint-state method (Plessix, 2006). We use the limited-memory Broyden-Fletscher-Goldfarb-Shanno (L-BFGS) algorithm (Nocedal and Wright, 2006) as an optimisation method for minimising the misfit

function. This method is less robust than the pre-conjugate gradient method but converges faster for multiparameter FWI (Brossier et al., 2009). For the misfit definition, we use the L2 norm, in which the misfit is scaled with the energy of the observed seismograms.

Pre-processing of field data

Pre-processing steps for FWI are the same as for the conventional VSP processing flow (correlation with the pilot sweep, assigning field geometry, the orientation of horizontal components towards the source, trace kill, stacking). Then, because the forward modelling in this package requires a causal wavelet, we convert the vibroseis data to the minimum-phase by applying a phase-shifting filter (Gibson and Larner, 1984). Furthermore, since the 2D forward modelling assumes 2D wave propagation, and our field data are collected in 3D space, we must also correct the data to 2D amplitudes by multiplying with $\sqrt{t}$ and convolving with $1/\sqrt{t}$ (Pica et al., 1990). Such corrected data of vertical and radial components, coupled with an elastic model, are used as inputs for the FWI.

The iterative process of inversion

We perform simultaneous inversion of all three elastic parameters. We apply the time-domain filtering multiscale approach. We use frequency filtering during the inversion. We define the corner frequency of the Butterworth low pass filter at the beginning of inversion and select a minimum number of iterations at the selected frequency. Once the misfit is smaller than the given value at the given frequency, the inversion is over and continued at the next frequency step.

As FWI is a computationally very demanding technique, the supercomputer is used to run the inversion code. Depending on the processor's availability and planned task (forward or inverse modelling), the local cluster at Exploration Geophysics and Magnus Supercomputer at Pawsey Supercomputing Centre are used. Both supercomputers have a significant number of central processing units (CPUs). Once the FWI parameters were defined, a test designed to compare the performance of inversion on a supercomputer revealed the optimum number of CPUs for the given task. For example, the inversion utilised 192 CPUs per job,

which resulted in around 32000 CPUs hours for the selected frequency range of the field data inversion.

5.2.2. Numerical study

We use the forward modelling results to test imaging parameters and assess the performance of FWI for single-shot data. In order to eliminate as many variables from the test, we choose to use the same modelling engine as is used for the inversion. We hope to use such a numerical study to show the viability and see the expected validity region of the inversion and the minimum errors we can expect from the inversion of the filed data. Therefore, we compute the synthetic VSP data from estimated elastic properties from GeoLab well using a forward modelling algorithm in IFOS2D.

One dimensional (1D) P-wave velocity (Vp) model is estimated from a near-offset DAS VSP experiment at GeoLab (Correa et al., 2017b), and S-wave velocity (Vs) and density are calculated using empirical relations (Castagna, 1985, Gardner, 1974). We refer to this model as a true model. A smoothed version of this elastic model used in the forward modelling is a starting model (M1) for FWI (Figure 5-1).

The model size is 1000 m x 960 m, with a cell size of 1x1 m. A high-resolution grid is needed to satisfy the spatial sampling conditions since the minimum propagation S-wave velocity in the near-surface layer is around ~400 m/s. The well is placed 80 m away from the left grid edge (Figure 5-1). It is populated with receivers, from 130 m to 870 m depth, with a receiver interval of 10 m. The source function is a wavelet extracted from the field data, and the source type is a vertical force source. The source is placed 715 m away from the well, which is the same offset of the source from the well as for the field data we will use later. This type of source excites both P- and S-waves in such a position. The modelling parameters are given in Table 5-2.

We inverted the data from a shot location distanced 715 m using receivers from 130 m to 870 m depth interval for the frequency range 6-65 Hz. A smoothed version of the elastic model (with a 200m long-running average operator) used in the forward modelling is a starting model (M1) for FWI.

Table 5-2. Modelling parameters

Parameters	Properties
Computation mode	Elastic
FD order / weights	8th order /Holberg operator
Boundary conditions	Free surface (top), PML (sides and bottom)
2D grid size	1000 m x 960 m
Cell grid size	1 m x 1 m
Time of wave propagation	1 s
Sample rate	0.0001 s
Source type/wavelet	Point source with directive force in the vertical direction / extracted from the field data
Receiver step / depth coverage	10 m / from 130 m to 870 m
Number of CPUs	48

5.2.3. Field data

Selected shot-gather from source location S63 is firstly pre-processed. The pre-processing includes correlation, field geometry assignment, horizontal component orientation towards the source, minimum-phase conversion, and correction to 2D amplitudes. In addition to pre-processing, the VSP data was processed to an upgoing-wavefield and migrated using the Kirchhoff migration algorithm (Dillon, 1988). Pre-processing and processing steps are given in Table 5-3 and performed in MATLAB and Radex software packages.

The application of FWI of field data, using elastic parameters created for the numerical study, has not been successful, most likely due to the lateral inhomogeneity observed in field gathers (for more details, see 5.3.2.1. Investigation of inversion's failure and conventional processing results).

Therefore, we needed to create a new starting model for which we used the 1D Vp profile obtained by inverting the first arrival travel times using fast marching eikonal solvers (Kroon, 2021). Vs and density properties were derived using the same empirical relations as for the synthetic model. We refer to this model M2 (Figure 4). We inverted field data from S63 using receivers 130 m to 870 m depth interval for the frequency range of 11 – 105 Hz. Apart from the elastic properties, all other modelling properties are indicated in Table 5-2 .

Table 5-3. Processing workflow

General pre-processing steps	
1. Read raw .sgy data	
2. Data editing	
3. Correlation with a pilot sweep	
4. Assign field geometry	
Specific steps	
FWI pre-processing:	**Conventional processing:**
1. Orientation of horizontal components	1. Spherical divergence correction
2. Conversion to minimum phase	2. Deconvolution
3. Correction to 2D amplitudes	3. Wavefield separation using 2D median filtering
4. Export to .su format and ready for the inversion	4. 2D VSP Kirchhoff migration using 1D interval velocity model.

5.2.4. Integrated interpretation

Single-shot VSP data have low illumination, and it is expected that the inversion results will have strong artefacts. Therefore, it is important to incorporate all available datasets to understand the FWI results better.

The list of available datasets is given in Table 5-4. OpendTect software package is used to incorporate the datasets.

Table 5-4. Datasets available for the interpretation

Available datasets	Dimensionality
Well / Stratigraphy logging	1D
Gamma-ray (GR) logging	1D
VSP migration image	2D
Inverted P-wave image	2D
Inverted S-wave image	2D
Calculated Poisson's ratio (PR) image	2D

Stratigraphy log for GeoLab well (Figure 4-2) consists of Q – Quaternary sediments, Tkm – Tertiary Kings Park Formation - Mullaloo Sandstone unit, TK – undivided Tertiary Kings Park Formation, Tkc – Tertiary Kings Park Formation - Como Sandstone unit, Kwlw – Cretaceous Leederville formation-Wanneroo unit, Kwlm – Cretaceous Leederville formation-Mariginiup unit, Kws – Cretaceous South Perth Shale, Kwg – Cretaceous Gage Formation and Ju – Jurassic Yarragadee Formation. The lithological description is given in Well Completion report (Rockwater, 2016).

Absolute values of the gamma-ray (GR) log can be found in Figure 4-2. GR log can also be used qualitatively to identify rocks with higher clay content and more shaly rocks (high GR). In opposite, low GR will identify rocks with higher content of sand and silica.

5.3. Results and discussion

5.3.1. FWI of synthetic VSP data

Figure 5-1. shows the true and starting Vp models used in the numerical study and the inverted Vp models from FWI. We observe that the inverted model converges well with the true model resolving thin layers of different velocities at

depth (indicated by the arrows in the figure). Most of the model updates occurred within the area of reflection points illuminated by the source and recorded on the receiver array. The wave propagation artefacts affect the rest of the model.

The ten-meter thick high-velocity layer (enclosed by a red dashed box in the figure) at a depth of 130 m could not be well reconstructed, probably due to inadequate receiver coverage for the reflected waves and a maximum inversion frequency of 65 Hz. Nevertheless, the synthetic modelling results confirm that the FWI of single-shot VSP data produces an adequate subsurface image in the half-offset distance, even though the wave propagation artefacts are present in the other parts of the image.

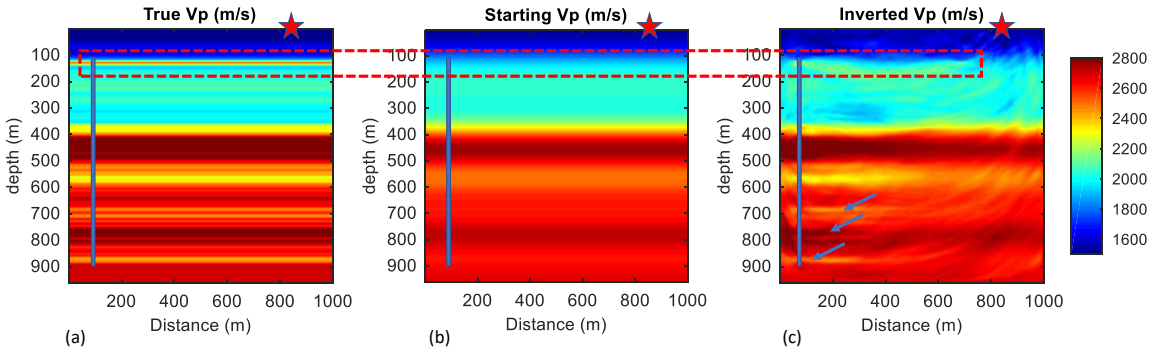

Figure 5-1. Vp models of synthetic data: (a) True model, (b) Starting model M1, and (c) Inverted model. The blue line shows receivers and red star source location. The arrows point to the well-resolved thin layers.

5.3.2. FWI of field VSP data

We first used the same FWI parameters for the field data as for the synthetic study. However, the inversion of the field data did not converge even for low frequencies.

5.3.2.1. Investigation of inversion's failure and conventional processing results

After several unsuccessful inversion attempts, we assessed the walkaway VSP seismograms more closely and noticed the presence of diffracted waves. The diffracted waves can be observed on every seismogram on the collected walkaway dataset, and they are imprinted in the first break arrivals. Examples of three different seismograms from shot locations 23, 35 and 48 are shown in Figure 5-2.

The interval velocities calculated from the VSP data heavily rely on the picked first-break times. In our field data, the diffracted waves are best observed between 350 m to 600 m depth and marked with red circles in Figure 5-2. The graph with interval velocities (Figure 5-3) confirms an increase in DAS (black line) and geophone (pink) interval velocities at the same depth interval. Therefore, diffracted waves may have introduced an error in calculating the interval velocities and reduced their accuracy. This is the most likely reason for the inversion's constant failures.

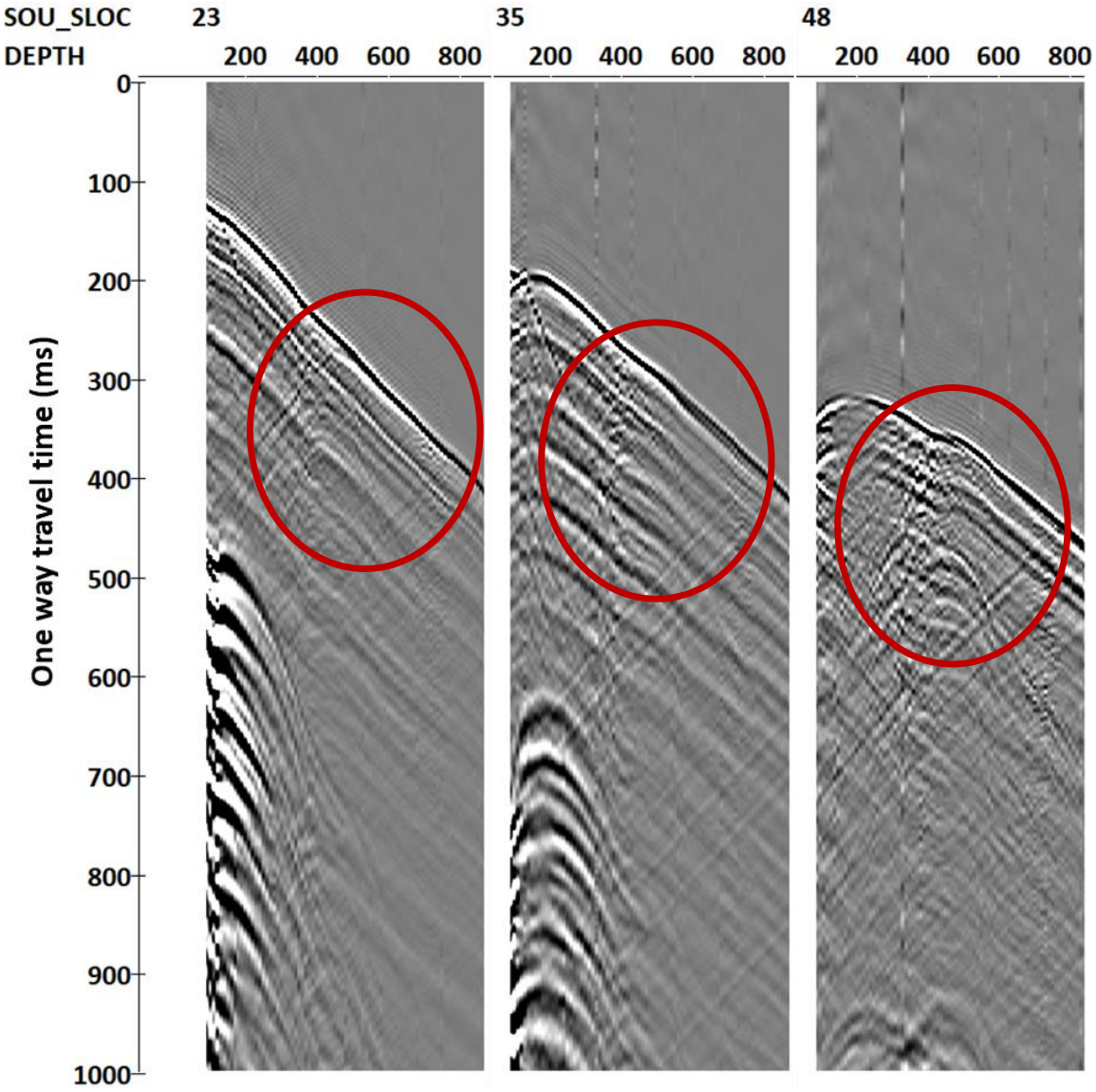

Figure 5-2. Three shot gathers from source locations 23, 35 and 48. Red circles show observed diffracted waves.

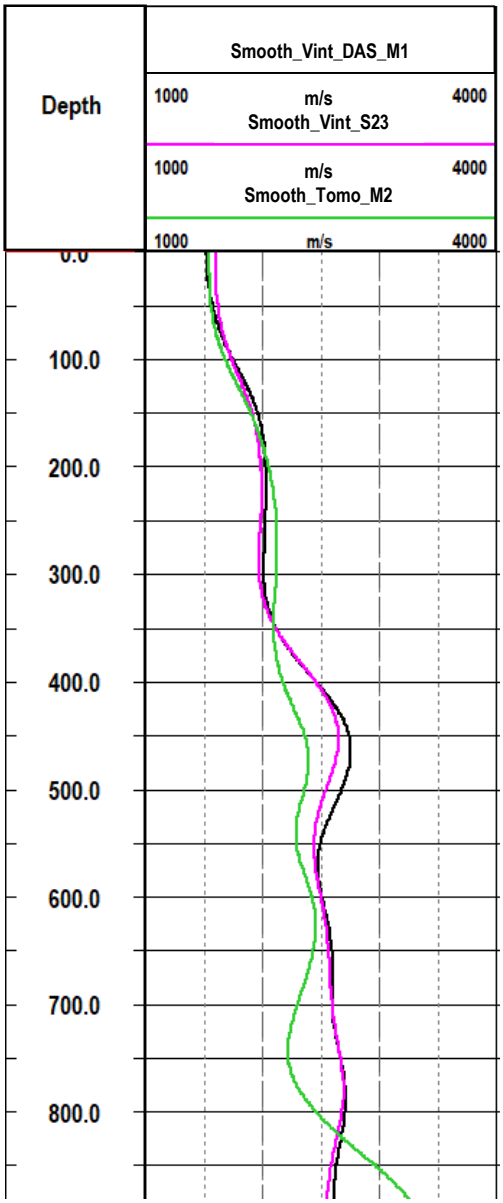

Figure 5-3. Comparison of interval velocities obtained from near-offset DAS VSP (black line labelled “smooth_DAS_M1”), shot location S23 (pink line labelled “smooth_Vint_S23”) and tomography results (green line labelled “smooth_Tomo_M2”).

One of the conventional VSP processing products is the migration of reflection events to a common imaging plane. The conventional processing flow was applied (Table 5-3), and the processed upgoing wavefield from shot location S63 was firstly migrated with interval velocities (smooth_Vint_S23) velocities (Figure 5-4). The figure also shows stratigraphy and gamma-ray logs, apart from the migration image. The horizontal line at the top of the Cretaceous Wanneroo unit (Kwlw) at a depth of 400 m is a clear indication of inappropriate interval velocities used for migration.

The migration result is an additional confirmation that the starting velocity model was not sufficiently accurate. Although the zero offset VSP is the most accurate method to obtain seismic velocities along the borehole (Cassell, 1990), the use of these velocities away from the borehole assumes lateral homogeneity. However, such an assumption is not always met in practice.

To overcome this issue, a new starting velocity model is created. The model is obtained by applying travel time tomography. We picked the first arrival times from S63. We used tomography with fast marching (1D) eikonal solver-based (Kroon, 2021) that accounts for the refracted waves present on raw gather to construct the velocity model.

This approach gave us a new interval velocity model - M2, shown in Figure 5-3 as a green line. It can be noticed that the main difference to other velocity models is observed at the same depth interval where diffracted waves are observed. We migrated the data from this location with tomography velocities (Figure 5-5). The horizontal line observed in Figure 5-4 is resolved now. However, the depth interval from 350 m to 500 m still does not look best resolved. It may indicate additional lateral complexity at this interval. It is also important to mention that the used migration algorithm assumes no lateral velocity changes.

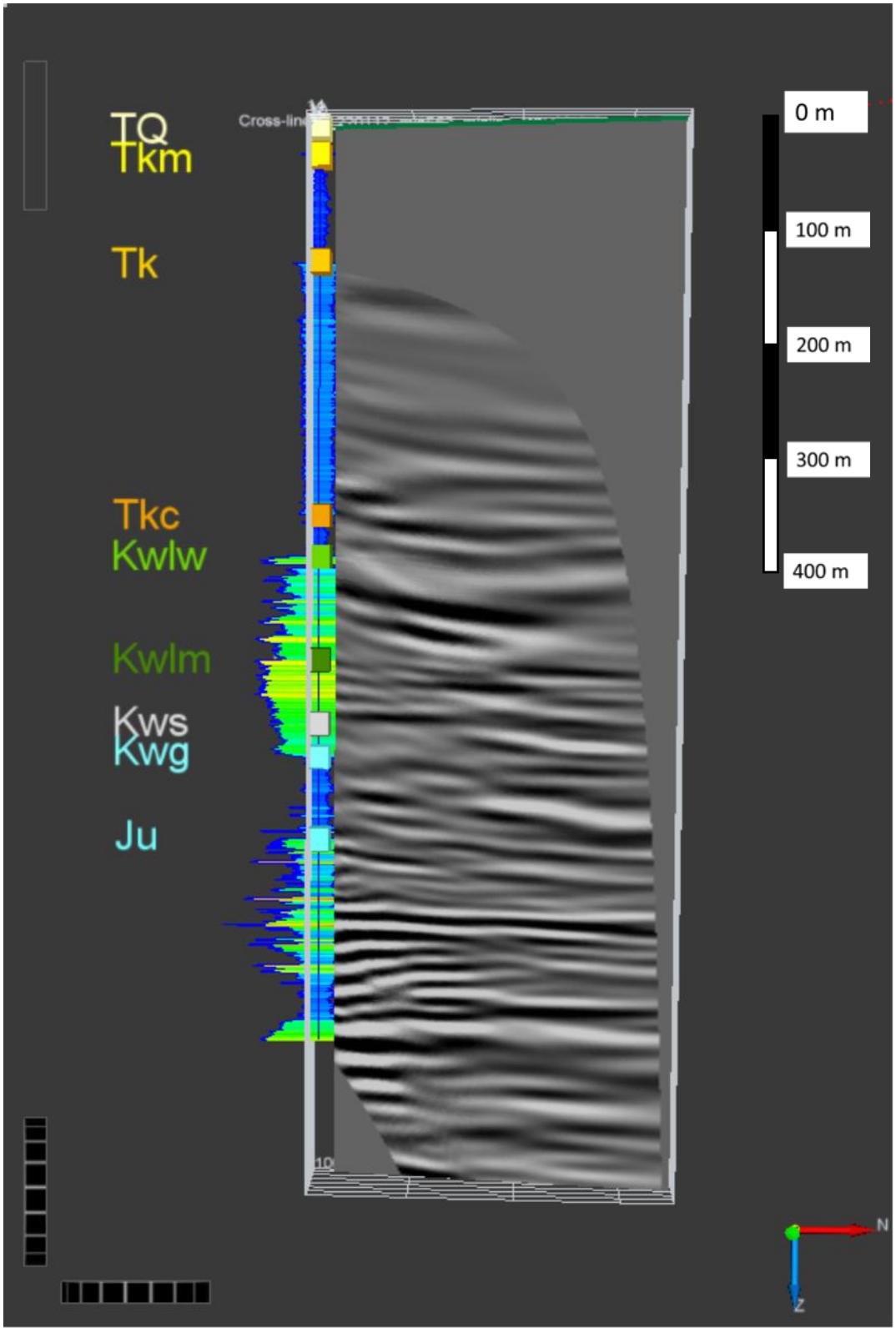

Figure 5-4. VSP migration of S63 with interval velocities from a near-offset VSP.

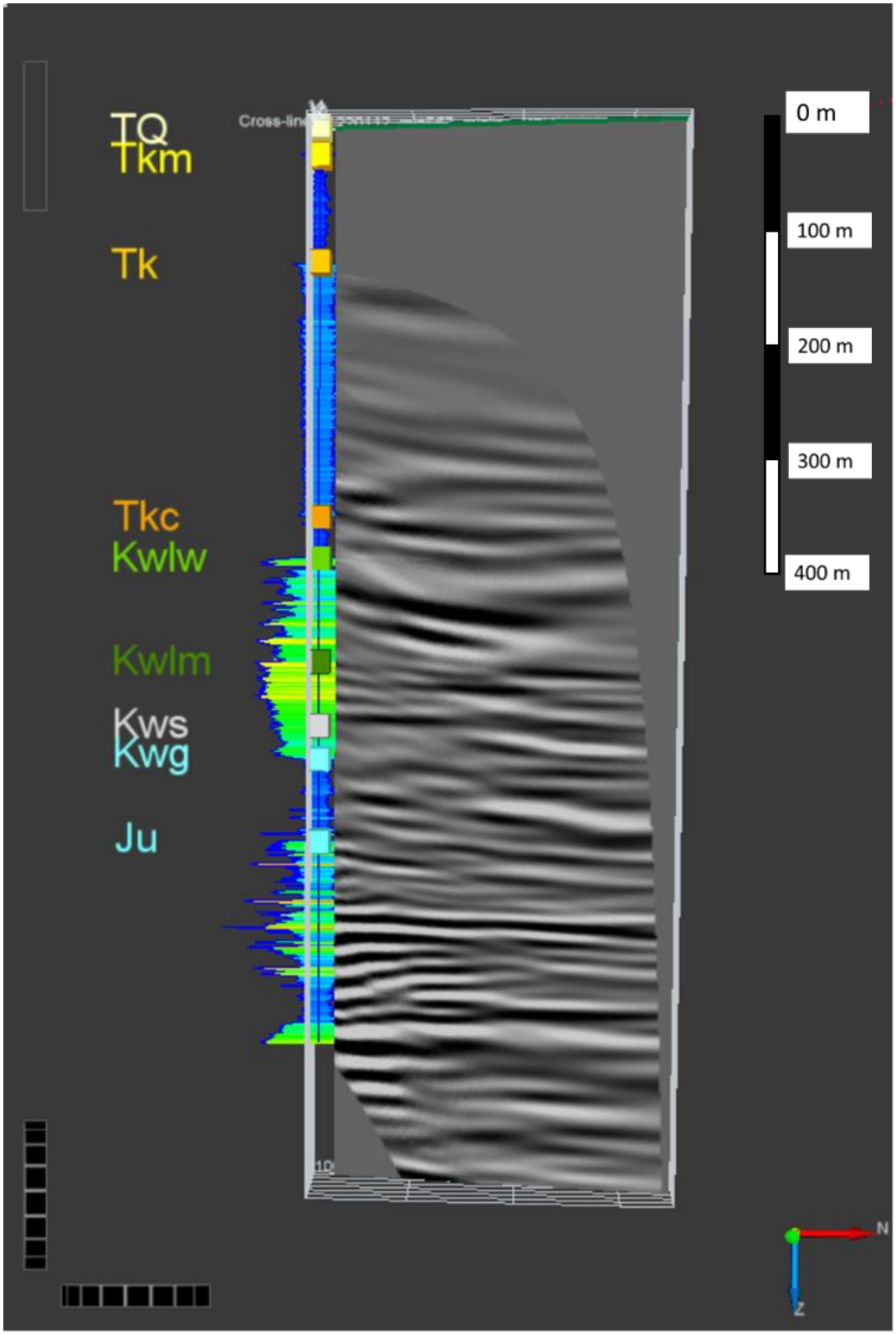

Figure 5-5. VSP migration of S63 with velocities obtained by tomography.

5.3.2.2. FWI with M2 parameter model

To address the issues mentioned in previous section, we used the M2 model as a starting P-wave velocity model, and S-wave velocity and density parameters are derived using empirical relations described in section

5.2.2. Numerical study. The inversion process started at 11 Hz with an increment step of 1 Hz. The synthetic data created with new elastic parameters (M2) fitted field data much better. The inversion is stopped at 105 Hz. The time limitation at Pawsey Supercomputer per single job required that the inversion be done in stages. One stage includes inversion for a frequency band of 10 Hz.

The results from FWI applied to field data using M2 are shown in Figure 5-6 for three frequency steps: 11 Hz (top), 40 Hz (middle) and 105 Hz (bottom). There are three seismograms for the frequency steps – synthetic seismogram for the given model (left column), field seismogram (middle column) and difference (misfit in right column) between synthetic and field data. The horizontal lines observed in all seismograms are low-quality traces from the field data removed prior to the inversion. As the number of iterations and frequency increases, the contribution of converted and reflected waves increases. The presence of these waveforms in VSP data is a great advantage for the inversion process, as these waves represent constraints of the inversion.

The starting M2 and final inverted model of P-wave velocities are shown in Figure 5-7.

As observed in the numerical study, the wave propagation artefacts dominate at a distance larger than the half offset. Hence, we limit the FWI interpretation from the well to 360 m away from the well (half offset).

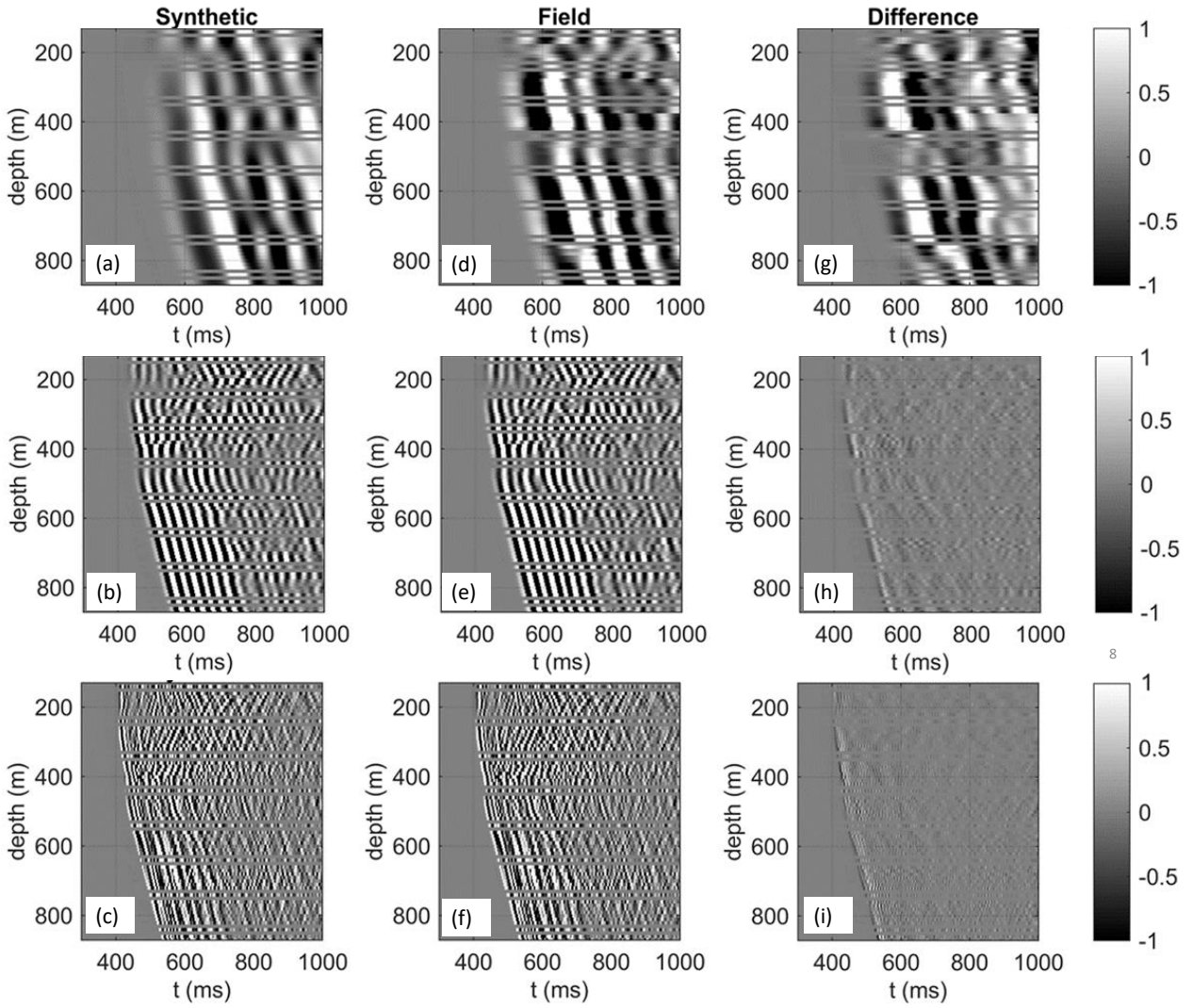

Figure 5-6. VSP seismograms from different frequency steps (11 Hz (top), 40 Hz (middle) and 105 Hz (bottom). From left to right: modelled (2a-2c), field (2d-2f) and calculated misfit (difference) (2g-2i) gathers.

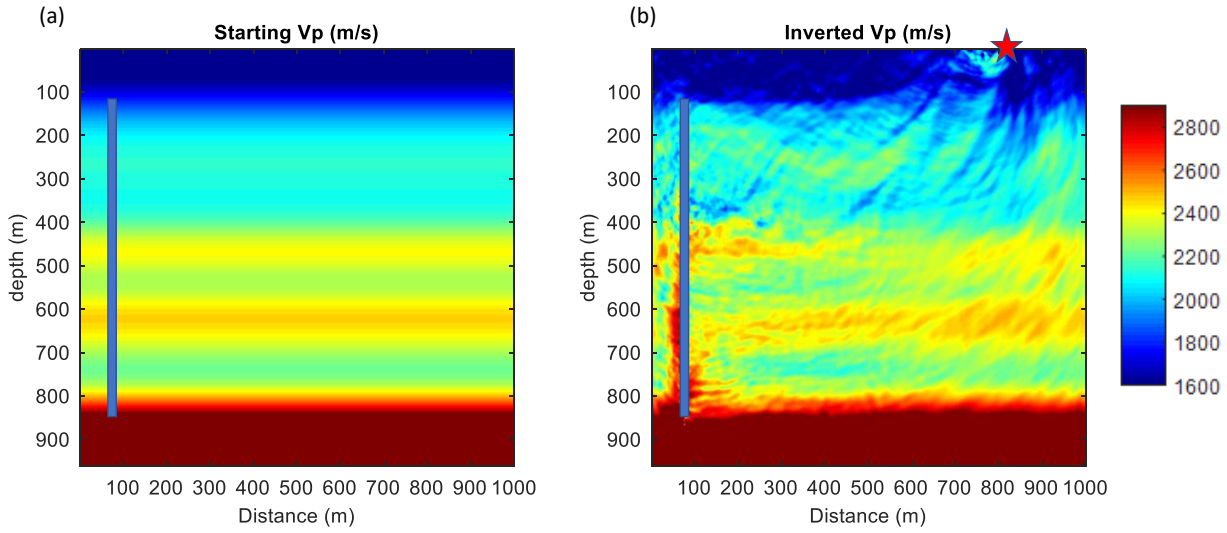

Figure 5-7. The full extent of the starting and inverted Vp model for field data. The blue line shows receivers and red star source location.

Figure 5-8 shows the starting M2 model (Vp and Vs) and the results of FWI to a half-offset distance. The FWI images of Vp and Vs contain still some artefacts. Mostly because the single offset VSP has a limited coverage, which was also reduced by excluding low signal to noise traces from the inversion (see the missing traces in Figure 5-6). However, FWI seems to resolve thin velocity layers around the well, indicated by the arrow in Figure 5-8.

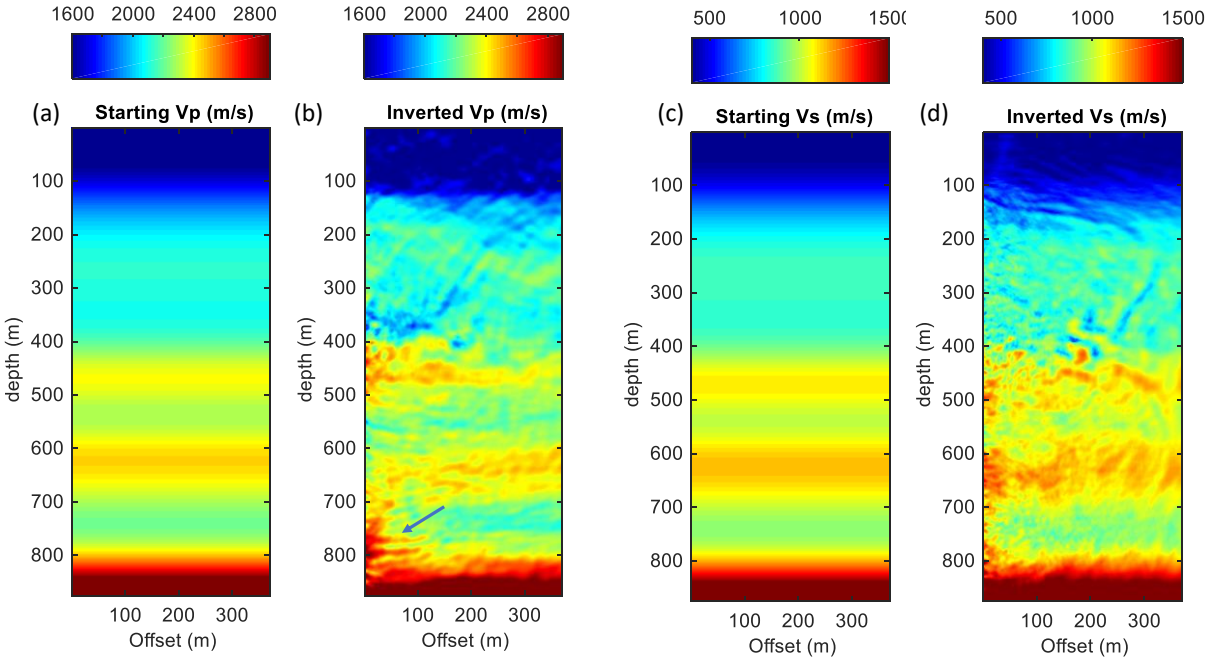

Figure 5-8. Results from FWI of data with source S63. (a) Starting Vp model (M2), (b) Inverted Vp model, (c) Starting Vs model, (d) Inverted Vs model.

One of the advantages of elastic FWI is that inversion returns both P- and S-wave velocities. This allows for the calculation of Poisson's ratio (PR) of the investigation area. PR is the ratio of transverse contractional strain to longitudinal extensional strain (Sheriff, 2002) and controls the ratio of the P- and S-wave velocities. The practical meaning of this property is that it measures the degree to which material expands/contracts when squeezed/stretched.

Earlier studies that utilised the same FWI workflow (Egorov et al., 2017) indicate that applied amplitude correction of 3D to 2D amplitude affects the inverted density data since the density inversion is controlled only by the amplitude information. Therefore I did not use or analyse the density data.

5.3.3. Results of the integrated interpretation

In geoscience, it is widely accepted that the geological/stratigraphy log from boreholes is the ground truth for any interpretation, including geophysical. Therefore, this log will guide the direction of the interpretation. Figure 5-9 shows three resulting images with logging data (stratigraphy indicating the top of the unit

and gamma-ray log). The resulting images (inverted Vp, Poisson's ratio) are superimposed over the VSP migration image with a transparency of 50 %.

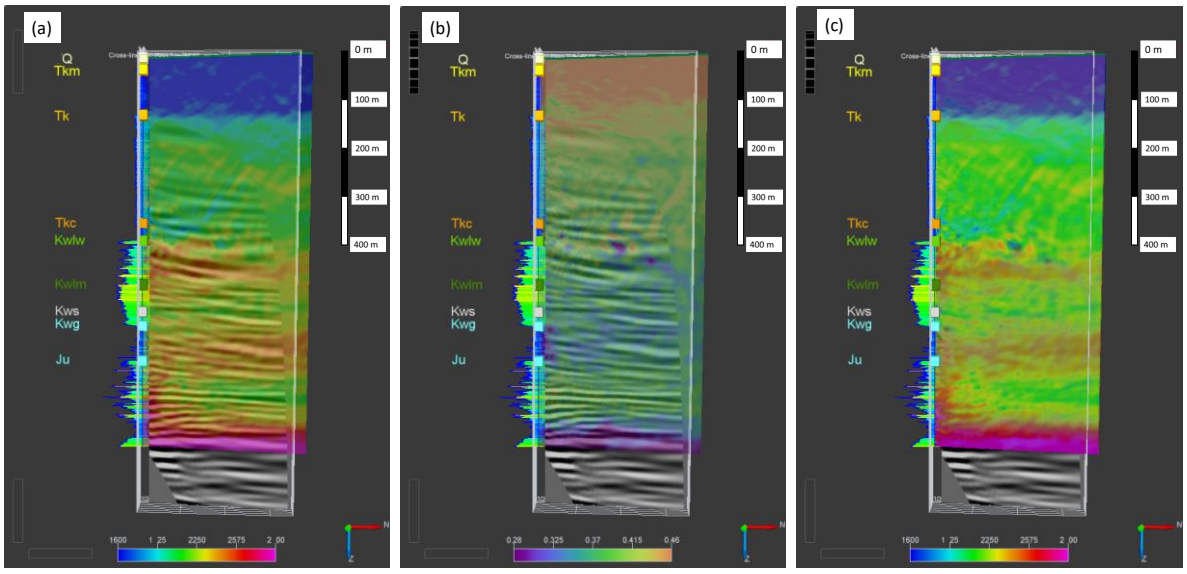

Figure 5-9. Superimposed results with logging data (gamma-ray and stratigraphy). (a) Inverted P-wave image over VSP migration image; (b) Poisson's ratio image over VSP migration image; (c) Poisson's Ratio image over inverted P-wave velocity image with VSP migration image in the background.

Based on the stratigraphy log, the first major change in velocity correlates to the contact between Mullaloo Sandstone Member of the Kings Park formation (Tkm) and undivided Kings Park formation (Tk). Gamma-ray log also changes the character at this depth, from very low to low. These changes in velocity and GR correspond well to the observed rocks. The Mullaloo unit comprises medium to very coarse-grained, moderately to poorly sorted quartz sand. The Tk sediments are much finer-grained and comprise carbonaceous siltstone and mudstone overlain with silt and fine to medium-grained sandstone. A broad, subtle undulation in the Vp image is observed away from the well towards the north, along with the same contact. The PR image (Figure 5-9b) shows a distinctive line at the same contact, but that could be attributed to the artefact as the line curves significantly. Such a steep curve is hard to geologically explain in these relatively young rocks. Migrated VSP does not have this contact imaged.

Next stratigraphic contact occurs at 360 m between the Tk sediments and Como Sandstone (Tkc) unit. A mild decrease in P-wave velocity has a limited spatial distribution. GR also decreases. This agrees with the lithology description. The

Como Sandstone unit comprises of very coarse-grained, moderately sorted quartz sand. Apart from GeoLab well, this unit was intersected in only two other artesian monitoring wells. It is believed that it probably occupies a secondary fluvial channel of a limited extent near the base of Tk (Department of Water, Government of Western Australia, 2008). The PR image has a few small lows in this area, and it is unclear if it is due to the artefacts or geology. At the bottom of Tkc is the Kings Park Unconformity, a major paleovalley (Rockwater, 2016), which overlies the Cretaceous sediments. The unconformity zone is where diffracted waves are observed, and VSP migration struggled. The inverted Vp image distinguishes the Tertiary and Cretaceous sediments from the well and reveals several gentle undulations that characterise this unconformity. Interesting features are observed on the PR image described by a significant PR decrease in two undulations, 170 and 240 meters horizontally away from the well (Figure 5-9c). These could indicate a different rock deposited in minor/secondary paleochannel known to exist near the base of Tk. The local heterogeneities can also explain the observed diffracted waves on the shot records and the struggle of using the 1D velocity model for the migration. This hypothesis was tested with forward modelling. A small feature (50 m x 20 m) with lower Vp was placed within the M2 model at the same location as the observed anomaly. The diffracted waves were observed in the resulting synthetic seismogram at similar depth/time samples (Figure 5-10).

Once within the Cretaceous sediments, Wanneroo (Kwlw) and Mariginiup (Kwlm) members of Leederville formation, the GR log has more character change as these units comprise of interbedded sandstone and siltstone. The inverted velocity is higher for Kwlw than Kwlm. Higher content of calcareous cement could explain higher Vp in Kwlw. Migrated VSP has several reflections in this zone, originating from interbedded sandstone and siltstone.

The Gage Formation has significantly lower GR due to high sandstone content. The contact between top South Perth Shale and Gage is well observed on inverted Vp image, but not so well at the top of Yarragadee (Ju), even though log reports unconformity. There is a good distinction between the Gage and Yarragadee on PR image, where it appears that Gage formation has much lower

PR and a limited spatial extension. However, the latter could also be due to the weak illumination.

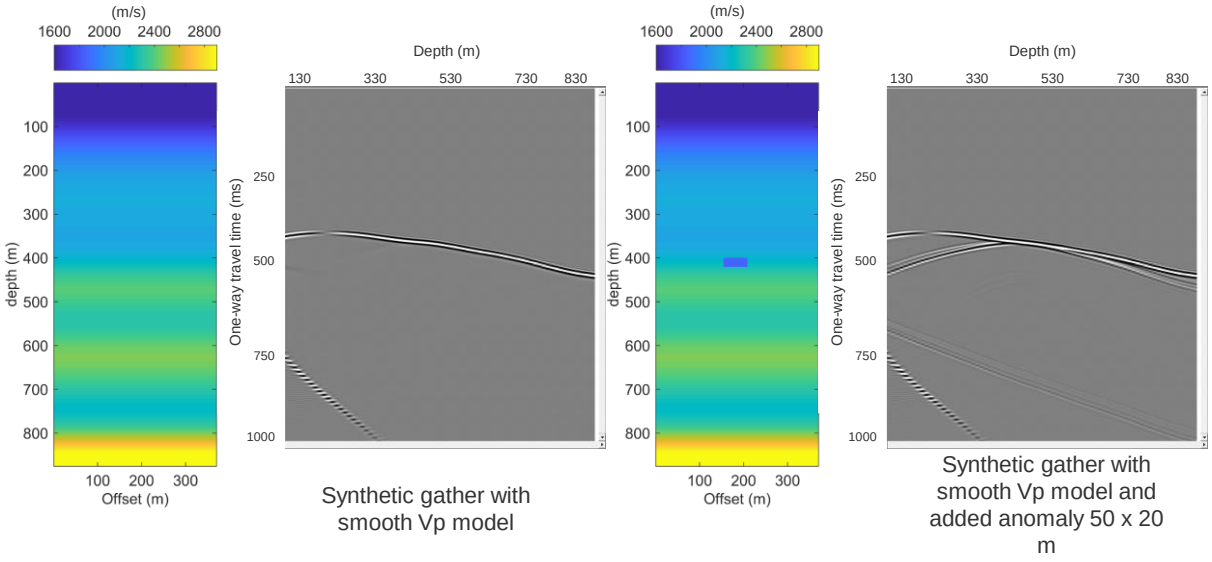

Figure 5-10. Testing hypothesis of paleochannel – Anomaly validation, source located at 700 m away from the well with an anomaly positioned at 400 m depth.

5.4. Conclusions

The single-shot VSP dataset is processed, migrated, and applied elastic FWI workflow to invert P- and S-wave velocities (Vp and Vs, respectively). The FWI workflow applied to VSP data can provide additional value for the subsurface characterisation. The critical step for a successful FWI application is to have an appropriate starting velocity model, which can be obtained from a near-offset VSP. In the case of lateral heterogeneity, as observed here, it was necessary to apply tomography to get an appropriate starting velocity model. The lack of lateral consistency in velocity distribution is due to the limited illumination of single or limited offset FWI applied to borehole seismic data provides valuable insights about the subsurface, including detailed rock properties. While the illumination is limited for a single offset VSP and numerous artefacts are observed in the images built using FWI, the integrated interpretation can reduce many uncertainties. There is a good correlation between VSP migration image, FWI results, gamma-ray log, and stratigraphy. Elastic FWI allows the calculation of Poisson's ratio image, which can also be used to identify local anomalies and potential targets. FWI can resolve small geological features. Overall, the described method allowed

the imaging of the subsurface and the identification of geological contacts and their shapes. The artefacts could be significantly reduced by constraining the FWI with data from other source locations. In the case of the GeoLab walkaway experiment, the recording geometry and presence of diffractions (subsurface complexity) indicate that one may need to apply 3D FWI workflow to account for them. Using the results of FWI for depth migration can improve seismic imaging, particularly in complex geological terrains often found in mineral exploration.

6 Conclusions and outlook

The main objectives of this research were to investigate the current VSP application in mineral exploration in Australia, identify the challenges and study how these challenges could be mitigated.

The current VSP application described in this thesis is merely limited to zero-offset single source location surveys. Such application is justified by the inherited risk of borehole surveys in an open hole environment. Since most of the boreholes in mineral exploration are deviated, the illumination of such zero-offset VSP is often increased. The VSP imaging allows for correlating seismic events directly to known geological features with great confidence, depth accuracy, and higher resolution than surface seismic imaging. However, the illumination of zero-offset VSP collected at the deviated borehole is still insufficient to image dips at and around the borehole accurately. Accurate imaging of dips can be achieved with a multi-offset VSP survey. The cost of a multi-offset VSP survey can be reduced by utilising distributed acoustic sensing technology. However, further field DAS trials are needed to address challenges related to specifics of the DAS survey (deployment, selection of cable type, adjusting recording parameters, etc.). A limited number of field DAS trials is related to the high cost of DAS interrogators and poor understanding of an appropriate DAS deployment technique in small-diameter non-cased boreholes. Therefore, the trials should be carefully planned, executed, and conducted at an acceptable "research and development" cost for the mining industry.

The presented VSP cases demonstrate that the seismic reflectivity of typical targets in a hard-rock environment can be quite high. Furthermore, these cases

support that the seismic reflectivity is controlled by the contrast of acoustic impedance, which is strongly affected by numerous structural and textural features. The structural-textural features like shears, faults, foliation, bedding, and fracturing, often indicate a zone of significant change or interest within mineral deposits, and their imaging is important for exploration. Interpretation of rock properties, with a comparison of velocity measurements collected in-situ and on the core, indicates that a common procedure of taking measurements on the core should be done if wireline measurements are not available, and it should be done with caution.

A good understanding of a novel technology is best achieved in a controlled environment at designated test sites that can allow for the repetition of the experiment using different parameters and sensors in stable conditions. Once the technology is well understood in such conditions, DAS VSP surveys should become a routine during a seismic program in mineral exploration. Contribution to a greater understanding of DAS technology is given in comparison of amplitudes collected with both geophone and DAS. To compare the data, I first brought these two datasets to the same physical properties and calibrated them to the absolute strain rate. The amplitude spectrum of the entire absolute strain-rate wavefield (uncorrelated) and the first-break amplitudes (correlated) for DAS and converted geophone are then compared. In addition to amplitude spectrum analysis, the applied method allowed the simulation of different gauge lengths. Despite different factors that affect these two sensors' performance, the comparison demonstrated that the observed absolute values of strain-rate amplitude have similar values. Although similarity in absolute response is surprisingly good, we do not expect this finding to be universal; different cable designs, coupling, etc., can produce situations where geophone and DAS responses can be different.

A denser geophone dataset can be used to simulate DAS response and study how different acquisition parameters such as gauge length affect the wavefields. It can also help with further understanding of strain-rate / DAS data (e.g., adaptation of existing particle velocity processing workflows to DAS workflows). In the absence of standardisation of DAS systems (i.e., different DAS systems

may have fixed or variable gauge length parametrisation), one can study the gauge length effect from the converted geophone wavefield and potentially use it for the sensitivity optimisation for a target wavelength.

The FWI workflow has been applied to the field VSP dataset. This type of imaging provided valuable information about the subsurface that could not be imaged with a conventional processing workflow. Additionally, elastic FWI allows the calculation of Poisson's ratio image, which can be used to identify local small-scale anomalies and potential targets. The critical step for successful FWI application is to have an appropriate starting velocity model, which can be obtained from a near-offset VSP. In the case of lateral heterogeneity, as observed in the field example, it was necessary to apply the tomography to get an appropriate starting velocity model. The lack of lateral consistency in velocity distribution is due to the limited illumination of single or limited offset. FWI applied to borehole seismic data provides valuable insights about the subsurface, including detailed rock properties. While the illumination is limited for a single offset VSP and numerous artefacts are observed in the images built using FWI, the integrated interpretation can reduce many uncertainties. Furthermore, there is a good correlation between VSP migration image, FWI results, gamma-ray log and stratigraphy. Overall, the described method allowed the imaging of the subsurface and the identification of geological contacts and their shapes.

The recommendation for future works are:

- To conduct more "research and development" field DAS VSP trials to determine the most cost-effective deployment type that secures quality data acquisition in a small-diameter open hole environment (75-96 mm);

- Due to the absence of standardisation of the DAS system, comparison to the conventional sensor (geophone) is always recommended when a new type of DAS interrogator is being used. Ideally, there should be a designated test site where the DAS systems could be compared.

- Increase the confidence of FWI results by constraining the inversion with more shot locations.

- Use FWI results for depth migration.

The above-mentioned recommendations can improve seismic imaging, particularly in complex geological terrains, and significantly assist subsurface characterisation in mineral exploration.

References

Adam, E., Perron, G., Milkereit, B., Wu, J., Calvert, A. J., Salisbury, M., Verpaelst, P., Dion, D. J. (2000). A review of high-resolution seismic profiling across the Sudbury, Selbaie, Noranda, and Matagami mining camps. *Canadian Journal of Earth Sciences,* ***37****,* 503-516. https://doi.org/10.1139/e99-064

Ajo-Franklin, J. B., Dou, S., Lindsey, N. J., Monga, I., Tracy, C., Robertson, M., Rodriguez T. V., Ulrich, C., Freifeld, B., Daley, T., Li, X. (2019). Distributed Acoustic Sensing Using Dark Fiber for Near-Surface Characterization and Broadband Seismic Event Detection. *Sci Rep* ***9****,* 1328. https://doi.org/10.1038/s41598-018-36675-8

Aldawood, A., Alfataierge, E., Bakulin, A. (2020). *Introducing a New DAS Test Facility for Evaluating Emerging DAS Technologies* [Paper presentation] First EAGE Workshop on Fibre Optic Sensing, Mar 2020, https://doi.org/10.3997/2214-4609.202030021

ALT. (2014). *User Guide, QL40 FWS – Full Waveform Sonic V12.10.01*. Advanced Logic Technology, Luxembourg.

Bakku, S. K. (2015). *Fracture characterisation from seismic measurements in a borehole.* [Doctoral dissertation, Massachusetts Institute of Technology]. http://hdl.handle.net/1721.1/97331

Barberan, C., Allanic, C., Avila, D., Hy-Billiot, J., Hartog, A., Frignet, B., Lees, G. (2012). *Multi-offset Seismic Acquisition Using Optical Fibre Behind Tubing* [Paper presentation] 74th EAGE Conference and Exhibition incorporating EUROPEC 2012, cp-293. https://doi.org/10.3997/2214-4609.20148798

Bellefleur, G., Matthews, L, Roberts, B., McMonnies, B., Salisbury, M., Perron, G., Snyder, D., McGaughey, J. (2004). *Downhole seismic imaging of the Victor kimberlite, James Bay Lowlands, Canada: A feasibility study* [Paper

presentation] 74th Annual International Meeting, SEG Technical Program, Expanded Abstracts, 1229-1232. https://doi.org/10.1190/1.1845103

Bellefleur, G., Schetselaar, E., Wade, D., White, D., Enkin, R. and Schmitt, D.R. (2020). Vertical seismic profiling using distributed acoustic sensing with scatter-enhanced fibre-optic cable at the Cu–Au New Afton porphyry deposit, British Columbia, Canada. *Geophysical Prospecting*, **68**, 313, https://doi.org/10.1111/1365-2478.12828

Bohlen, T., Saenger, E. H. (2006). Accuracy of heterogeneous staggered-grid finite-difference modeling of Rayleigh waves. *Geophysics*, **71(4)**, T109-T115.
https://doi.org/10.1190/1.2213051

Bohlen, T., et al. (2016). *IFOS2D, Version 2.0.3. [Code]* https://git.scc.kit.edu/GPIAG-Software/IFOS2D

Bona, A., Dean, T., Correa, J., Pevzner, R., Tertyshnikov, K., Van Zaanen, L. (2017). *Amplitude and Phase Response of DAS Receivers* [Paper presentation] 79th Conference and Exhibition, EAGE, Extended Abstracts. https://doi.org/10.3997/2214-4609.201701200

Bona, A., Pevzner, R. (2018). *Distributed acoustic sensing for mineral exploration: case study* [Paper presentation] AEGC 2018, Extended Abstracts.
https://doi.org/10.1071/ASEG2018abW8_4F

Brossier, R., Operto, S., Virieux, J. (2009). Seismic imaging of complex onshore structures by 2D elastic frequency-domain full-waveform inversion. *Geophysics*, **74(6)**, WCC105–WCC118. https://doi.org/10.1190/1.3215771

Cassell, B.R. (1990). *Reliability of walkaway VSP imaging given inaccurate velocity estimates* [Paper presentation] EAGE/SEG Research Workshop, cp-53-00035.
https://doi.org/10.3997/2214-4609.201411882

Castagna, J.P., Batzle, M.L., Eastwood, R.L. (1985). Relationships between compressional-wave and shear-wave velocities in clastic silicate rocks. *Geophysics*, **50(4)**, 571-581. https://doi.org/10.1190/1.1441933

Charara, M., Barnes, C., Tarantola, A. (1996). *The state of affairs in inversion of seismic data: An OVSP example* [Paper presentation] 66th Annual International Meeting SEG. 1999-2002. https://doi.org/10.1190/1.1826558

Claerbout, J. F. (1971). Toward a unified theory of reflector mapping. *Geophysics*, **36(3)**, 467-481. https://doi.org/10.1190/1.1440185

Cosma, C., Heikkinen, P., Keskinnen, J., Enescu, N. (2001). VSP in crystalline rocks-from downhole velocity profiling to 3D fracture mapping. *International Journal of Rock Mechanics and Mining Sciences,* **38**, 843–850. https://doi.org/10.1016/S1365-1609(01)00049-1

Cosma C., Heikkinen, P., Keskinen, J. (2003). Multiazimuth VSP for Rock Characterization of Deep Nuclear Waste Disposal Sites in Finland. In B. Milkreit, D. Eaton, and M. Salisbury (Eds), *Hardrock Seismic Exploration* (pp. 207 – 226). Geophysical Developments No.10, SEG. https://doi.org/10.1190/1.9781560802396.ch14

Cosma, C., Enescu, N. (2011). *Seismic Side-Scan for Wide-Range High Resolution Imaging around Boreholes* [Paper presentation] EAGE Borehole Geophysics Workshop, BG22. https://doi.org/10.3997/2214-4609.20145265

Correa, J., Egorov, A., Tertyshnikov, K., Bona, A., Pevzner, R., Dean, T., Freifeld, B., Marshall, S. (2017a). Analysis of signal to noise and directivity characteristics of DAS VSP at near and far offsets — A CO2CRC Otway Project data example. *The Leading Edge,* **36(12)**, 994a1-994a7. https://doi.org/10.1190/tle36120994a1.1

Correa, J., Dean, T., Van Zaanen, L., Tertyshnikov, K., Pevzner, R., Bona, A. (2017b). *A Comparison of DAS and Geophones for VSP Acquisition At a Dedicated Field Laboratory* [Paper presentation] EAGE 79th Conference & Exhibition 2017 https://doi.org/10.3997/2214-4609.201701100

Correa, J., Dean, T., Van Zaanen, L., Tertyshnikov, K., Pevzner, R., Bona, A. (2017c). *DAS Versus Geophones: a Quantitative Comparison of a VSP Survey at a Dedicated Field* [Paper presentation] EAGE, Fourth EAGE Workshop on Borehole Geophysics Nov 2017. https://doi.org/10.3997/2214-4609.201702477

Correa, J., Pevzner, R., Bona, A., Tertyshnikov, K., Freifeld, B., Robertson, M., Daley, T. (2018a). 3D VSP acquired with DAS on tubing installation: A Case Study from the CO2CRC Otway Project. *Interpretation*, **7**, SA11-SA19. https://doi.org/10.1190/INT-2018-0086.1

Correa, J. (2018b). *Distributed Acoustic Sensing for Seismic Imaging and Reservoir Monitoring Applied to CO2 Geosequestration* [Doctoral dissertation, Curtin University]. http://hdl.handle.net/20.500.11937/75668

Daley, T. M., Miller, D. E., Dodds, K., Cook, P., Freifeld, B. M. (2016). Field testing of modular borehole monitoring with simultaneous distributed acoustic sensing and geophone vertical seismic profiles at Citronelle, Alabama. *Geophysical Prospecting*, **64(5)**, 1318–1334. https://doi.org/10.1111/1365-2478.12324

Dean, T., Cuny, T., Hartog, A.H. (2017). The effect of gauge length on axially incident P-waves measured using fibre optic distributed vibration sensing. *Geophysical Prospecting*, **65**, 184-193. https://doi.org/10.1111/1365-2478.12419

Dean, T., Tertyshnikov, K., Pevzner, R., Calbris, G., Jestin, C., Lanticq, V. (2019). *Experimental Measurement of the Effects of Acquisition Parameters on DAS Data Quality* [Paper presentation] 81st EAGE Conference &

Exhibition 2019. https://doi.org/10.3997/2214-4609.201901245

Dillon, P. B. (1988). Vertical seismic profile migration using the Kirchhoff integral. *Geophysics*, **53**, 786-799. https://doi.org/10.1190/1.1442514

Department of Water, Government of Western Australia (2008)., *Perth Regional Aquifer Modelling System (PRAMS) model development: Hydrogeology and groundwater modelling* (report no. HG20). https://www.water.wa.gov.au/__data/assets/pdf_file/0015/5280/71802.pdf

Egorov, A., Pevzner, R., Bóna, A., Glubokovskikh, S., Puzyrev, V., Tertyshnikov, K., Gurevich, B. (2017). Time-lapse full-waveform inversion of vertical seismic profile data: Workflow and application to the CO2CRC Otway Project. *Geophysical Research Letters*, **44**, 7211–7218. https://doi.org/10.1002/2017GL074122

Egorov, A., Correa, J., Bona, A., Pevzner, R., Tertyshnikov, K., Glubokovskikh, S., Puzyrev, V., Gurevich, B. (2018). Elastic full-waveform inversion of vertical seismic profile data acquired with distributed acoustic sensors. *Geophysics*, **83(3)**, r273–r281. https://doi.org/10.1190/geo2017-0718.1

Evenden, B.S., Stone, D.R. (1971). *Seismic prospection instruments. Volume 2 Instrument Performance and Testing*, Geoexploration Monographs, ISBN 978-3-443-13004-6.

Eaton, D., Milkereit, B., Salisbury, M. (2003). Mature technologies adapted to new exploration targets, Foreword to hardrock seismic exploration. In D. Eaton, B. Milkereit, M. Salisbury (Eds), *Hardrock seismic exploration* (pp. 1–6). SEG https://doi.org/10.1190/1.9781560802396.fm

Fessenden, R. (1917). Method and apparatus for locating ore bodies; U.S. Patent No. 1,240,328. https://patents.google.com/patent/US1240328A/en

Foley, A., Jones, S., Turner, G. (2018). *Fast-Tracking Gold Exploration Below 300m around a mature mine complex – 3D Seismic Case History of the Darlot – Centenary Gold Mine* [Paper presentation] ASEG Extended Abstracts, 2018. https://doi.org/10.1071/ASEG2018abW8_3F

Fouqué, F. (1888). *Les tremblements de terre*. Paris : Librairie J.-B. Baillière. https://babel.hathitrust.org/cgi/pt?id=uc1.b4175887&view=1up&seq=9

Gardner, G.H.F.; Gardner L.W.; Gregory A.R. (1974). Formation velocity and density -- the diagnostic basics for stratigraphic traps. *Geophysics*, **39**, 770–780. https://doi.org/10.1190/1.1440465

Gal'perin, E.I. (1974). *Vertical Seismic Profiling*. Translation by The Society of Exploration Geophysicists.

Gal'perin, E. I. (1985) *Vertical Seismic Profiling and Its Exploration Potential*. D. Reidel Publishing Company.

Geoscience Australia. (2020). *Australian Government, Digital Publication, Mineral exploration*. https://www.ga.gov.au/digital-publication/aimr2020/mineral-exploration#fn11

Gibson, B., Larner K. (1984). Predictive deconvolution and the zero-phase source, *Geophysics*, **49**, 379-397. https://doi.org/10.1190/1.1441674.

GoldFields. (2012). *Annual Report* https://www.goldfields.com/reports/annual_report_2012/minerals/pdf/stives.pdf

GoldFields (2016). *Annual Report* https://www.goldfields.com/reports/annual_report_2016/minerals/reg-aus-darlot-geology.php .

Greenwood, A., Dupuis, C., Hashemi, A., Urosevic, M. (2010). *Hydrophone VSP imaging in the Agnew-Wiluna Belt, Western Australia* [Paper presentation] 21st International Geophysical Conference and Exhibition, ASEG, Preview

147.
https://doi.org/10.1081/22020586.2010.12041992

Greenwood, A. (2013). *Application of Vertical Seismic Profiling for the characterisation of hard rock* [Doctoral dissertation, Curtin University]. https://espace.curtin.edu.au/handle/20.500.11937/826

Hardage, B. A. (2000). *Vertical Seismic Profiling*. Principles: Pergamon.

Hartog, A. H. (2017). *An introduction to distributed optical fiber sensors*. CRC Press.
https://doi.org/10.1201/9781315119014.

Hinds, R. C., Anderson, N. L., Kuzmiski, R. (1996). *VSP interpretive processing: Theory and practice*. Soc. Exploration Geophysicists.

Isaenkov, R., Glubokovskikh, S., Tertyshnikov, K., Pevzner, R., Bona, A. (2020). *Effect of Rocks Stiffness on Observed DAS VSP Amplitudes* [Paper presentation] EAGE Workshop on Fiber Optic Sensing for Energy Applications in Asia Pacific, November 2020. https://doi.org/10.3997/2214-4609.202070003

Juhlin, C. (1990). Interpretation of the reflections in the Siljan Ring area based on results from the Gravberg-1 borehole. *Tectonophysics*, **173 (1-4)**, 345-360.
https://doi.org/10.1016/0040-1951(90)90229-2

Juhlin, C., Lindgren, J., Collini, B. (1991). Interpretation of seismic reflection and borehole data from Precambrian rocks in the Dala Sandstone area, central Sweden. *First Break*, **9**, 24–36. https://doi.org/10.3997/1365-2397.1991002

Karaev N.A., Rabinovich, G.Y. (2000). *Ore Seismic Prospecting*. Moscow, Geoinformmark (in Russian).

Komatitsch, D., Martin, R. (2007). An unsplit convolutional perfectly matched layer improved at grazing incidence for the seismic wave equation. *Geophysics*, **72(5)**, SM155–SM167. https://doi.org/10.1190/1.2757586

Köhn, D. (2011). *Time domain 2D elastic full waveform tomography* [Doctoral dissertation, Christian-Albrechts-Universität zu Kiel]. https://macau.uni-kiel.de/servlets/MCRFileNodeServlet/dissertation_derivate_00003917/Diss_DKoehn.pdf

Kroon, D.J. (2021). *Accurate Fast Marching, MATLAB Central File Exchange.* https://www.mathworks.com/matlabcentral/fileexchange/24531-accurate-fast-marching].

Kukkonen, I. T. (ed). (2011). *Outokumpu deep drilling project 2003-2010, special paper 51.* Geological Survey of Finland. https://tupa.gtk.fi/julkaisu/specialpaper/sp_051.pdf

Levander, A. R. (1988). Fourth-order finite-difference P-SV seismograms. *Geophysics*, **53(11)**, 1425-1436. https://doi.org/10.1190/1.1442422

Lawton, D.C., Osadetz, K.G., Saeedfar, A., Macquet, M. (2017). Monitoring technology innovation at the CaMI Field Research Station, Brooks, Alberta. *Journal of CMC Research Institutes*.

Lindsey N. J., Martin, E. R., Dreger, D. S., Freifeld, B., Cole, S., James, S. R., Ajo-Franklin, J. B. (2017). Fiber-optic network observations of earthquake wavefields. *Geophysical Research Letters*, **44**, 11,792–11,799, https://doi.org/10.1002/2017GL075722

Lindsey, N. J., Dawe, T.C., Ajo-Franklin, J.B. (2019). Illuminating seafloor faults and ocean dynamics with dark fiber distributed acoustic sensing. *The American Association for the Advancement of Science*, **366(6469)**, 1103-1107.
https://doi.org/10.1126/science.aay5881

Malehmir, A., Durrheim, R., Bellefleur, G., Urosevic, M., Juhlin, C., White, D.J., Milkereit, B., Campbell, G. (2012). Seismic methods in mineral exploration and mine planning: A general overview of past and present case histories and a look into the future, *Geophysics*, **77 (5)**, WC173 – WC190.

https://doi.org/10.1190/geo2012-0028.1

Malehmir, A., Andersson, M., Lebedev, M., Urosevic, M., Mikhaltsevitch, V. (2013). Experimental estimation of velocities and anisotropy of a series of Swedish crystalline rocks and ores. *Geophysical Prospecting*, **61**, 153-167. https://doi.org/10.1111/j.1365-2478.2012.01063.x

Mateeva, A., Mestayer, J., Cox, B., Kiyashchenko, D., Wills, P., Lopez, J., Grandi, S., Hornman, K., Lumens, P., Franzen, A., Hill, D., and J. Roy. (2012*). Advances in Distributed Acoustic Sensing (DAS) for VSP* [Paper presentation] 2012 SEG Annual Meeting, Las Vegas, Nevada. https://doi.org/10.1190/segam2012-0739.1

Mateeva, A., Lopez, J., Potters, H., Mestayer, J., Cox, B., Kiyashchenko, D., Wills, P. (2014). Distributed acoustic sensing for reservoir monitoring with vertical seismic profiling. *Geophysical Prospecting*, **62(4)**, 679-692. https://doi.org/10.1111/1365-2478.12116

Mateeva, A., Duan, Y., Kiyashchenko, D., Lopez, J. (2021). On the Surmountable Limitations of Distributed Acoustic Sensing (DAS) Vertical Seismic Profiling (VSP) – Depth Calibration, Directionality, and Noise, Learning from Field Trials. In Y. Li, M. Karrenbach, J. B. Ajo-Franklin (Eds), *Distributed Acoustic Sensing in Geophysics: Methods and Applications*. Geophysical Monograph Series, American Geophysical Union. https://doi.org/10.1002/9781119521808.ch6

Mestayer, J., Cox, B., Wills, B., Kiyashchenko, D., Lopez, J., Costello, M., Bourne, S., Ugueto, G., Lupton, R., Solano, G., Hill, D., Lewis, A. (2011). *Field Trials of Distributed Acoustic Sensing for Geophysical Monitoring* [Paper presentation] SEG Technical Program, Expanded Abstracts, . 4253-4257 https://doi.org/10.1190/1.3628095

Mueller, C., Bellefleur, G., Adam, E., Perron, G., Mah, M., Snyder, D. (2012). Performance of low-fold scalar migration for downhole seismic imaging of massive sulphide ore deposits at Norman West, Sudbury, Canada.

Geophysics, **77**. https://doi.org/10.1190/geo2011-0482.1

Nocedal, J., Wright, S. (2006). *Numerical Optimization*. Springer, New York.

Northern Star Resources. (2021). *Geology and mineralisation,* https://www.nsrltd.com/our-assets/kalgoorlie-production-centre/carosue-dam-operations

Parker, T., Shatalin, S., Farhadiroushan, M. (2014). Distributed Acoustic Sensing – a new tool for seismic application. *First Break*, **32**, 61-69. https://doi.org/10.3997/1365-2397.2013034

Pevzner, R., Bona, A., Correa, J., Tertyshnikov, K., Palmer, G., Valishin, O. (2018a). *Optimising DAS VSP data acquisition parameters: theory and experiments at Curtin training facility* [Paper presentation] EAGE 80th Annual Conference and Exhibition. https://doi.org/10.3997/2214-4609.201801923

Pevzner, R., Tertyshnikov, K., Bona, A. (2018b). *Feasibility of Passive Vertical Seismic Profiling Using Distributed Acoustic Sensing for Monitoring Applications* [Paper presentation] EAGE 80th Annual Conference and Exhibition. https://doi.org/10.3997/2214-4609.201801473

Pica, A., Diet, J. P., Tarantola, A. (1990). Nonlinear inversion of seismic reflection data in a laterally invariant medium. *Geophysics*, **55(3)**, 284–292. https://doi.org/10.1190/1.1442836

Plessix, R. E. (2006). A review of the adjoint-state method for computing the gradient of a functional with geophysical applications. *Geophysical Journal International*, **167**, 495-503. https://doi.org/10.1111/j.1365-246X.2006.02978.x

Pretorius, C. C., Muller, M. R, Larroque, M., Wilkins, C. (2003). A review of 16 years of hard rock seismics on the Kaapvaal Craton, in Eaton, D. W., B. Milkereit, and M. H. Salisbury, eds., *Hardrock seismic exploration*: SEG,

247–268.
https://doi.org/10.1190/1.9781560802396.ch16

Pretorius, C. C., Gibson, M., Snyman, Q. (2011). Development of high resolution 3D vertical seismic profiles. *Journal of the South African Institute of Mining and Metallurgy*, **111(2)**, 117–125. Retrieved October 10, 2022, from http://www.scielo.org.za/scielo.php?script=sci_arttext&pid=S2225-62532011001400010&lng=en&tlng=en

Radivojević, M., Roberts, B.W. (2021). Early Balkan Metallurgy: Origins, Evolution and Society, 6200–3700 BC. *J World Prehist* **34**, 195–278. https://doi.org/10.1007/s10963-021-09155-7

Riedel, M., Cosma, C., Enescu, N., Koivisto, E., Komminaho, K., Vaittinen, K., Malinowski, M. (2018). Underground Vertical Seismic Profiling with Conventional and Fiber-Optic Systems for Exploration in the Kylylahti Polymetallic Mine, Eastern Finland. *Minerals*, **8(11)**, 538, https://doi.org/10.3390/min8110538

Rockwater Pty Ltd. (2016). *Yarragadee aquifer geophysical instrument calibration bore – completion report*.

Sallas, J.J. (1984). Seismic vibrator control and the downgoing P-wave. *Geophysics*, **49(6)**, 732-740. https://doi.org/10.1190/1.1441701

Schneider, W. A. (1978). Integral formulation for migration in two and three dimensions. *Geophysics*, **43**, 49-76. https://doi.org/10.1190/1.1440828

Sidenko, E., Pevzner, R., Bona, A., Tertyshnikov, K., (2020). *Experimental Comparison of Directivity Patterns of Straight and Helically Wound DAS Cables* [Paper presentation] 82nd EAGE Conference & Exhibition 2020. https://doi.org/10.3997/2214-4609.202011548

Sheriff, R. E. (2002). *Encyclopaedic Dictionary of Applied Geophysics*. Society of Exploration Geophysicists.

Schilke, S., Donno, D., Chauris, H., Hartog, A., Farahani, A., Pico, Y., Schlumberger. (2016). *Numerical evaluation of sensor coupling of distributed acoustic sensing systems in vertical seismic profiling* [Paper presentation] SEG International Exposition and 86th Annual Meeting. https://doi.org/10.1190/segam2016-13527500.1

Shulakova, V., Tertyshnikov, K., Pevzner, R., Kovalyshen, Y., Bona, A., Gurevich., B. (2020). *Ambient Seismic Noise in Urban environment: Case study using downhole DAS at Curtin University Campus* [Paper presentation] EAGE Workshop on Fiber Optic Sensing for Energy Applications in Asia Pacific, Nov 2020. https://doi.org/10.3997/2214-4609.202070019

State of Western Australia, Department of Mines, Industry Regulation and Safety. (2020). 1:50000 Geological series maps https://dasc.dmirs.wa.gov.au/home?productAlias=50KPerth

Steffen, Roberston and Kirsten. (2004). *An independent technical report on St Ives Gold Mine*. SRK Consulting 2004. https://www.sec.gov/Archives/edgar/data/1203464/000110465904037462/a04-13277_1ex99d3.htm#Figure7_1

Sun, Y., Xue, Z., Hashimoto, T., Lei, X., Zhang, Y. (2020). Distributed Fiber Optic Sensing System for Well-Based Monitoring Water Injection Tests—A Geomechanical Responses Perspective. *Water Resources Research*, **56**, https://doi.org/10.1029/2019WR024794

Tarantola, A. (1984). Inversion of seismic reflection data in acoustic approximation. *Geophysics*, **49**, 1259-1266. https://doi.org/10.1190/1.1441754

Tarantola, A. (1986). A strategy for nonlinear elastic inversion of seismic reflection data. *Geophysics*, **51(10)**, 1893–1903. https://doi.org/10.1190/1.1442046

Tertyshnikov, K., Pevzner, R., Freifeld, B., Ricard, L., Avijegon, A. (2019). *3D DAS VSP for characterisation of the CO2 shallow release site: CSIRO In-*

Situ Laboratory case study [Paper Presentation] 2nd EAGE-VPI Conference on Reservoir Geoscience. https://doi.org/10.3997/2214-4609.201977064

Tertyshnikov, K., Pevzner, R. (2019). *Performance of Different Seismic Sources for DAS VSP Acquisitions: a Case Study at Curtin Well Site* [Paper presentation] 81st EAGE Conference & Exhibition 2019. https://doi.org/10.3997/2214-4609.201900693

Tertyshnikov, K., Pevzner, R. (2020). *3C VSP with DAS – an Obvious Approach* [Paper presentation] 82nd EAGE Conference & Exhibition 2020. https://doi.org/10.3997/2214-4609.202030016

Tertyshnikov, K., Yurikov, A., Bona, A., Urosevic, M., Pevzner, R., Cristall, J. (2020). *3D VSP for Coal Seams Exploration using Permanently Installed DAS* [Paper presentation] EAGE Workshop on Fiber Optic Sensing for Energy Applications in Asia Pacific, Nov 2020. https://doi.org/10.3997/2214-4609.202070021

Tertyshnikov, K., Zulic, S., Yurikov, A., Yavuz, S., Sidenko, E., Isanekov, R., Pevzner, R. (2021). *Curtin In-Situ GeoLab – advancing geophysical sensing* [Paper presentation] 3rd Australasian Exploration Geoscience Conference, 244 . https://doi.org/10.1080/14432471.2021.1957452

Urosevic, M., and B. Evans. (2000). Surface and borehole methods to delineate kimberlite pipes in Australia. *The Leading Edge*, **19**, 756–758. https://doi.org/10.1190/1.1438712 .

Van Zaanen, L., Bona, A., Correa, J., Dean, T., Pevzner, R., Tertyshnikov, K. (2017*). A comparison of borehole seismic receivers* [Paper presentation] SEG International Exposition and 87th Annual Meeting. https://doi.org/10.1190/segam2017-17799478.1

Verliac, M., Lesnikov, V., Euriat, C. (2015). *The Rousse-1 DAS VSP experiment – Observations and comparisons from various optical acquisition systems*. SEG Technical Program Expanded Abstracts : 5534-5538.

https://doi.org/10.1190/segam2015-5886544.1

Virieux, J. (1986). P-SV wave propagation in heterogeneous media: Velocity-stress finite-difference method. *Geophysics*, **51(4)**, 889–901. https://doi.org/10.1190/1.1442147

Vujić, S. (2003). Mining on the Ground of the Central Balkans: Eight thousand years of history. In S. Vujić, B. Jovanović, Č. Jordović,(Eds), *Mining on the Ground of the Central Balkans: Eight thousand years of history*. Serbian Academy of Sciences and Arts, Science Gallery and Museum of Science and Technology, Belgrade (In Serbian).

Vujić, S. (2014). The history of Serbian Mining. In S. Vujić, A. Grubić, R. Jelenković (Eds), *Serbian Mining and Geology in the Second Half of XX Century*, (pp. 1-38), Academy of Engineering Sciences of Serbia, Matica srpska and Mining Institute of Belgrade, 564 p. http://ribeograd.ac.rs/wp-content/uploads/2018/08/Istorija-srpskog-rudarstva-EN.pdf

Wuestefeld, A., Stokkan, S., Baird, A., Oye, V. (2021). *NOR-FROST: A near-surface test site for fibre optic sensing* [Paper presentation] EAGE GeoTech 2021 Second EAGE Workshop on Distributed Fibre Optic Sensing, March 2021 https://doi.org/10.3997/2214-4609.202131027

Wyatt, K., Wyatt, S. (1981). *The determination of subsurface structural information using the vertical seismic profile* [Paper presentation] SEG 51st Annual International Meeting.

Yu, G., Xiong, J.L., Wu, J.J., Chen, Y.Z., Zhao, Y.S. (2020). Enhanced surface seismic data processing using simultaneous acquired DAS-VSP data. *First Break*, **38(6)**, 29-36. https://doi.org/10.3997/1365-2397.fb2020039

Zulic, S., Tertyshnikov, K., Yurikov, A., Sidenko, E., Isaenkov, R., Pevzner, R. (2020). *Curtin Geolab Research Facility: Walkaway VSP with DAS and Geophones* [Paper presentation] EAGE Workshop on Fiber Optic Sensing for Energy Applications in Asia Pacific, November 2020. https://doi.org/10.3997/2214-4609.202070031

Zulic, S., Sidenko, E., Yurikov, A., Tertyshnikov, K., Bona, A., Pevzner, R. (2021). *Comparison of Amplitude Measurements on Borehole Geophone and DAS Data* [Poster presentation] AGU Fall Meeting 2021. https://doi.org/10.1002/essoar.10510092.1

Zulic, S., Bona, A., Tertyshnikov, K., Yurikov, A., Pevzner, R. (2021). *Subsurface characterisation using full waveform inversion of vertical seismic profile data: Example from the Curtin GeoLab well* [Paper presentation] 3rd Australasian Exploration Geoscience Conference. https://doi.org/10.1080/14432471.2021.1957452

Every reasonable effort has been made to acknowledge the owners of copyright material. I would be pleased to hear from any copyright owner who has been omitted or incorrectly acknowledged.